DESIGNING FIXED DOSE COMBINATION OF GLIPIZIDE AND FELODIPINE USING FUSED DEPOSITION MODELING 3D PRINTING

BY
MR. Kasitpong THANAWUTH

A Thesis Submitted in Partial Fulfillment of the Requirements
for Doctor of Philosophy PHARMACEUTICAL ENGINEERING
(INTERNATIONAL PROGRAM)
Silpakorn University
Academic Year 2025

DESIGNING FIXED DOSE COMBINATION OF GLIPIZIDE AND FELODIPINE USING FUSED DEPOSITION MODELING 3D PRINTING

By
MR. Kasitpong THANAWUTH

A Thesis Submitted in Partial Fulfillment of the Requirements
for Doctor of Philosophy PHARMACEUTICAL ENGINEERING
(INTERNATIONAL PROGRAM)
Silpakorn University
Academic Year 2025

Thesis Title	DESIGNING FIXED DOSE COMBINATION OF GLIPIZIDE AND FELODIPINE USING FUSED DEPOSITION MODELING 3D PRINTING
By	MR. Kasitpong THANAWUTH
Field of Study	PHARMACEUTICAL ENGINEERING (INTERNATIONAL PROGRAM)
Thesis Advisor	Professor Pornsak Sriamornsak, Ph.D.

Faculty of Pharmacy, Silpakorn University in Partial Fulfillment of the Requirement for the Doctor of Philosophy

..... Dean of the Faculty of Pharmacy

(Professor Pornsak Sriamornsak, Ph.D.)

Thesis COMMITTEE

..... Chairperson

(Professor Sontaya Limmatvapirat, Ph.D.)

..... Advisor

(Professor Pornsak Sriamornsak, Ph.D.)

..... Committee

(Associate Professor Prasert Akkaramongkolporn, Ph.D.)

..... Committee

(Assistant Professor Vipaluk Patomchaiviwat, Ph.D.)

..... External examiner

(Associate Professor Kampanart Huanbutta, Ph.D.)

60365802: MAJOR PHARMACEUTICAL ENGINEERING (INTERNATIONAL PROGRAM)
Keyword: Fixed-dose combination tablets, Dual-drug release, Immediate-release Glipizide tablet, Controlled-release Felodipine tablet, Fused deposition modeling (FDM)

MR. Kasitpong THANAWUTH : DESIGNING FIXED DOSE COMBINATION OF GLIPIZIDE AND FELODIPINE USING FUSED DEPOSITION MODELING 3D PRINTING Thesis Advisor : Professor Pornsak Sriamornsak, Ph.D.,

Poor medication adherence in chronic diseases such as hypertension and diabetes affects approximately 50% of patients, primarily due to complex dosing regimens. This research investigated fused deposition modeling (FDM) 3D printing technology to develop personalized pharmaceutical dosage forms with controlled release profiles, comprising three studies: (i) controlled-release felodipine tablets with varying internal geometries, (ii) immediate-release glipizide tablets using low-temperature printing, and (iii) fixed-dose combination tablets incorporating both drugs. Drug-loaded filaments were prepared via hot-melt extrusion; felodipine filaments (5% w/w in PVA) were extruded at 185°C, while glipizide filaments (12% w/w with Kollidon® VA64, mannitol, triethyl citrate) required low-temperature processing at 60°C to preserve drug stability. 3D printing was performed using a dual-nozzle Flashforge Creator Pro at 195°C for felodipine and 90°C for glipizide. Characterization techniques included DSC, TGA, PXRD, SEM, and SRXTM analysis, and drug release was evaluated using followed USP dissolution methods with mathematical modeling. The first study revealed controlled-release felodipine tablets with constant volume but varying geometries (round, square, hexagonal, triangular) exhibited drug release governed by the surface area-to-volume (SA/V) ratios rather than surface area alone. Round geometry (SA/V=0.55) showed the fastest release, while triangular (SA/V=0.41) had the slowest. Peppas-Sahlin modeling confirmed swelling-controlled mechanisms, with polymer relaxation dominating (65-75%) over Fickian diffusion. Tablets with similar SA/V ratios demonstrated comparable dissolution profiles (f_2>50). The second study developed immediate-release glipizide tablets through factorial design optimization. Grid infill pattern, single shell, and 0.3 mm layer thickness provided optimal rapid release by maximizing porosity and surface contact. A mathematical model predicted tablet thickness for 5-15 mg dosages. All formulations achieved >80% release within 30 min, meeting USP criteria with ± 5% content uniformity. The third study produced fixed-dose combinations using three designs: stacked-layer, core-shell (felodipine core/glipizide shell), and inverted core-shell. All achieved dual-release profiles with immediate glipizide release (>80% at 30 min) and controlled felodipine release over 24 h. The stacked-layer showed the fastest felodipine release due to enhanced hydration, the core-shell demonstrated the slowest release following Hopfenberg erosion model, and the inverted core-shell produced glipizide profiles similar to commercial tablets (f_2=60.06). Key innovations include establishing predictive geometry-release relationships, achieving successful low-temperature processing for thermolabile drugs, and creating sophisticated dual-release polypills. This research demonstrates FDM 3D printing's potential for personalized medicine, enabling customized dosage forms tailared to individual patient needs, with precise control over drug release through geometric design and process optimization, and offers the potential to revolutionize pharmaceutical manufacturing via point-of-care production to improve patient compliance in chronic disease management.

ACKNOWLEDGEMENTS

First and foremost, I would like to express my deepest gratitude to my advisor, Professor Dr. Pornsak Sriamornsak, for his invaluable guidance, continuous support, and providing me with numerous opportunities to conduct research. His mentorship has been instrumental in developing my critical thinking, learning abilities, and research planning skills throughout my doctoral studies. His dedication and expertise have shaped my academic journey in countless ways.

I wish to extend my sincere appreciation to Professor Dr. Sontaya Limmatvapirat and Professor Dr. Thawatchai Phaechamud, faculty members in the Pharmaceutical Engineering program, for their assistance, valuable advice, and encouragement that helped me successfully complete my Ph.D. studies. Their expertise and support have been crucial to my academic achievement.

I am deeply grateful to my colleagues at College of Pharmacy, Rangsit University, who provided continuous support and encouragement throughout my doctoral studies. Their collaboration and friendship have been invaluable in pushing forward my Ph.D. research to completion.

My heartfelt thanks go to my fellow graduate students who shared this academic journey with me, as well as all the scientists and staff members at the Faculty of Pharmacy, Silpakorn University, who provided assistance and moral support throughout my research work. Their camaraderie and professional support created an environment conducive to learning and research.

Finally, I wish to dedicate my deepest appreciation to my family, who have shown endless patience, love, and encouragement throughout this challenging journey. Without their unwavering support and understanding, this accomplishment would not have been possible. Their belief in me has been my greatest source of strength. To all those who have contributed to my success in ways both large and small, I am eternally grateful.

Kasitpong THANAWUTH

TABLE OF CONTENTS

Page

LIST OF TABLES

Page

LIST OF FIGURES

Page

LIST OF ABBREVIATION

3D	Three dimention
% w/w	Percent weight per weight
°/s	Angle per second
ABS	Acrylonitrile butadiene styrene
AIC	Akaike information criterion
AM	Additive manufacturing
APIs	Active pharmaceutical ingredients
ASTM	The American Society for Testing and Materials
BCS	Biopharmaceuticals classification system
CAD	Computer aided design
DLP	Digital light processing
DMSO	Dimethyl sulfoxide
DSC	Differential scanning calorimetry
f_2	Similarity factor
FDC	Fixed-dose combination
FDM	Fused deposition modeling
FDP	Felodipine
FFF	Fused filament fabrication
g/mm^2	Gram per square millimeter
GPZ	Glipizide
h	Hour (s)
HME	Hot-melt extrusion
HPLC	High-performance liquid chromatography
HPMC	Hydroxypropyl methyl cellulose
keV	Kiloelectronvolt
kg	Kilogram
KVA64	Kollidon® VA 64
mg	Milligram
mg/L	Milligram per litter

mg/mL	Milligram per millitter
min	Miniute (s)
mL/min	Millite per miniute
mm	Millimeter
mm^2	Square millimeter
mm^3	Cubic millimeter
mPa.s	MilliPascal-second
N	Newton
NCDs	Non-communicable diseases
nm	Nanometer
°C	Degree celcious
PEG	Poly (ethylene glycol)
PEGDA	Poly (ethylene glycol) diacrylate
PEO	Poly (ethylene oxide)
PLA	Poly (lactic acid)
PVA	Poly (vinyl alcohol)
PXRD	Powder X-ray diffractometry
R^2	Correlation coefficient
SA/V	Surface area-to-volume
SEM	Scanning electron microscope
SLA	Stereolithography
SLS	Selective laser sintering
SRXTM	Synchrotron radiation X-ray tomographic microscopy
T2DM	Type 2 diabetes mellitus
TEC	Triethyl citrate
T_g, t_g	Glass transition temperature
TGA	Thermogravimetric analysis
T_m, t_m	Melting point temperature
XTM	X-ray tomographic microscopy
XμCT	X-ray micro-computed tomography

CHAPTER 1
INTRODUCTION

1.1. Statement and significance of the problems

Chronic diseases are indispositions that last for 1 year or more and require ongoing medical attention or limit activities of daily living or both. Chronic diseases such as diabetes, heart disease, asthma, Alzheimer's disease, epilepsy, arthritis, and cancer, etc. Almost elderly patients have more than one chronic disease. They have to acquire a lot of medicines for long-term treatment. Patients have to remember time for taking medicines. In addition, they are often required to spilt the dosage unit which may lead to under- or over-dose of drug for treatment. Therefore, patient compliance has been a challenge problem [1].

Personalized medicine, which may be thought of as tailoring medical treatment, is a medical procedure used for diagnosis, intervention, and selection of an effective drug therapy for a patient based on patient's parameters such as pharmacological profile, body weight, gender, metabolism, age and patient's comorbidities [2].

Although the conventional pharmaceutical industrial techniques are produced for large-scale, they are limited to small batch preparation of individual doses because of their multistep such as mixing, milling, and conversion of granules into tablets using compression [3]. These multistep processes are inappropriate for the development of personalized and complex drug dosage forms. In the past decade, many researchers have started exploring 3D printing to prepare pharmaceutical dosage forms. The 3D printing involves with making solid objects (layer-by-layer process) by using computer aided design (CAD) data. The fused deposition modeling (FDM) is one of the 3D printing techniques which demonstrates the most interesting in fabricating pharmaceutical because FDM printers are easy to operate, movable, and inexpensive. These techniques combine hot-melt extrusion with 3D printing techniques [3-5]. FDM process uses an ink that prepared raw material to be filament and pass it through extrusion nozzle to melt the filament and deposit it onto building. Several academic publications have shown that FDM enables adjustment of the drug dosing easily and

customized dosage forms in different shapes and sizes of tablet. These advantages could be beneficial for preparing controlled-release dosage forms for individual.

The goal of this study is to improve patient compliance in managing a variety of chronic diseases by utilizing FDM 3D printing technologies to innovate the creation of a polypill or a single dosage tablet. Felodipine (FDP) and glipizide (GPZ), selected as model drugs, are prevalent in the treatment protocols of patients contending with multiple chronic diseases such as hypertension and diabetes. Currently, none of the commercial products combining antihypertensive agents and antidiabetic drugs have been launched. Additionally, these medications demand administration at varied dosages and intervals, making their incorporation into a single tablet challenging. In this research, the formulation of multi-drug 3D-printed dosage forms is meticulously planned. Poly (lactic acid) and/or polyvinyl alcohol have been selected as bases, instrumental in the controlled release of the drugs. In contrast, Kollidon® VA64 (vinylpyrrolidone-vinyl acetate copolymer) has been chosen to facilitate the study of immediate drug release mechanisms. Furthermore, this study will further investigate the drug release mechanisms inherent to these 3D-printed tablets, aiming to elucidate the influence of FDM 3D printing technology on drug release kinetics.

1.2. Objective of the research

The main objectives of this research were:

(1) To fabricate 3D-printed tablets loaded with FDP that feature various internal surface geometries while maintaining a constant surface area, using polylactic acid (PLA) for the outer compartment.

(2) To develop a filament containing GPZ using Kollidon® VA 64 and to produce immediate-release glipizide tablets through FDM 3D printing at low temperatures.

(3) To investigate the preparation of fixed-dose combination tablets containing two drugs, FDP and GPZ, with varying drug release profiles using the FDM 3D printing technique.

CHAPTER 2
LITERATURE REVIEW

2.1. 3D printing technologies and application of 3D printing in healthcare

2.2. 3D Printing in personalized drug delivery

2.3. Fused deposition modeling 3D printing

2.4. Printing materials for FDM 3D printing

2.5. Working process parameters of FDM-3D printing technique

  2.5.1. Drug loading filament process using hot melt extrusion method

  2.5.2. Mechanical characterization of filament

  2.5.3. 3D printing process parameter

2.6. Physicochemical and therapeutic dosage of the model drugs

  2.6.1. Felodipine

  2.6.2. Glipizide

2.1. 3D printing technologies and application of 3D printing in healthcare

The 3D printing is a recently innovative technology that has been revolutionary in engineering, product design, aerospace, architecture, military, chemical industry, food industry, and fashion industry [6]. The importance of 3D printing is not only limited to these industrial areas, but it is also expanding in the medical field in a wide range of applications such as tissue designs, tissue engineering, organ printing, diagnostic platforms, dentistry, biomedical devices, anatomical models, drug designing, and drug delivery systems [7]. For the application of 3D printing technology in healthcare, it has been continuously improved. At the present, this technology can be used directly for a variety of biomedical applications. For example, Jakab et al. proposed that multicellular spheroids can be used as bioink for 3D organ printing [8], Barron et al. utilized laser-based technology to deposit mammalian cells onto a biopolymer matrix [9], and Duan et al. developed artificial heart valve by 3D printing with alginate/gelatin hydrogel [10], etc. For the application of 3D printing technology in pharmaceutical field, it has become an interesting innovation over the last decade. From the published research articles, 3D printing technologies have variously developed. For instance, complex drug release profiles, personalized and unique drug dosage, customized and on-demand drug printing, and implantable drug delivery devices [3, 11].

This technology, also known as additive manufacturing (AM), builds three-dimensional objects layer-by-layer from a digital model, providing precise the design and composition of the final product. In 2009, the American Society for Testing and Materials (ASTM) has grouped these technologies into seven major categories according to the methods of adding material and working principle to produce the desired 3D object, including binder jetting, vat photopolymerization, powder bed fusion, material jetting, material extrusion, directed energy deposition and sheet lamination [12]. The most prominent techniques are detailed below.

- Vat photopolymerization (stereolithography - SLA / Digital light processing – DLP) uses a light source (a laser for SLA, a digital projector for DLP) to selectively cure a liquid photopolymer resin in a vat, layer by layer. It is known for its exceptionally high resolution and precision, making it ideal for fabricating intricate structures such as microneedles for transdermal drug delivery, complex scaffolds for tissue engineering, and custom dental appliances. The primary challenges are the limited availability of

biocompatible and FDA-approved resins and the potential for photochemical reactions with the active drug ingredients [13, 14].

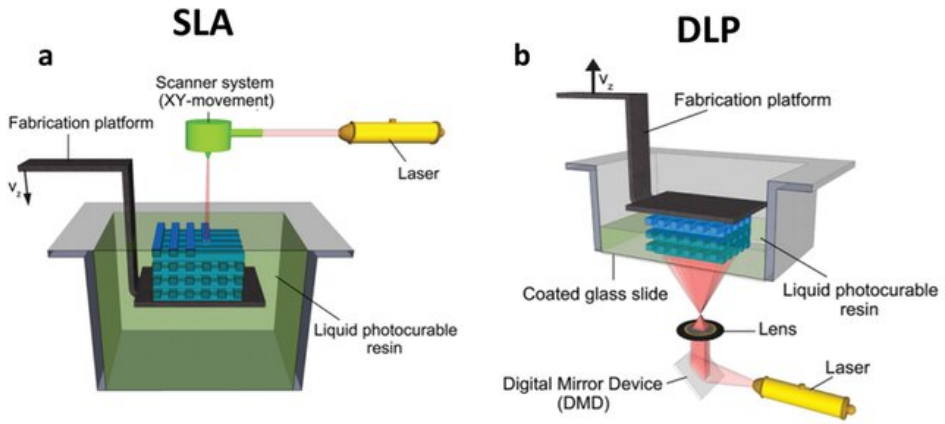

Figure 1. Scheme of stereolithography (SLA) and digital light processing (DLP) 3D printing.

- Powder bed fusion (selective laser sintering - SLS) uses a high-power laser to fuse or sinter powdered materials together. This technique is highly versatile as it does not require support structures and can work with a range of materials, including polymers and metals like titanium alloys, which are used for orthopedic and dental implants [16]. In pharmaceuticals, it allows for the creation of porous tablets with modified drug release without the need for binders, but the high temperature involved may degrade thermally sensitive drugs [17, 18].

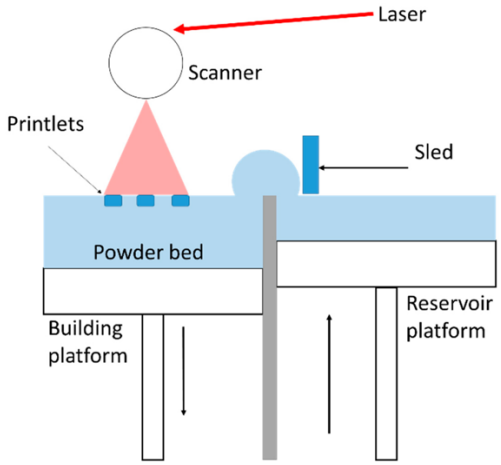

Figure 2. Scheme of selective laser sintering (SLS) 3D printing.

• Material jetting, including inkjet and binder jetting, works by depositing tiny droplets of a drug-polymer formulation onto a substrate, similar to how a standard inkjet printer operates. This approach enables accurate control over drug dose and spatial distribution, making it suitable for producing rapidly disintegrating tablets, uniform coatings, and combination therapies with multiple active ingredients [19-22].

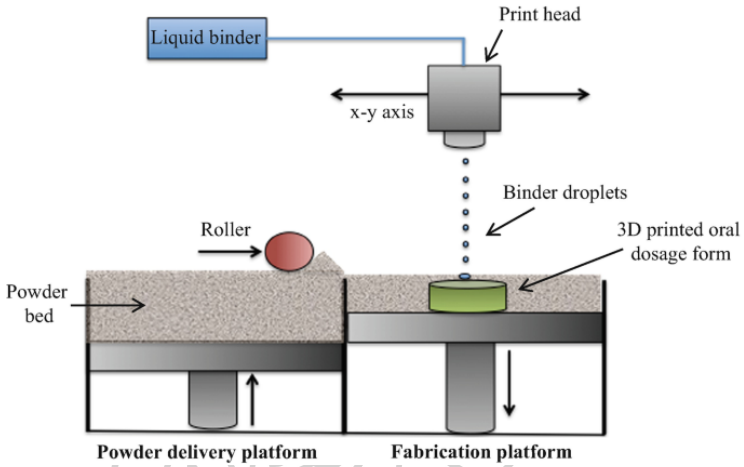

Figure 3. Scheme of binder jetting 3D printing.

Table 1. Summary of current 3D printing techniques used in pharmaceutical applications

3D printing method	Materials used	Design strategies	Drug delivery mechanism	Advantages	Limitations	Reference
FDM 3D printing	Thermoplastic polymers	Layer-by-layer deposition	Immediate and sustained release	Cost-effective, scalable	Limited to thermally stable drugs	[24]
Inkjet printing	Drug solutions/ suspensions, polymers	Drop-on-demand	Localized drug delivery	High resolution, low waste	Limited to low-viscosity formulations	[25]
SLA 3D printing	Photosensitive resins	UV-curing layer-by-layer	Controlled release	High precision and complexity	Limited biocompatible resins	[26]
SLS 3D printing	Powdered polymers	Laser sintering of layers	Modified drug release	No need for binders	High temperature may degrade drugs	[27]

2.2. 3D Printing in personalized drug delivery

Personalized medicine is a medical procedure used for diagnoses, intervention, and selection of efficient drug therapies for the patient based on patient's parameters such as pharmacological profile, body weight, gender, metabolism, and age. The conventional pharmaceutical industrial techniques are limited to small batch preparation of individual doses due to their multisteps, mainly mixing, milling, and conversion of granules into tablets using compression [3]. These multistep processes were found to be inappropriate for the development of personalized and complex drug dosage forms. In addition, 3D printing has emerged as a powerful solution, offering the remarkable versatility to create drugs with accurate concentrations, complex geometries, and tailored release profiles that are ideal for personalized therapy. This technology is particularly beneficial for patient populations with unique needs, such as children, the elderly, and individuals with rare diseases or complex combination therapy regimens.

One of the most significant advantages of 3D printing is its ability to improve patient compliance, especially for those with multiple chronic diseases, by fabricating "polypills.". A polypill is a single dosage form that combines multiple active pharmaceutical ingredients (APIs), which can reduce pill burden and simplify treatment regimens. For example, Khaled et al. successfully fabricated a polypill with five compartments which represented a cardiovascular treatment regimen was developed using semi-solid based extrusion 3D printing (Figure 4). The tablet composed of aspirin and hydrochlorothiazide in two immediate release compartments and pravastatin, atenolol, and ramipril in three sustained release chambers, showcasing the ability to integrate different release kinetics within one unit [28]. Further advancing this concept, Sadia et al. utilized dual FDM 3D printer to manufacture multi-layered tablets containing various APIs with compartmentalized release profiles for hypertension control, illustrating how such systems can be tailored to complex clinical needs [29]. Addressing the challenge of differing absorption sites, Gioumouxouzis et al. used a dual-layer 3D printing approach to create an anti-diabetic formulation containing both metformin and glimepiride. This design allowed for distinct release characteristics for each drug, enabling concurrent weekly administration [30]. These examples highlight

the unique capability of 3D printing to create complex drug delivery systems that are difficult, if not impossible, to produce using traditional methods. The ability to precisely control the spatial distribution of multiple drugs within a single tablet opens the door to highly sophisticated and personalized therapeutic strategies. Table 2. summarizes some studies which were fabricated 3D printed polypill under each technology from the literature.

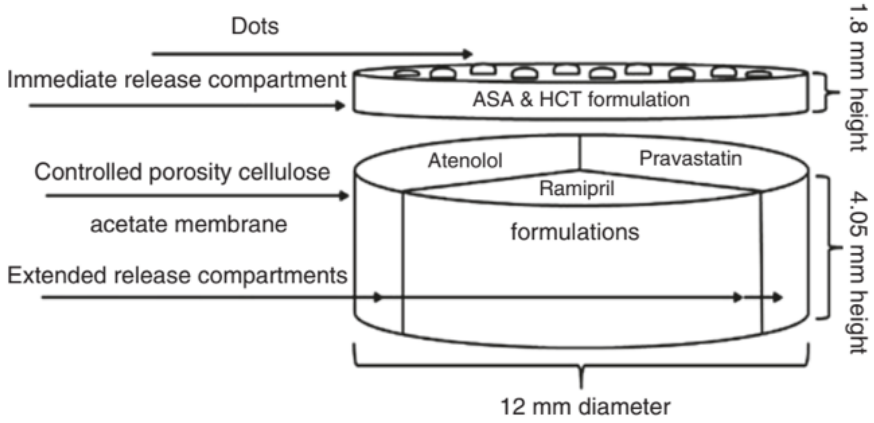

Figure 4. 3D printed polypill containing five different drugs with different release profiles.

Table 2. Polypills that were developed by 3D printing technology.

3DP technology	APIs	Ink formulation	Reference
Extrusion 3D printing	Atenolol, pravastatin, ramipril, aspirin, HCTZ	HPMC 2208, lactose, sodium starch glycolate, polyvinylpyrollidone K30	[28]
FDM 3D printing	Lisinopril, indapamide, rosuvastatin, amlodipine	Poly(vinyl alcohol) (PVA), sorbitol, titanium dioxide	[31]
Extrusion 3D printing	Caffeine, vitamin B1, B3, B6	Craft Blend R30M, R4H Tween 80, water	[28]
SLS 3D printing	Amlodipine, lisinopril	Poly(ethylene oxide) (PEO) 100,000	[32]
SLA 3D printing	Irbesartan, atenolol, HCTZ, amlodipine	Poly(ethylene glycol) (PEG300), poly(ethylene glycol) diacrylate (PEGDA)	[33]
FDM 3D printing	Isoniazid, rifampicin	Hydroxypropyl cellulose, hypromellose acetate succinate	
FDM 3D printing	Enalapril, HCTZ	Eudragit® EPO, tri-calcium phosphate, triethyl citrate	[29]
Extrusion 3D printing	Nifedipine, glipizide, captopril	HPMC 2208, PEG 6000, tromethamine, lactose	[34]

The adaptability of 3D printing makes it especially useful for both pediatrics and geriatric. In pediatrics, children often struggle with unpleasant tastes, awkward textures, or the need for precise, weight-based dosing that standard tablets cannot meet. 3D printing can help overcome these issues. For example, Zhu et al. used semi-solid extrusion to produce child-friendly orodispersible propranolol gummies tailored to pediatric dosage requirements [35]. Likewise, Goyanes et al. created chewable isoleucine tablets in kid-appealing flavors (lemon, raspberry, coconut) and colors (light green, yellow, orange) to improve acceptance in patients with maple syrup urine disease [36]. For geriatric applications, polypharmacy and swallowing difficulties can reduce adherence to treatment. 3D printing offers solutions to these challenges. For instance,

printed polypills combine multiple medications into a single tablet, streamlining complex regimens. Fast-disintegrating tablets and oro-dispersible films can be produced to assist patients who have trouble swallowing. Additionally, for individuals with dementia or cognitive impairment, printed dosage forms can include tactile markers or scannable QR codes that display customized instructions—such as date, time, or day of the week—to improve safety and ensure doses are taken correctly [37].

2.3. Fused deposition modeling 3D printing

The FDM or Fused filament fabrication (FFF) is a method of 3D printing that incorporates the hot-melt extrusion (HME) process for manufacturing a filament that can be fed directly to an extrusion head for melt-deposition of 3D printer in a layer-by-layer. HME is a process for the production of pharmaceutical dosage forms which ensures free-solvent production, low-cost in scale-up, and increased solubility and bioavailability of poorly water-soluble drugs. The advantages of FDM are less expensive than other techniques, no post-printing processes, and movable. The limitations of this technique are high temperature process leading to material degradation and preparation of filaments is required [5].

The process of preparation of FDM 3D-printed dosage forms starts from creating the dosage form model by using the digital design software such as Autocad, Autodesk, Solidworks, Creo parametric, Onshape, Mimics, 3Matic, and Google SketchUp, etc. Then, this digital model is converted into .stl digital file format. The .stl file is subsequently changed to G code file by using slicer software before sending the information for command the 3D printer [38]. Before printing of dosage forms, the materials have to be filament forms. Drug loading into the filament process is an important process for the fabrication of the dosage form with the FDM-3D printing technique. The drug should be loaded into filament before printing. This process has two techniques: impregnation and HME. After that, the filament is passed through printing nozzle to melt the filament and deposit it onto building plate. The object is sequentially printed layer-by-layer until it has done.

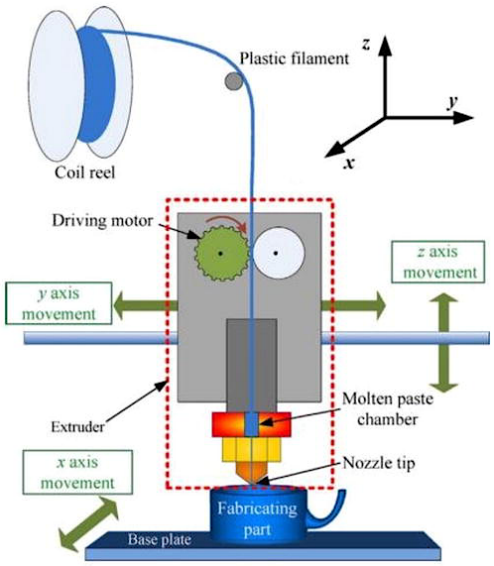

Figure 5. Scheme of fused deposition modeling 3D printing.

2.4. Printing materials for FDM 3D printing

FDM is thermo-based techniques, thus the melting point (T_m), glass transition temperature (T_g), thermal-degradability and viscosity of melted material are significant criteria for selecting of suitable material for drug devices. T_m and T_g are significant for appropriate selection of extrusion temperature during the process. While viscosity of melted material depends on the temperature that generates the flow required to the material through the barrel. For FDM 3D printing techniques, the polymers are used as drug-loaded filament for providing controlled drug release. Several pharmaceutical materials have been investigated for FDM including polyvinyl alcohol, cellulose-based polymers, polylactic acid, polycarpolactone, polyvinylpyrrolidone, poly methyl methacrylate (Eudragit®), Soluplus®, and Kollicoat®, etc. [40, 41].

PVA is the most wildly used commercial polymer in 3D printed drug delivery systems. Because it is biocompatibility, biodegradability, good water solubility. It exhibits a relatively low glass transition temperature (~45 °C) that confers flexibility during filament handling, hile its melting point of PVA ranges from 180 ºC to 228 ºC depending on the degree of hydrolysis of acetate groups [41] and inherently high melt viscosity dictate the extrusion and printing temperature window—typically 180–210 °C—and often require plasticizers (e.g., sorbitol) to improve flow and filament

toughness [42]. However, its hygroscopic nature necessitates careful dry storage to maintain print quality, and the relatively high processing temperatures can restrict its use with heat-sensitive additives or APIs in pharmaceutical printing.

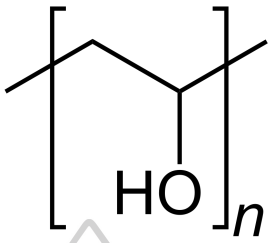

Figure 6. The chemical structure of polyvinyl alcohol.

Kollidon® VA 64 (KVA64), a copovidone copolymer of vinylpyrrolidone and vinyl acetate, is an ideal excipient for FDM in pharmaceutical 3D printing due to its balanced thermal and mechanical properties. With a glass transition temperature around 101 °C, it can be processed at relatively low temperatures (70–210 °C), minimizing the risk of drug degradation while accommodating moderately thermolabile APIs [43]. Its water solubility and hydrophilicity facilitate rapid tablet disintegration and the formation of stable amorphous solid dispersions, ensuring both high drug loading and uniform API distribution. Moreover, KVA 64 exhibits excellent miscibility with a wide range of small-molecule drugs—miscibility that can be further enhanced by acidic additives or plasticizers—resulting in consistent dissolution profiles for immediate-release formulations. Although neat KVA 64 filaments tend to be brittle and may challenge filament flexibility, blending with ductile polymers (such as Affinisol® or Kollicoat® IR) or incorporating low-molecular-weight plasticizers like PEG significantly improves toughness, lowers melt viscosity, and enhances printability [44]. Consequently, when appropriately formulated, KVA64 enables the reliable production of personalized dosage forms with rapid release characteristics and robust mechanical performance throughout the extrusion and printing processes.

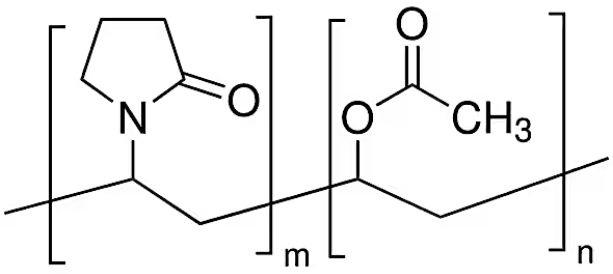

Figure 7. The chemical structure of Kollidon® VA 64.

PLA is increasingly favored for pharmaceutical FDM 3D printing because it couples biocompatibility with processability, enabling the fabrication of drug-delivery constructs and biomedical scaffolds that meet stringent safety requirements. With a glass transition temperature of roughly 60–71 °C and a melting range of 150–170 °C, PLA can be extruded at temperatures low enough to protect many heat-sensitive drugs from thermal degradation, while still providing sufficient flow for precise layer deposition [45]. Its FDM-induced micro- to sub-micron-scale surface roughness, together with design-controlled porosity (typically 24–76 %), promotes both drug loading and tissue ingrowth, making printed objects highly adaptable as controlled-release matrices or regenerative scaffolds [46]. Although neat PLA is somewhat brittle, its mechanical strength, degradation rate, and bioactivity can be tuned by blending with additives such as hydroxyapatite or graphene oxide, yielding constructs appropriate for load-bearing bone applications and targeted release kinetics [46, 47]. Careful attention to material quality and surface chemistry remains essential, as FDM processing can introduce surface oxidation or redistribute additives within pores, potentially altering drug stability and cell interactions [45, 47]. Overall, PLA's inherent biocompatibility, moderate thermal window, and easily adjustable structure render it a prime candidate for customized pharmaceutical devices, provided that formulation and printing parameters are optimized to balance mechanical demands, degradation behavior, and therapeutic performance.

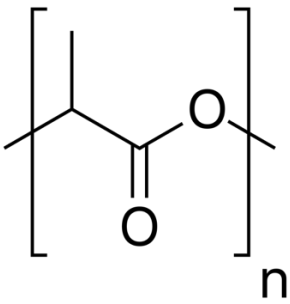

Figure 8. The chemical structure of polylactic acid.

2.5. Working process parameters of FDM-3D printing technique

Practical consideration with FDM comprises printing material, especially physical and mechanical properties of a 3D object are important criteria in material selection, for example, thermal property and rheology of materials. Drug loading into the filament process is one of the crucial steps for consideration with the fabrication of drug delivery devices. The APIs should be incorporated into filament before printing. Impregnation and hot-melt extrusion are two techniques used in this procedure. The printing process parameters are essential for evaluating the properties of a product. For example, infill density, infill pattern, extrusion speed, height of layers, and nozzle temperature, etc. [40, 48, 49].

2.5.1. Drug loading filament process using hot melt extrusion method

HME is a general method of filament preparation for FDM-3D printing technique. In this method, the active substances and polymer are loaded through the hopper and then mixed in the screw before it extruded from the nozzle as a filament with the diameter suitable for FDM 3D printing machine [50]. This process is shown in Figure 9. The extrusion equipment is composed of a feeding hopper, barrels, screws and a die. The process parameters of the filament extrusion are screw configuration, screw speed, feed rate, barrel temperature, and tractor speed.

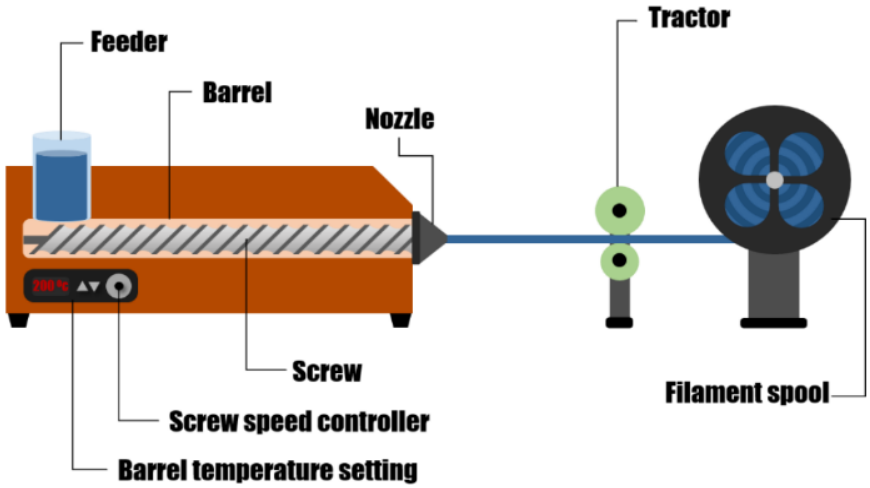

Figure 9. General schematic of the filament hot-melt extrusion process

2.5.2. Mechanical characterization of filament

The mechanical characteristics of the filaments which are suitable for FDM 3D printing should be considered. HME filaments should be able to endure the mechanical stress experienced during loading and printing. Filaments with weak mechanical characteristics have a higher chance of breaking and clogging the nozzle. The determination of the stiffness of the filaments is conducted in a tensile test [48, 51] The tensile test is a destructive test process that provides information about the tensile strength, yield strength, and ductility of the material. It measures the force required to break a composite or plastic specimen and the extent to which the filament stretches or elongates to that breaking point [52]. Table 3. displays the characterization techniques that may be used to assist researchers in designing formulas and determining the appropriateness of filaments for FDM 3D printing.

Table 3. Characterization methods for determining the suitability of filaments for FDM 3D printing.

Characterization method	Parameters studied	Processing window	Reference
Three-point bend test	Brittleness	Breaking stress > 2,941 g/mm^2, breaking distance > 1 mm	[54]
Repka-Zhang test	Brittleness/stiffness	Stiffness > 20,758 g/mm^2	[55]
Stiffness test	Toughness	Toughness > 80 g/mm^2	[56]
Hooke's law	Constant ''k"	''K" value > 40 g/mm^2	[57]
FDM feedability testing	Flexibility	Correlation score > 0.5	[58]
Dynamic mechanical analysis	Brittleness	Brittleness > 0.0002%Pa	[38]
Tensile test and three-point bend test	Young's modulus and distance at break	Young's modulus > 300 N/mm^2; distance at break > 1.125 mm	[48]

2.5.3. 3D printing process parameter

One of the challenges of 3D printing is to explore the adequate printing parameters with respect to the material that is being used and design one intends to print. This part will discuss optimal parameters to take into account to obtain a successful print.

The temperature from the heating coil in the head of the printer or printing nozzle will be changed to melt the filament. The bed platform where the material is deposited and requires an appropriate temperature to aid the first layer of the material into the bed platform. If the temperature in the system is inappropriate for the bed platform, it might lead to warping, distortions, or failure to print the object [59].

The flow of filament into the printer refers to the percentage of material or filament that is deposited in the bed platform. This parameter depends on the filament diameter. In general, the diameter size of the filament used is $1.75 - 3.00$ mm. If the

filament is smaller, the flow can be increased in order to prevent any voids or air gaps in the printed objects. While the filament is too large, clogging can occur [60].

The layer thickness is the thickness of the layer that is deposited by the nozzle of the printer (Figure 10). This parameter depends on the size of the nozzle tip. The diameter size of nozzle tip most commonly is used 0.4 mm - 0.8 mm [61].

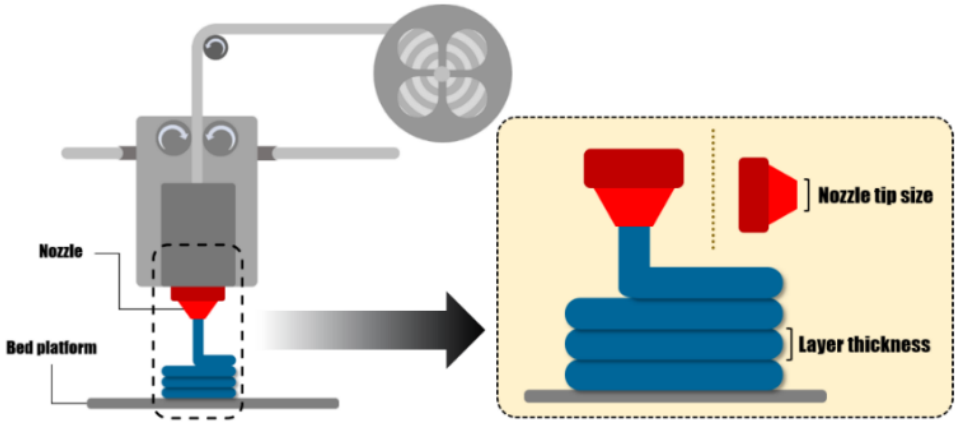

Figure 10. Layer thickness

The printing speed can prevent printing defects such as delamination or a deposition. The causes of the defects are the speed is too fast and the counter perimeter or oven the infill is not able to stick into the previous printed layer leading to cause the gaps between layers. Thus, printing speed can help to fabricate an object at an efficient time [60].

Infill pattern is the pattern of the material that is internally located in the object. The different infill patterns that can use for printing are illustrated in Figure 11. For infill density, it is the printing volume of the object. It varies from 25% – 100%. These parameters impact on dissolution behavior of API because of the porosity of the internal structure of the object [62]. For instance, Goyanes et al. fabricated individual tablets by changing infill percentage in the printer software (Figure 12) [63]. The results showed release profiles depended on the infill percentage used to print the tablet. When tablets containing different infill percentages were printed, it was found that tablets containing less infill exhibited a faster drug release. Conversely, tablets with higher infill percentages showed extended-release profiles.

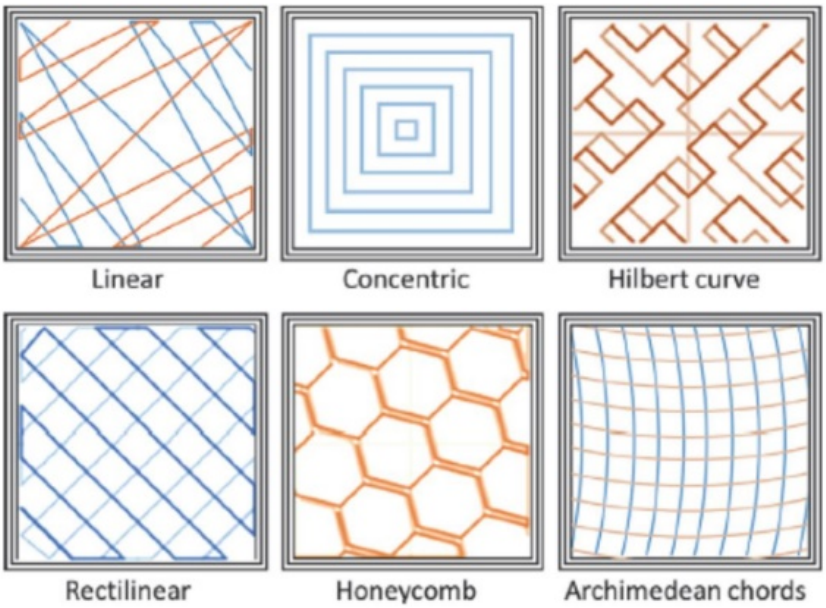

Figure 11. Different infill patterns used for 3D printing.

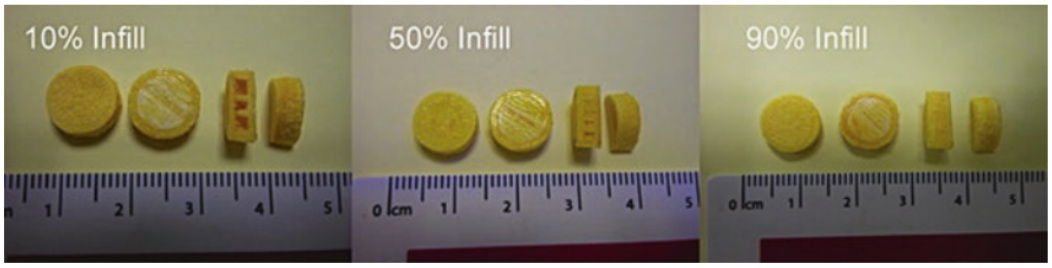

Figure 12. Images of tablet which have different percentage infill (from left to right): top, base, internal and lateral views.

2.6. Physicochemical and therapeutic dosage of the model drugs

2.6.1. Felodipine

FDP is a calcium channel blockers type of antihypertensive agents. It is used to treat high blood pressure. The dosage of treatment of FDP is initial 2.5-10 mg daily and maximum 20 mg/day [64]. According to the biopharmaceuticals classification system (BCS), it is a class II drug. The melting point of this drug is 144-145 ºC and the

degradation temperature is 190.62 ºC . The solubility of FDP is 19.7 mg/L in water, 20 mg/ml in ethanol and 30 mg/ml in dimethyl sulfoxide (DMSO) [65].

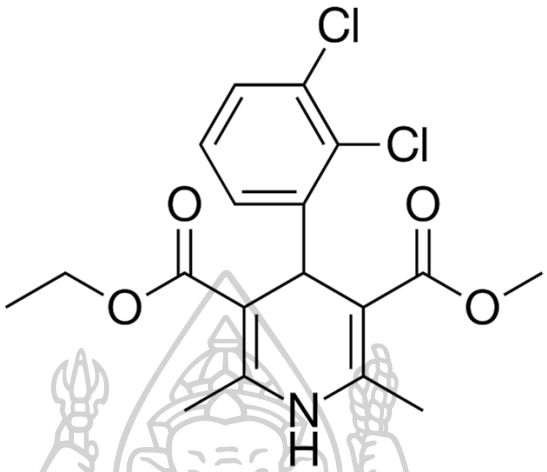

Figure 13. The chemical structure of felodipine.

2.6.2. Glipizide

GPZ is an oral antidiabetic drug, which takes an initial dosage 5 mg twice daily before each meal, is used for the treatment of type 2 diabetes mellitus and maximum 20 mg/day [64]. GPZ is an BCS Class II drug. For physicochemical of GPZ, it is a crystalline white or almost white powder and a melting point of 208-209 ºC. GPZ has been reported as a drug practically insoluble in water, and slightly soluble in ethanol [66].

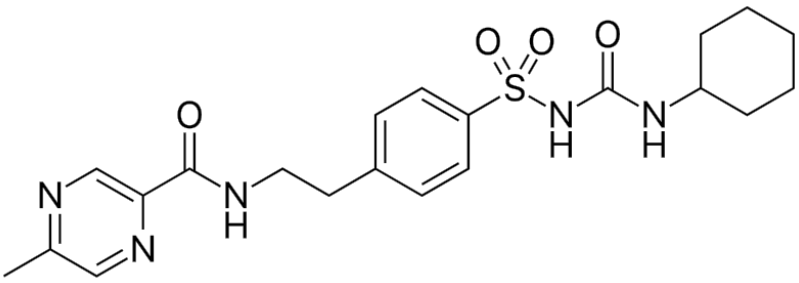

Figure 14. The chemical structure of glipizide.

CHAPTER 3
CONTROLLED RELEASE OF FELODIPINE FROM 3D-PRINTED TABLETS WITH CONSTANT SURFACE AREA: INFLUENCE OF SURFACE GEOMETRY

3.1. Introduction

3D printing technology involves creating three-dimensional objects or materials by adding layers based on digital designs. This technology has garnered significant interest across various sectors, including architecture, automotive, engineering, biomedical, and pharmaceuticals. Notably, the FDA approved the first 3D-printed pharmaceutical dosage form, the Spritam™ tablet for seizure treatment, in August 2015 [67]. Since then, the number of 3D-printed drug products has been increasing. The advantages of 3D printing in pharmaceuticals include improved controlled drug release, reduced risk of adverse effects, the ability to design high drug loadings, and the production of personalized dosage forms.

The ASTM classifies 3D printing technologies into seven categories: binder jetting, direct energy deposition, material extrusion, material jetting, powder bed fusion, sheet lamination, and vat photopolymerization [68]. Among these, material extrusion is particularly popular for creating solid objects and is frequently used in the pharmaceutical industry to manufacture dosage forms due to its flexibility. FDM is a notable example of material extrusion-based 3D printing. In FDM, solid materials are heated and melted during the printing process to form the desired objects. This method constructs objects layer by layer from the bottom up using thermoplastic filaments [69]. Additionally, FDM does not require post-processing steps after printing. Therefore, the polymers used in this process must melt at the printing temperature. Thermoplastic polymers are commonly employed in FDM because they can withstand the high temperatures involved in production. For example, acrylonitrile butadiene styrene (ABS) is used for creating matrix models, while PLA and PVA are used for producing tablets [70]. These polymers are preferred for FDM printing due to their suitable physical properties, which are crucial in selecting materials for 3D printing.

Currently, producing traditional pharmaceutical dosage forms, particularly tablets, involves several processes that need modification to achieve the desired properties. Recently, the tablet fabrication process has been refined by altering various physical barrier patterns, such as coatings on membranes and release matrices, both inside and outside the tablets. However, this process has limitations, including being time-consuming and requiring multiple modification steps. Additionally, changing the shape and size of tablets may necessitate new equipment or modifications to manufacturing

facilities. To address these issues, three-dimensional printing technology has been developed for producing pharmaceutical products.

As previously mentioned, 3D printing technology is a promising option for fabricating pharmaceutical dosage forms, particularly tablets. Tablets produced using FDM have been developed into various types, including immediate, sustained, and time-released tablets. These 3D-printed tablets can be easily customized to achieve different drug release patterns by selecting suitable polymers, modifying geometric designs, and compartmentalizing the matrices within the formulated products. Although several methods exist to control drug release, only a few studies have focused on geometric design modifications [71]. Therefore, this study aimed to produce an FDM filament containing a model drug in a water-soluble polymer (such as PVA) and to create 3D-printed tablets with different inner surface geometries and a constant surface area by printing PLA for the outer compartment. The study also investigated the relationship between the inner compartment's surface geometric patterns and the dissolution behavior of the drug-loaded 3D-printed tablets.

3.2. Materials and methods

3.2.1. Materials

FDP, an antihypertensive agent used as the model drug (BCS Class II, characterized by low solubility and high permeability, with a molecular weight of 384.26 g/mol, was sourced from Xilin Pharmaceutical Raw Material Co., Ltd. (Jiangsu, China). PVA powder (Parteck® MXP), designed specifically for hot-melt extrusion applications to enhance solubility, was provided by Merck (Darmstadt, Germany). Parteck® MXP is a semi-crystalline polymer with a molecular weight of 32,000 g/mol, a glass transition temperature of 40–45 °C, a melting temperature of 170 °C, a decomposition temperature above 250 °C, and a melt viscosity of 345.3 ± 7.8 mPa.s at D = 200 s^{-1} [72, 73]. PLA filament with a diameter of 1.75 mm was obtained from Zhejiang Flashforge 3D Technology Co., Ltd. (Zhejiang, China). Polysorbate 80 (Tween® 80) was purchased from PanReac AppliChem (Barcelona, Spain).

3.2.2. Preparation of FDP-loaded filaments

The FDP-loaded PVA filament, containing 5% w/w FDP and 95% w/w PVA, was produced using a single-screw extruder (model Wellzoom™ C desktop extruder, Shenzhen Mistar Technology Co., Ltd., Shenzhen, China) with a nozzle diameter of 1.75 mm at a temperature of 185 °C. The screw speed of the extruder was set to 12 rpm. Before printing, the filament was stored in a desiccator at room temperature.

3.2.3. Design and fabrication of FDP-loaded 3D-printed tablets

The controlled release of FDP-loaded 3D-printed tablets with two compartments was designed using Fusion 360 software (Autodesk Inc., San Rafael, CA, USA). The tablet models are depicted in Figure 15. Various geometries for the inner compartment, including round, square, hexagon, and triangle, were created. The volume of the inner compartment was kept constant (Table 4). According to our preliminary studies (data not shown), the inner tablet volume required to achieve the desired FDP dose (5 mg/tablet) was 79.97 mm^3. The outer compartment of all tablets was made using PLA.

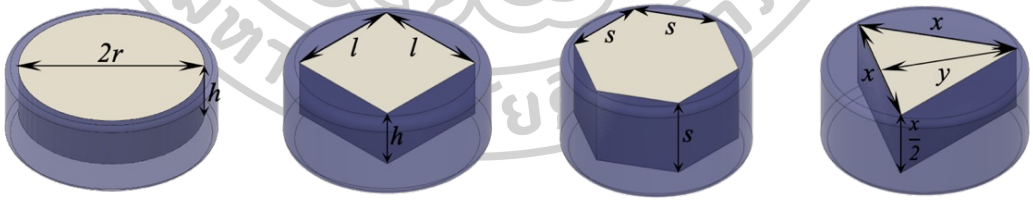

Figure 15. Design of FDP-loaded 3D-printed tablets with different internal surface geometries (left to right; round, square, hexagon, and triangle).

Table 4. Physical parameters for FDP-loaded 3D-printed tablets with an inner compartment volume constant.

Surface Geometry of Inner Tablet	Volume Equation	Inner Tablet Dimensions (mm)	Inner Tablet Volume (mm^3)	Surface Area (mm^2)
Round	$v = \pi r^2 h$	$r = 3.50$, $h = 2.00$	79.97	38.48
Square	$v = l^2 h$, $h = \frac{l}{2}$	$l = 5.36$, $h = 2.38$	79.97	28.72
Hexagon	$v = \frac{3\sqrt{3}}{2} s^3$	$s = 3.09$	79.97	24.88
Triangle (TX)	$v = \frac{x^2 y}{4}$, $y = \frac{x\sqrt{3}}{2}$	$x = 7.08$, $y = 6.13$	79.97	21.73
Triangle (T2X)	$v = \frac{x^2 y}{4}$, $y = \frac{x\sqrt{3}}{2}$	$x = 8.93$, $y = 7.73$	159.94	34.49

Note: v represents the volume of inner compartment tablet, r, h, l, s, x, and y represent the dimensions of inner compartment tablet as shown in Figure 3.1.

For the 3D-printing process, the model tablets were converted to gcode files using FlashPrint software version 3.28.0 (Zhejiang Flashforge 3D Technology Co., Ltd., Zhejiang, China). The tablets were printed on the Flashforge Creator Pro (Zhejiang Flashforge 3D Technology Co., Ltd., Zhejiang, China) using two printing nozzles. The outer compartment, made from commercial PLA filament, was printed with the right nozzle at 200 °C. For the inner compartment, the FDP-loaded PVA filament was extruded through the left nozzle at 195 °C. Other printing settings included a bed temperature of 60 °C, a printing speed of 50 mm/s, a moving speed of 70 mm/s, a 100% infill density with a line pattern, and a layer thickness of 0.12 mm.

3.2.4. Characterization of FDP-loaded 3D-printed tablets

3.2.4.1. Morphological characteristics of tablets

The morphological characteristics of the FDP-loaded 3D-printed tablets were examined using a SEM (model Mira 3, Tescan, Brno, Czech Republic). Dried samples, including whole tablets and cross-sectioned tablets cut with a cutter, were mounted on SEM stubs and coated with a gold layer. These samples were then

analyzed under the SEM. Images of the tablet surfaces and cross-sections were captured at a voltage of 5 kV with a working distance of approximately 30 mm. The morphology of the tablets was subsequently analyzed.

3.2.4.2. Differential scanning calorimetry (DSC)

The thermal properties of the materials, including FDP, PVA powder, physical mixtures of FDP and PVA, and FDP-loaded PVA filaments, were examined using a DSC 8000 (PerkinElmer, Waltham, MA, USA). Samples weighing between three to five milligrams were placed in solid aluminum pans, sealed, and heated from 20 to 250 °C at a rate of 10 °C/min. During the experiment, the nitrogen purge rate was maintained at 20 mL/min. The data were analyzed using Pyris software.

3.2.4.3. Thermogravimetric analysis (TGA)

TGA was employed to assess the thermal stability of the samples during filament extrusion and 3D-printing processes using a simultaneous thermal analyzer (model STA 6000, PerkinElmer, Waltham, MA, USA). For the analysis, samples weighing between 3 to 5 mg were placed in open ceramic pans and heated from 35 to 600 °C at a rate of 10 °C/min under a nitrogen purge with a flow rate of 20 mL/min.

3.2.4.4. Powder X-ray diffractometry (PXRD)

The crystalline or amorphous nature of all samples was examined using a PXRD (model MiniFlex II, Rigaku, Tokyo, Japan). The scanning conditions included a voltage of 30 kV and a current of 15 mA, with an angle range from 5° to 45°. The scanning speed was set at 4°/min, utilizing Cu-Kα radiation (0.154 nm).

3.2.4.5. Synchrotron radiation X-ray tomographic microscopy (SRXTM)

The porosity and pore surface area of the inner compartment of FDP-loaded 3D-printed tablets were examined using the Synchrotron XTM beamline (BL1.2 W: X-ray imaging and tomographic microscopy) at the Synchrotron Light Research Institute in Nakhon Ratchasima, Thailand. During the experiment, the inner

compartment of the tablets could not remain stable under direct synchrotron radiation. Therefore, SRXTM imaging was conducted using a polychromatic X-ray beam with a mean energy of 11.5 keV. The specimens were mounted on the sample stage after being attached to the sample carrier. X-ray tomography 3D imaging was then performed by rotating the 3D-printed tablet around an axis from 0 to 180° with an angular increment of 0.4°/s. For each sample, a total of 500 projection images were collected and processed through correction, stitching, and reconstruction using Octopus reconstruction software (Tescan, Gent, Belgium). The processed images were analyzed for porosity using Octopus analysis software (Tescan, Gent, Belgium), and the resulting 3D images were rendered using Drishti software (National Computational Infrastructure, Canberra, Australia).

3.2.5. Drug content of FDP-loaded filaments and 3D-printed tablets

The drug content of the FDP-loaded PVA filament and FDP-loaded 3D-printed tablets was assessed using high-performance liquid chromatography (HPLC) (model Agilent 1100 series HPLC system, Agilent Technologies, CA, USA). To ensure uniformity, three different segments of the filament were collected for drug content analysis. Additionally, 100 mg of each 3D-printed tablet was weighed and dissolved in 25 mL of 1% w/v polysorbate 80. The sample solutions were filtered through a 0.45-μm filter and then 20 μL was injected into a 150 × 4.6 mm Luna 5u C18 column (Phenomenex, Cheshire, UK). The mobile phase, consisting of acetonitrile, methanol, and phosphate buffer (40:20:40), was pumped at a flow rate of 1 mL/min at a controlled temperature of 35°C. The phosphate-buffered solution was prepared by dissolving 6.9 g of monobasic sodium phosphate in water, adding 8 mL of 1 M phosphoric acid, and diluting with water to a final volume of 100 mL. Absorbance was measured at a wavelength of 254 nm. All samples were analyzed in triplicate.

3.2.6. *In Vitro* drug release of 3D-printed tablets

The method for analyzing the in vitro drug release of the FDP-loaded 3D-printed tablet was adapted from the United States Pharmacopeia (USP 43-NF 38) protocol for felodipine extended-release tablets. In this procedure, 750 mL of 1% w/v

polysorbate 80 was added to the vessels of a USP dissolution apparatus II (model AT Xtend™, Sotax, Westborough, MA, USA). The FDP-loaded 3D-printed tablet was submerged in the medium within the vessel, and the tests were conducted at a paddle speed of 100 rpm with a controlled temperature of 37 ± 0.5°C. Samples of 3 mL were withdrawn at various time intervals (45 min, 1, 2, 4, 6, 8, 10, 12, 14, 16, 18, 20, 22, and 24 hours). To maintain sink conditions, 3 mL of fresh medium solution was added after each sample withdrawal. Drug concentrations were determined using HPLC, as described in Section 3.2.5.

3.2.7. Mathematical description of drug release

3.2.7.1. Drug release kinetics modeling

Six different kinetic models were considered to fit the observed data to determine the release behavior from the 3D-printed tablets. Model 1 is provided by the zero-order equation (Equation (1)).

$$C_t = C_0 - k_0 t \quad (1)$$

where C_t is the amount of drug released at time t, C_0 is the initial drug concentration, and k_0 is the zero-order rate constant. In zero-order kinetics, the drug release rate is constant over time, independent of the drug concentration.

Model 2 describes first-order kinetics, where the drug release rate is proportional to the drug concentration. The first-order equation (Equation (2)). is:

$$\log C_t = \log C_0 - \left(\frac{k_t}{2.303}\right) \quad (2)$$

where C_t is the amount of drug released at time t, C_0 is the initial drug concentration, and k_t is the is the first-order constant.

Model 3 is the Higuchi model. This model is often used to explain drug release from the inert matrix system. Equation (3) is illustrated the equation of the Higuchi model.

$$\frac{C_t}{C_\infty} = k_H t^{1/2} \quad (3)$$

where C_t and C_∞ are the drug release amounts at time t and infinite time, respectively, and k_H is the release constant of Higuchi.

Model 4 is based on the Korsmeyer–Peppas model. The model is utilized to describe the drug release from the polymer matrix. Equation (4) is employed the Korsmeyer–Peppas kinetics equation.

$$log(\frac{C_t}{C_\infty}) = log\ k + n\ log\ t \quad (4)$$

where C_t and C_∞ are the cumulative drug release at time t and infinite time, respectively. k is a constant depending on the structure and geometrical characteristic of the system, and n is the exponent indicating the drug release mechanism. For designed FDP-loaded 3D-printed tablets, only one side of the tablet contacted the medium. Therefore, they might have a planar geometry system, and when n = 0.5, the drug release mechanism is the Fickian diffusion. An anomalous transport mechanism is observed when n is between 0.50 and 1.0. When n = 1.0, the drug release mechanism is Case II transport. Finally, if the value of n is more than 1, the drug release is the Super Case II model.

Model 5, the Hopfenberg model, Equation (5) creates a mathematical Hopfenberg model to predict drug release from surface-eroding polymers, providing a surface area that remains consistent during the degradation process [74].

$$\frac{C_t}{C_\infty} = 1 - (1 - (\frac{k_{HB}t}{C_0 a_0}))^n \quad (5)$$

where C_t and C_∞ are the drug release amounts at time t and infinite time, respectively, C_0 is the initial drug release concentration, k_{HB} is the erosion constant, a_0 is the half thickness of the film or the radius of a sphere or cylinder, and n is an exponent that changes with geometry, with n = 1, 2, and 3 for slab (flat), cylindrical, and spherical geometry, respectively [75].

Model 6 represents the Peppas–Sahlin model. This model is expressed to simultaneously describe two contribution mechanisms from the polymeric matrix (diffusional and relaxational). The Peppas–Sahlin kinetics equation is shown in Equation (6).

$$\frac{C_t}{C_\infty} = k_1 t^m + k_2 t^{2m} \quad (6)$$

where C_t and C_∞ are the drug release amounts at time t and infinite time, respectively, k_1 is the diffusion rate constant, k_2 is the relaxation rate constant, and m is the diffusion exponent.

All the above mathematical models are only valid in the 5 to 60% range of drug release from in vitro drug release. The experimental data for mathematical models of drug release were analyzed using the DDSolver program with Microsoft Excel software [76]. The correlation coefficient (R^2) values and Akaike information criterion (AIC) were used to determine the best-fit model for drug release, with statistically higher R^2 and lower AIC.

3.2.7.2. Comparison of drug release profiles

The two dissolution profiles were compared using similarity factors (f_2). The f_2 value is described by an equation derived from the logarithmic reciprocal square root transformation of the sum of squared errors. This measurement was expressed as the percent (%) similarity of dissolution between the two curves, calculated by Equation (7):

$$f_2 = 50 \cdot log\left\{\left[1 + \left(\frac{1}{n}\right)\sum_{t=1}^{n}|R_t - T_t|^2\right]^{-0.5} x\ 100\right\} \quad (7)$$

where R_t and T_t are drug release percentages at time points of reference and test sample, respectively, and n is the number of time points. The f_2 was calculated using the DDSolver software. The f_2 value is between 50 and 100, implying the similarity of the two release profiles. The similarity factors were computed in accordance with the best-fit model obtained from drug release kinetic analysis.

3.2.8. Stability studies

FDP 3D-printed tablets with a triangular surface geometry (TX, T2X (5% FDP), and T2X (10% FDP)) were stored in a desiccator chamber maintained at 40% relative humidity. The samples were kept at room temperature (around 28 °C) for 12 months. After this period, the drug content of the FDP 3D-printed tablets was evaluated.

3.3. Results and Discussion

3.3.1. Preparation of FDP-loaded filaments

PVA, a water-soluble polymer, is frequently used in 3D printing due to its advantageous properties, such as thermoplastic behavior and biodegradability.

Consequently, it was chosen to produce the filaments for 3D printing. The extrusion process was conducted at 185 °C with an extrusion speed of 12 rpm. The results indicated that a smooth, uniform filament was successfully produced under these conditions, with no defects observed along the fabricated filament (Figure 16A).

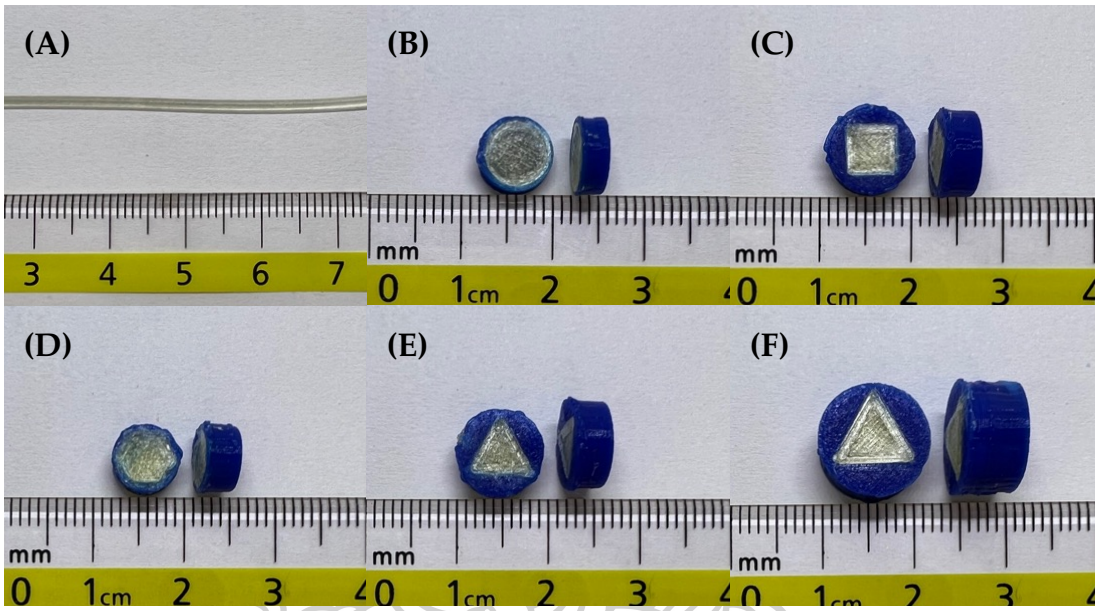

Figure 16. The photo images include (A) the FDP-loaded PVA filament, FDP-loaded 3D-printed tablets with various internal surface geometries: (B) round, (C) square, (D) hexagon, and (E) triangle, as well as (F) an FDP-loaded 3D-printed tablet with a triangular surface geometry and double the volume of the inner compartment.

3.3.2. Design and fabrication of FDP-loaded 3D-printed tablets

As shown in Table 3.1., variations in tablet geometry resulted in different surface areas, even though the inner tablet volume remained constant. This discrepancy arose because different geometric patterns required different formulas to achieve the same volume. For example, at a constant volume, the height (*h*) of the tablets varied between round and other geometric designs, leading to differences in calculated surface areas. It was observed that the round-shaped tablet had the largest inner compartment surface area, followed by the square, hexagon, and triangle shapes, respectively. These findings indicate that, despite having the same volume, the total surface area of each tablet differed, which would likely affect the drug release. The subsequent section

evaluates the drug release pattern to confirm this. The diameter and thickness of the FDP-loaded 3D-printed tablets are provided in Table 5.

Table 5. The diameter and thickness of the FDP-loaded 3D-printed tablets.

Surface Geometry of Inner Tablet	Diameter (mm)	Thickness (mm)
Round	8.23 ± 0.12	2.92 ± 0.01
Square	9.26 ± 0.15	3.92 ± 0.07
Hexagon	7.53 ± 0.16	3.81 ± 0.01
Triangle (TX)	9.12 ± 0.03	3.84 ± 0.05
Triangle (T2X)	11.53 ± 0.14	6.05 ± 0.10

3.3.3. Characterization of FDP-loaded filaments and 3D-printed tablets

3.3.3.1. The morphological characteristics of tablets

The photo images of FDP-loaded 3D-printed tablets are shown in Figure 16, demonstrating that all tablets were well-prepared without any defects. Figure 17. presents SEM images of the FDP-loaded 3D-printed tablets with different internal surface geometries. The top surfaces of the tablets were flat but relatively rough (Figure 17A-B), likely due to the high printing temperature and viscosity during both the extrusion and printing processes [55]. Figure 17C shows an inconsistent layer-by-layer printing pattern in the inner compartment of the 3D-printed tablets, resulting from a printing process defect. Various infill shapes may impact printing quality due to differences in the surface area being printed. Additionally, the outer compartments of all tablets were densely compacted, making them very difficult to cut. This could explain the layering issues observed in some FDP-loaded 3D-printed tablets when viewed under an SEM.

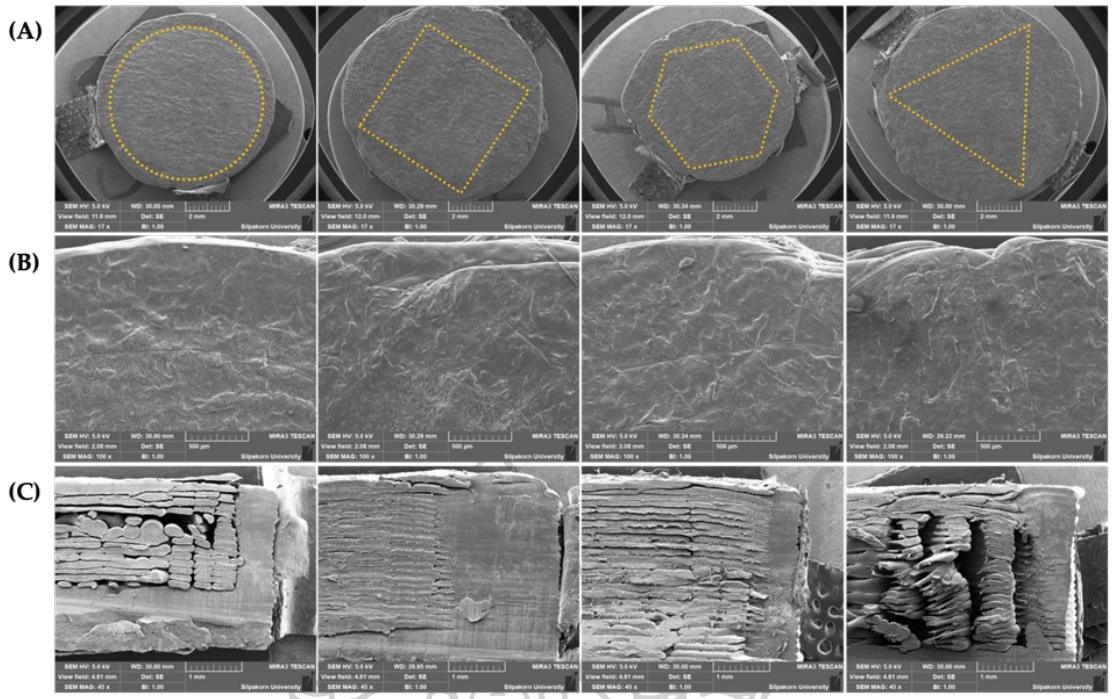

Figure 17. SEM images of FDP-loaded 3D-printed tablets with various internal surface geometries (from left to right: round, square, hexagon, and triangle), displaying **(A)** a top view of the entire tablet, **(B)** a close-up of the top surface, and **(C)** a cross-sectional view.

3.3.3.2. Differential scanning calorimetry

The DSC thermograms of PVA, FDP, physical mixtures of FDP and PVA, and FDP-loaded PVA filaments are shown in Figure 18A. The PVA powder exhibited glass transition endotherms at 57.3 °C and a broad endothermic peak around 193.3 °C, indicating its melting temperature. Additionally, due to its semi-crystalline nature, PVA did not display a sharp melting peak. FDP had a melting point of approximately 145.5 °C. In the physical mixture, the melting point remained similar to that of FDP. However, the thermogram of the FDP-loaded PVA filament did not show the FDP melting peak, suggesting that FDP was fully incorporated into the PVA matrix [77].

3.3.3.3. Thermogravimetric analysis

The TGA thermograms of PVA, FDP, physical mixtures of FDP and PVA, and FDP-loaded PVA filaments are illustrated in Figure 18B. The TGA curve for PVA showed a significant weight reduction at its degradation temperature of 293.6°C. FDP began to lose weight at around 261.4°C. Additionally, a slight weight loss was observed as the temperature increased, likely due to water evaporation, as reported in several studies [78-80]. These results indicate that both PVA and FDP are stable at the printing temperature of 195°C. The thermograms of PVA and the FDP-loaded PVA filament were nearly identical, suggesting that FDP was fully dispersed within the polymer matrix.

3.3.3.4. Powder X-ray Diffractometry

The PXRD patterns of PVA, FDP, physical mixtures of FDP and PVA, and FDP-loaded PVA filaments are shown in Figure 19. PVA exhibited a characteristic peak at 19.41°. In contrast, the crystalline drug FDP displayed several distinctive peaks with high intensities at 10.31°, 10.93°, 16.31°, 16.60°, 21.90°, 24.56°, 25.43°, 26.46°, and 27.19° [81, 82]. The diffractogram of the physical mixture showed a combination of the characteristic peaks of PVA and FDP, but with lower intensity. Notably, the crystalline peaks of FDP were completely absent in the FDP-loaded PVA filament, indicating a transition from a crystalline to an amorphous form. This result suggests that FDP was fully incorporated into the PVA matrix, which enhances the drug's dissolution rate and solubility. The PXRD findings are consistent with the DSC results, confirming the molecular dispersion of FDP within the PVA matrix.

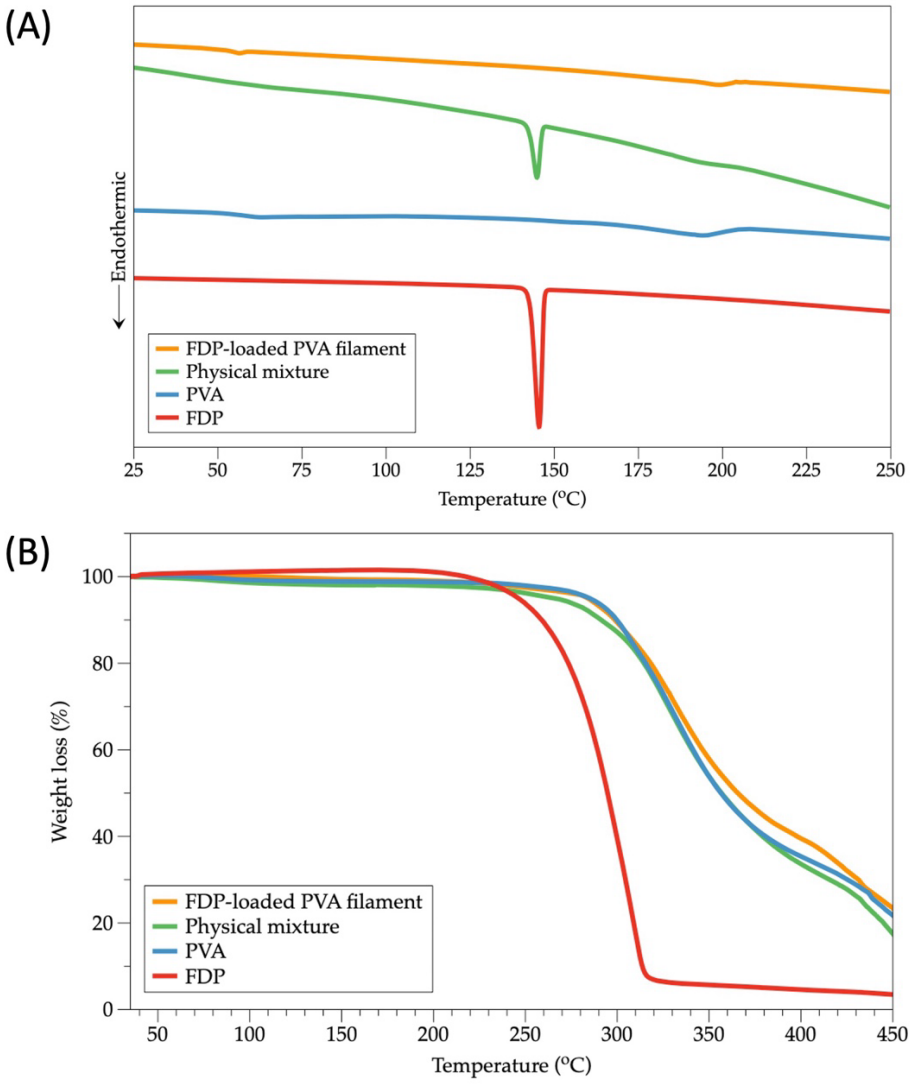

Figure 18. (A) DSC thermograms and **(B)** TGA thermograms of FDP, pure PVA, physical mixtures of FDP and PVA, and FDP-loaded PVA filaments.

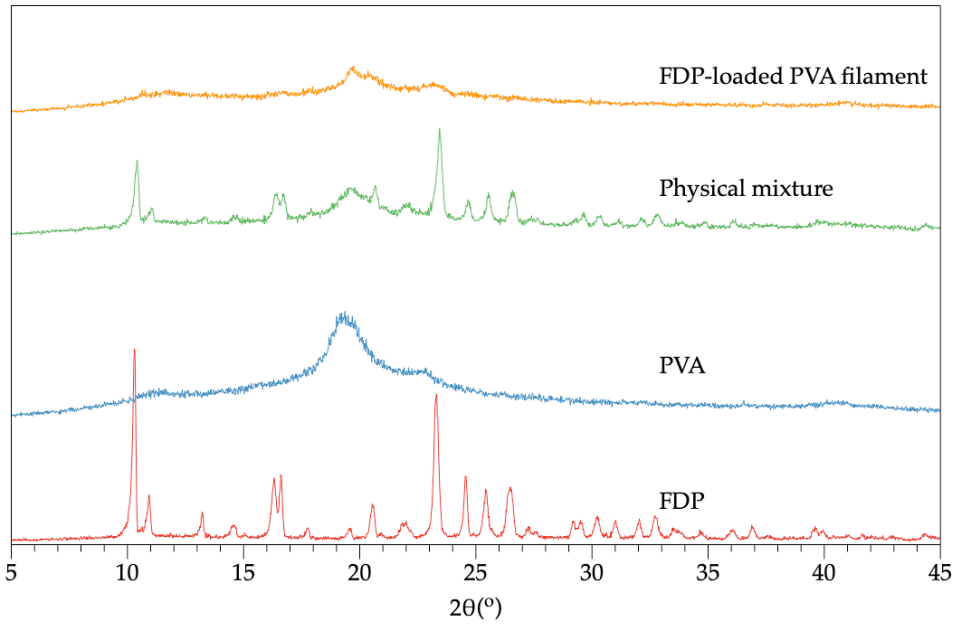

Figure 19. PXRD patterns of PVA, FDP, physical mixtures of FDP and PVA, and FDP-loaded PVA filaments.

3.3.3.5. Synchrotron radiation X-ray tomographic microscopy

The X-ray micro-computed tomography (XμCT) technique has proven to be an effective method for investigating the internal microstructure and porosity of 3D objects. This technique was used to conduct detailed studies on the morphology and internal structure of FDP-loaded 3D-printed tablets. The pore distribution within the inner compartment of these tablets was assessed and expressed as a percentage of porosity. As shown in Table 6., different geometric patterns resulted in varying porosity values. These differences in porosity may be due to the fact that all detected pore types were included in the XμCT analysis, including unexpected pores [83]. Additionally, pores can form during several stages of the FDM process. For instance, an uneven filament diameter can create pores during printing [84, 85]. When printing smaller objects, FDM 3D printing tools may not perform as effectively as they do with larger objects. According to SRXTM images, the % porosity of TX tablets was higher than that of T2X tablets because smaller tablets have a smaller surface area per layer, leading to a shorter cooling time before the next layer is printed [86]. This issue can affect the material's ability to partially solidify, and some extruded material may be

pulled during nozzle movement, resulting in more pores between layers in smaller tablets. In contrast, larger tablets have a larger surface area per layer, allowing more time for solidification before the next layer is printed, resulting in fewer gaps between layers. Figures 20 and 21. show that pore structures were present in all tablets. However, the porosity detected in the outer compartment was also converted to a porosity percentage, resulting in higher-than-expected porosity values.

Table 6. Porosity and pore surface area of inner compartments of FDP-loaded 3D-printed tablets using SRXTM.

Surface Geometry of Inner Tablet	Top Surface Area (mm^2) = TSA	Pore Surface Area (mm^2) = PSA	Total Surface Area (mm^2) (TSA + PSA) = TA	Inner Tablet Volume = V	TA/V Ratio	Porosity (%)
Round	38.48	5.31 ± 1.27	43.79 ± 1.27	79.97	0.55 ± 0.02	5.37 ± 2.89
Square	28.72	12.29 ± 1.03	41.01 ± 1.03	79.97	0.51 ± 0.01	30.78 ± 4.30
Hexagon	24.88	9.52 ± 0.16	34.40 ± 0.16	79.97	0.43 ± 0.01	22.12 ± 1.00
Triangle (TX)	21.73	11.01 ± 0.71	32.74 ± 0.71	79.97	0.41 ± 0.01	14.68 ± 2.89
Triangle (T2X)	34.49	7.68 ± 1.96	42.17 ± 1.96	159.94	0.26 ± 0.01	5.83 ± 1.48

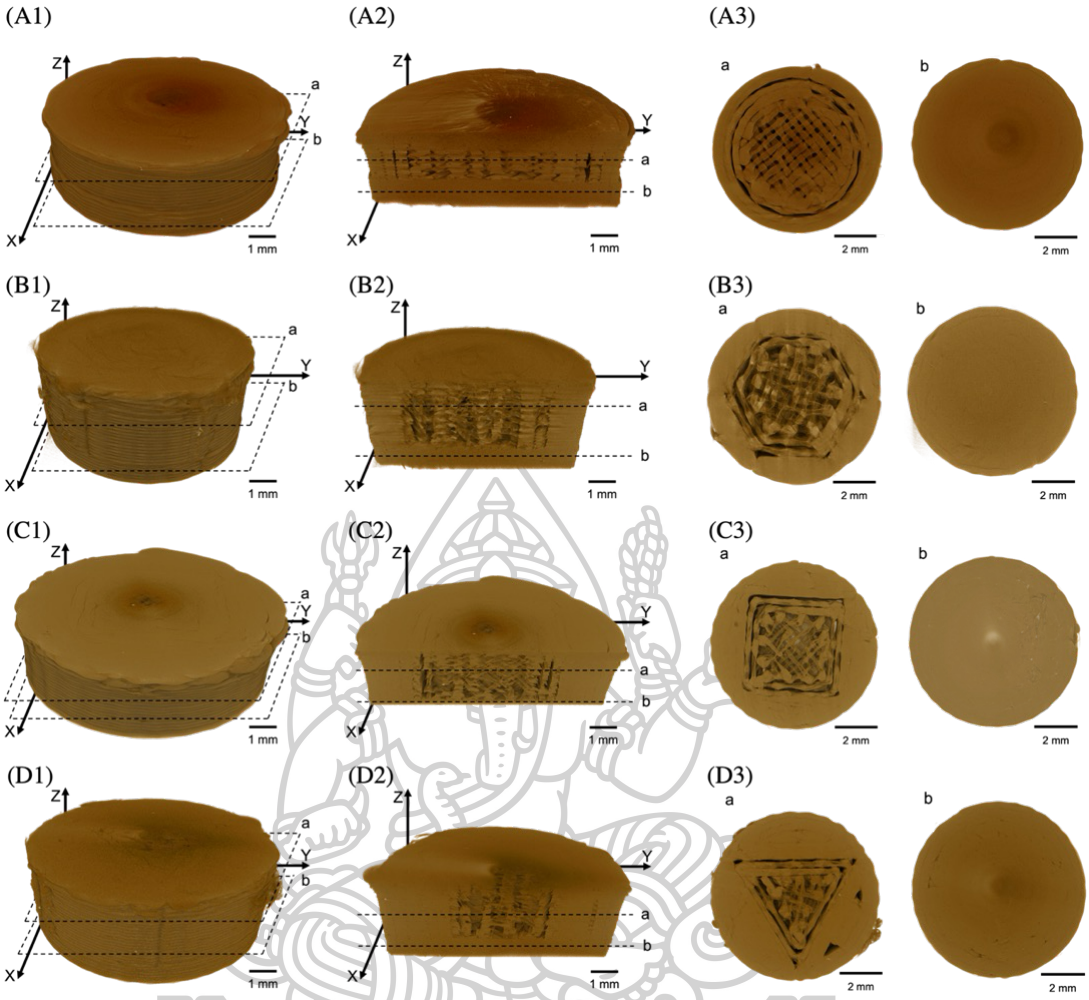

Figure 20. SRXTM images of FDP-loaded 3D-printed tablets with different inner surface geometries, showing **(A1,B1,C1,D1)** the entire tablet, **(A2,B2,C2,D2)** a vertical cross-section of the tablet, and **(A3,B3,C3,D3)** a horizontal cross-section of the tablet. The horizontal cross-section view images were created using the indicated positions (a and b).

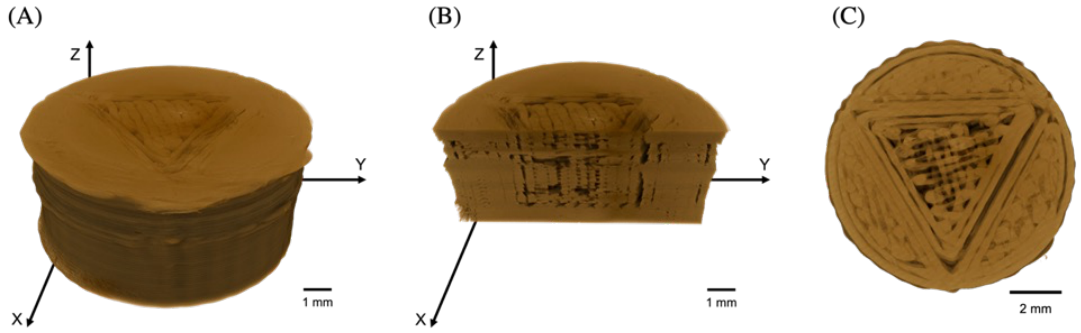

Figure 21. SRXTM images of FDP-loaded 3D-printed tablets with a triangle inner compartment (double the tablet volume, T2X), showing **(A)** the entire tablet, **(B)** a vertical cross-section, and **(C)** a horizontal cross-section of the tablet.

3.3.4. Drug content of FDP filament and 3D-printed tablets

The drug content is crucial for determining the properties of FDP-loaded 3D-printed tablets. The FDP content in the filament and the tablets with different surface geometries was quantitatively measured. The drug loading percentage in the filament was 98.11 ± 1.22%, while in the tablets with various geometries, it ranged from 94.68% to 98.36%. This suggests that no drug degradation occurred due to the high-temperature processes involved in both the HME and printing stages [87]. This finding is further supported by TGA results, which showed negligible changes in FDP weight at the printing temperature.

3.3.5. *In vitro* drug release of FDP-loaded 3D-printed tablets

Figure 22A shows the drug release percentage from 3D-printed tablets without an outer compartment. The drug release percentage was consistent across all geometric designs, with all tablets fully dissolving within 6 hours. In contrast, the presence of an outer compartment affected drug release (Figure 22B); tablets with round and square inner compartments released their drug content within 12 hours, indicating a slower release rate. The outer compartment likely influences drug release by limiting the penetration of the dissolution medium. After 24 hours, tablets with hexagonal and triangular inner compartments released approximately 80% of their drug

content. These findings align with the report by Kardy and colleagues [88]. The outer compartment reduced the drug release rate, likely by restricting the dissolution medium's access to the inner compartment, except from the top. This suggests that the outer compartment can be used to develop controlled-release tablets, while tablets without an outer compartment are better suited for immediate-release formulations.

Generally, increasing the drug concentration results in higher drug content and faster release [89]. To investigate this, we studied tablets of different volumes, TX and T2X (double the volume of TX), to examine the differences in drug release profiles. Figure 22C illustrates the impact of tablet volume and FDP concentration on drug release profiles.

The results indicated that increasing the tablet volume (from TX to T2X) significantly increased cumulative drug release for the same drug concentration (5% FDP). Additionally, comparing 10% FDP (T2X) with 5% FDP (T2X) showed nearly overlapping release profiles, suggesting that tablet volume significantly influences the drug release profile. The larger surface area of the tablets in contact with the dissolution medium, due to their higher volume, resulted in a significant increase in the dissolution rate.

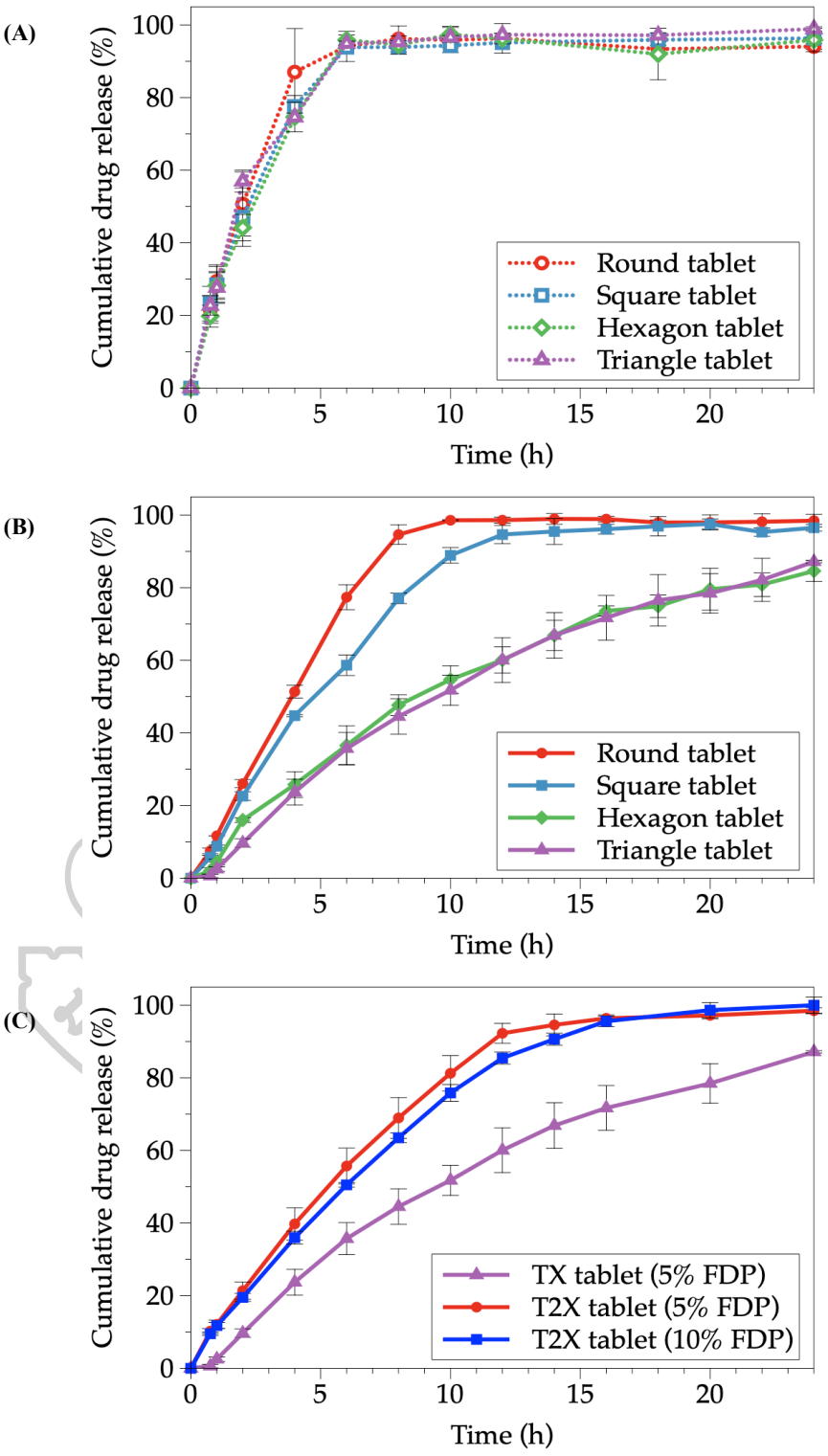

Figure 22. Cumulative drug release profiles of FDP-loaded 3D-printed tablets; (A) the tablets without an outer compartment, (B) the tablets with an outer compartment, (C) the tablets with triangle-shaped inner compartments having different inner compartment volumes or different drug concentrations.

Various mathematical models, including zero-order, first-order, Higuchi, Korsmeyer–Peppas, Peppas–Shalin, and Hopfenberg models, were employed to fit the experimental data and predict the release patterns and behaviors of the FDP-loaded 3D-printed tablets. The Higuchi model was deemed unsuitable for this purpose because the inner compartment, made of PVA polymer, was not an inert matrix, as indicated by the observed swelling [90]. The R^2 value from each model was used to compare the quality of the fits. The release profiles for all inner geometric designs followed the Peppas–Sahlin equation, with R^2 values ranging from 0.9977 to 0.9997, as shown in Table 7. This model demonstrated that the drug release mechanism involved both diffusion and relaxation. The k_2 values were higher than the k1 values, indicating that the relaxation release mechanism was more dominant than the diffusion mechanism for FDP-loaded 3D-printed tablets. Additionally, Table 7 shows that k_1 was highly negative in all formulations, suggesting that the Fickian diffusion mechanism played a minimal role in the drug release process. In other words, the diffusion processes in FDP-loaded 3D-printed tablets were almost negligible [91, 92].

Figure 23. shows the inner compartments with different surface geometries during the dissolution test. Upon exposure to the medium, the front surface of all 3D-printed tablets swelled, leading to the dissolution of the polymer matrix in the inner compartment. As noted in our previous reports [93], PVA, a water-soluble polymer produced through the HME process, swells when in contact with the dissolution medium and subsequently undergoes erosion [94].

Table 7. Release kinetics of FDP-loaded 3D-printed tablets with different surface areas.

Model	Surface Geometry of Inner Tablet	R^2	AIC	Parameters
Zero-order	Round	0.9982	11.0060	k_0 = 12.842
	Square	0.9894	24.6174	k_0 = 9.921
	Hexagon	0.9631	48.3447	k_0 = 5.247
	Triangle (TX)	0.9818	42.5807	k_0 = 5.097
	Triangle (T2X)	0.9800	26.4023	k_0 = 9.112
First-order	Round	0.9457	28.1522	k_1 = 0.189
	Square	0.9725	30.3707	k_1 = 0.151
	Hexagon	0.9937	32.4024	k_1 = 0.078
	Triangle (TX)	0.9864	39.3414	k_1 = 0.015
	Triangle (T2X)	0.9938	19.4127	k_1 = 0.135
Korsmeyer–Peppas	Round	0.9988	10.8932	K = 12.140, n = 1.036
	Square	0.9922	24.7875	K = 11.356, n = 0.926
	Hexagon	0.9866	41.2467	K = 8.475, n = 0.796
	Triangle (TX)	0.9953	31.8733	K = 1.894, n = 0.846
	Triangle (T2X)	0.9992	8.8577	K = 12.521, n = 0.825
Hopfenberg	Round	0.9985	12.2633	k_{HB} = 0.132
	Square	0.9943	22.8770	k_{HB} = 0.081
	Hexagon	0.9941	33.8798	k_{HB} = 0.008
	Triangle (TX)	0.9918	37.3964	k_{HB} = 0.030
	Triangle (T2X)	0.9986	12.5552	k_{HB} = 0.044
Peppas–Sahlin	Round	0.9997	5.8503	k_1 = −11.427, k_2 = 22.922, m = 0.414
	Square	0.9981	18.2374	k_1 = −35.371, k_2 = 44.718, m = 0.272
	Hexagon	0.9977	27.2436	k_1 = −42.867, k_2 = 47.858, m = 0.204
	Triangle (TX)	0.9993	17.7354	k_1 = −34.537, k_2 = 37.006, m = 0.242
	Triangle (T2X)	0.9993	10.1858	k_1 = −3.153, k_2 = 15.494, m = 0.384

Note: R^2 = correlation coefficient values, AIC = Akaike information criterion.

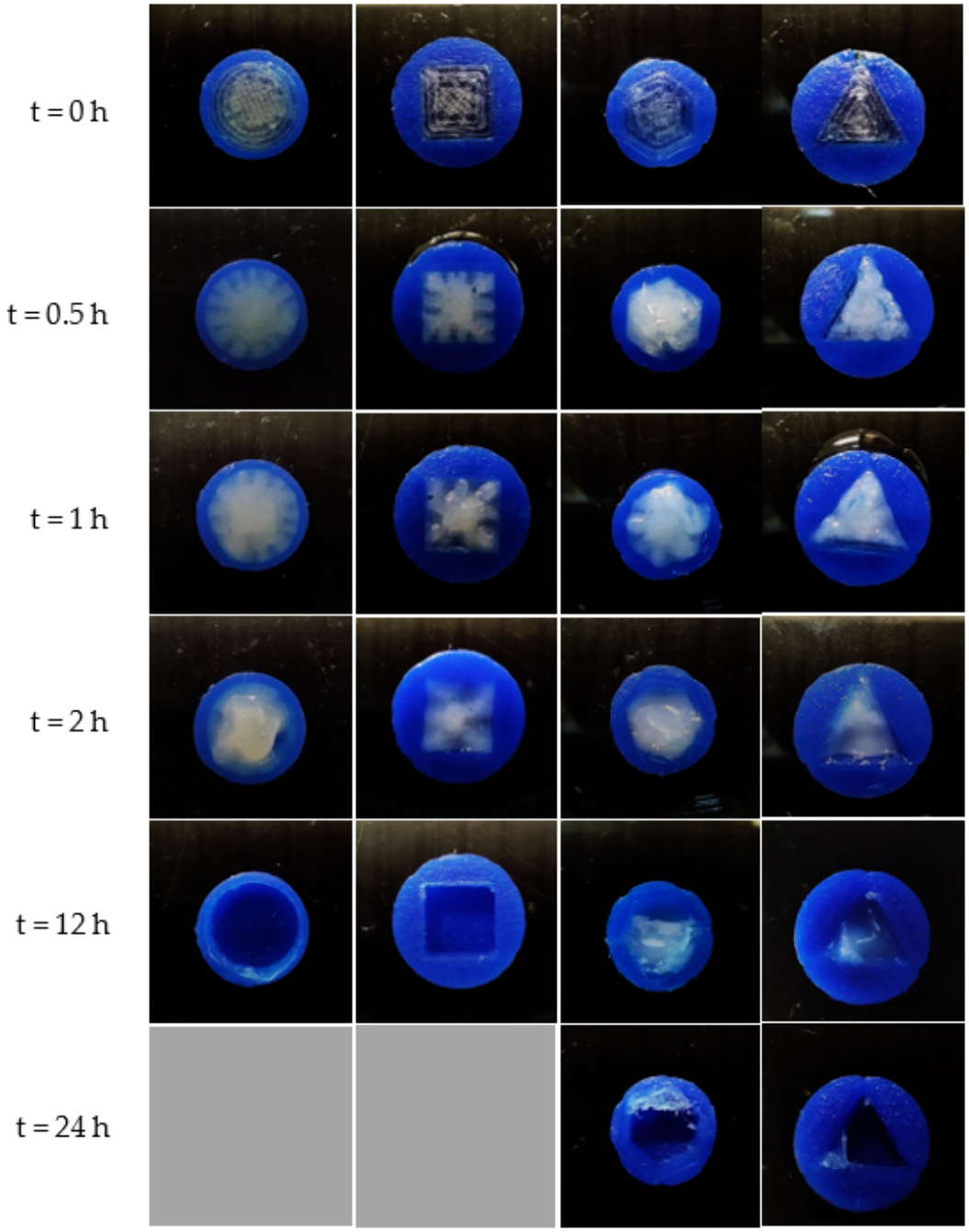

Figure 23. Top-view images of FDP-loaded 3D-printed tablets with round-, square-, hexagon-, and triangle-shaped inner compartments during the dissolution test.

3.3.6. Comparison of drug release profiles

The bootstrap f_2 tests for all FDP-loaded 3D-printed tablets were calculated to assess the similarity of release patterns among formulations with different geometric designs. The results are presented in Table 8. The findings showed that the f_2 values for comparisons between round and square shapes, and between hexagonal and triangular shapes, were above 50, specifically 51.82 and 76.51, respectively. This suggests that these geometric designs exhibited similar release profiles. In contrast, the f_2 values for other geometric design comparisons were significantly below 50, indicating dissimilar release profiles. These results highlight the importance of geometric design in determining drug release profiles, as the similarity in surface area-to-volume ratios was reflected in the f_2 values for round vs. square and hexagonal vs. triangular geometries [79, 95].

Table 8. Similarity factor (f_2) results for dissolution profile comparison of FDP-loaded 3D-printed tablets.

Comparison	Similarity Factors (f_2)	Interpretation
Round vs. square	51.82	Accept
Round vs. hexagon	32.48	Not accept
Round vs. triangle	30.89	Not accept
Square vs. hexagon	38.09	Not accept
Square vs. triangle	35.56	Not accept
Hexagon vs. triangle	76.51	Accept
Triangle (TX) vs. triangle (T2X)	39.47	Not accept

3.3.7. Stability studies

The stability of FDP-loaded 3D-printed tablets with a triangular surface geometry was assessed under long-term conditions (28 °C/40% RH) for 12 months. The FDP content in TX, T2X (5% FDP), and T2X (10% FDP) tablets was measured at 4.01 ± 0.13 mg, 4.25 ± 0.16 mg, and 8.25 ± 0.05 mg, respectively. These values were compared to the initial drug content immediately after printing, which was 4.23 ± 0.03

mg for TX, 4.53 ± 0.36 mg for T2X (5% FDP), and 8.59 ± 0.17 mg for T2X (10% FDP). As shown in Table 9., there was no significant difference in drug content before and after the stability studies ($p > 0.05$), as determined by a paired-samples t-test. This indicates that the FDP-loaded 3D-printed tablets remained stable during storage.

Table 9. Stability studies of 3D-printed tablets with triangle surface geometry.

Sample	Drug Content (mg)		Significance between Before and after Stability Tests (Paired-Samples *t* Test)
	0 Month	12 Months	
TX	4.23 ± 0.03	4.01 ± 0.13	No
T2X (5% FDP)	4.53 ± 0.36	4.25 ± 0.16	No
T2X (10% FDP)	8.59 ± 0.17	8.25 ± 0.05	No

3.4. Conclusions

The filaments produced through the hot-melt extrusion process were successfully prepared and utilized to create FDP-loaded 3D-printed tablets. The FDP was fully integrated into the PVA matrix, as confirmed by the measurement of physicochemical properties. The 3D printer was capable of producing FDP-loaded tablets in various shapes, including round, triangular, square, and hexagonal geometries. The drug release from these tablets was governed by swelling rather than the Fickian diffusion process. Additionally, the drug release patterns were primarily influenced by the surface-to-volume ratio, rather than the surface area alone. Tablets with similar surface-to-volume ratios exhibited similar dissolution patterns. Ultimately, fabricating 3D-printed tablets with different shapes and specific surface-to-volume ratios can potentially regulate or control drug release, aiding in the development of new dosage forms for specific applications.

CHAPTER 4
DEVELOPMENT AND OPTIMIZATION OF IMMEDIATE-RELEASE GLIPIZIDE TABLETS USING LOW-TEMPERATURE FDM 3D PRINTING

4.1. Introduction

3D printing technology has emerged as a transformative manufacturing approach in pharmaceutical research, providing novel possibilities for personalized medicine and on-demand drug production. FDM is a popular 3D printing technique due to its ease of use, low cost, and ability to generate complex geometries with precise control over drug release profiles [96]. The technology enables the fabrication of solid dosage forms with customizable features, such as tailored doses and specific release kinetics, which are difficult to achieve with traditional manufacturing.

FDM 3D printing is used in pharmaceutical manufacturing by extruding drug-loaded thermoplastic filaments through a heated nozzle and then deposition layer by layer to create three-dimensional structures. This technology has shown promise for developing modified-release formulations, whereas immediate-release drug delivery systems present new challenges and opportunities. Rapid drug dissolution and absorption required appropriate excipient selection and printing parameter optimization [97]. Modifying internal structure using FDM printing parameters including infill patterns, shell thickness, and layer height can modify drug release kinetics without changing formulation composition.

One of challenges in FDM 3D printing in pharmaceutical production is using high temperature processing, which can lead to thermal degradation of some APIs. The FDM 3D printing often operates at temperatures above 150°C, a temperature that can compromise the chemical stability of the drugs [98]. Therefore, the developing low-temperature FDM printing processes is essential for applying this technology to further pharmaceutical compounds. This necessitates the careful selection of polymers with low glass transition temperatures, as well as the use of appropriate plasticizers, in order to process at temperatures that preserve drug stability.

Recent studies have shown that tablet geometry and internal structure could be strategically manipulated to create immediate-release profiles. In addition, printing parameters affect the drug release [99-101]. Understanding structure-function relationships is essential for rational 3D-printed tablet design. Despite growing interest in pharmaceutical FDM printing, the literature on low-temperature immediate-release formulations is limited. The majority of published studies have used thermoplastic polymers to extend drug release in sustained or modified-release systems. Designs for

immediate-release formulations must emphasize rapid polymer dissolution and high tablet porosity [5]. Developing immediate-release formulations requires a shift in design knowledge, with a focus on rapid polymer dissolution and high tablet porosity [97]. This knowledge gap emphasizes the need for a thorough investigation into the formulation and process parameters that allow for rapid drug release from FDM-printed tablets.

In this study, GPZ, a second-generation sulfonylurea antidiabetic agent, provides a model drug to investigate immediate-release FDM 3D-printed formulations. Its melting point is approximately 212°C, but its chemical structure can change when exposed to high temperatures [102]. In addition, this drug has poor water solubility (BCS Class II). Thus, this property creates both challenges and opportunities for demonstrating the feasibility of low-temperature FDM printing for immediate-release oral dosage forms.

Therefore, this study was designed to develop and optimize immediate-release GPZ tablets using a low-temperature FDM 3D printing. The study aimed to: (1) formulate drug-loaded filaments with suitable mechanical properties for printing process; (2) investigate the effects of critical printing parameters on immediate drug release profile; and (3) establish a model for dose customization by modifying tablet geometry.

4.2. Materials and methods

4.2.1. Materials

GPZ was provided by Siam Pharmaceutical Co., Ltd. (Bangkok, Thailand). KVA 64 was supplied by BASF Pharma. Mannitol was purchased from Shandong Tianli Pharmaceutical Co., Ltd. (Shandong, Chaina) , and triethyl citrate (TEC) was obtained from Sigma-Aldrich (Missouri, USA). Analysis chemicals, including acetonitrile and methanol (HPLC grade) were obtained from RCI Labscan (Bangkok, Thailand). monobasic sodium phosphate and sodium hydroxide (analytical grade) were purchased from Ajax Finechem (NSW, Australia).

4.2.2. Preparation of GPZ-loaded filaments

The GPZ-loaded filament, comprising 12% w/w GPZ and other excipients including KVA 64, mannitol, and TEC, was prepared according to the composition shown in Table 10. A total of 30 g of each formulation was thoroughly mixed and fed into a single-screw extruder (Wellzoom™ C desktop extruder, Shenzhen Mistar Technology Co., Ltd., Shenzhen, China) equipped with a 1.75 mm diameter nozzle. Extrusion was performed at 60 °C with a screw speed of 10 rpm. Prior to 3D printing, the resulting filament was stored in a desiccator at room temperature.

Table 10. GPZ-loaded filaments formulations

	Amount (w/w)				Flexibility (mm)	Feedability	Hygro-scopic time (h)	Diameter (mm)
	GPZ	KVA 64	Mannitol	TEC				
F1	12	63	10	15	6.98 ± 0.27	No	2	1.80 ± 0.10
F2	12	68	10	10	3.48 ± 0.53	Yes	24	1.71 ± 0.06
F3	12	69	10	9	3.05 ± 0.25	Yes	30	1.74 ± 0.11
F4	12	70	10	8	2.10 ± 0.42	No	32	1.76 ± 0.13
F5	12	70.5	10	7.5	2.04 ± 0.43	No	32	1.74 ± 0.02
F6	12	78	10	-	NA	No	36	1.67 ± 0.07

Note. Glipizide (GPZ), Kollidon®VA64 (KVA64), Triethyl citrate (TEC)

4.2.3. Design and fabrication of GPZ 3D-printed tablets

The GPZ 3D-printed tablets were designed in cylindrical shape with dimensions of 10 x 2 mm in using Fusion 360 software (Autodesk Inc., San Rafael, CA, USA). Prior printing process, the slicing and printing parameters were set utilizing Simplify3D software (Simplify3D® LLC, USA), which produces the G-code for the 3D printer.

3D printing parameters that affected the drug release behavior of GPZ-loaded tablets were investigated using a mixed level factorial design. Three parameters were considered (Figure 24.): infill pattern (rectilinear and grid), number of shells (1, 2, and 3), and layer height (0.1, 0.2, and 0.3 mm). The experimental matrix included all

possible combinations of the variables, resulting in 18 unique 3D-printed tablets (Table 11).

Table 11. Experimental design for evaluating the effects of 3D printing parameters on % drug release of GPZ 3D-printed tablets.

Run	Infill pattern	Layer thickness (mm)	Shell number (layer)
1	Rectilinear	0.3	3
2	Rectilinear	0.3	1
3	Grid	0.2	1
4	Rectilinear	0.2	3
5	Grid	0.1	3
6	Rectilinear	0.1	2
7	Grid	0.2	2
8	Grid	0.1	1
9	Rectilinear	0.1	1
10	Rectilinear	0.1	3
11	Grid	0.3	2
12	Rectilinear	0.3	2
13	Grid	0.3	3
14	Grid	0.3	1
15	Rectilinear	0.2	2
16	Grid	0.1	2
17	Rectilinear	0.2	1
18	Grid	0.2	3

The printing process was performed using a Flashforge Creator Pro 3D printer (Zhejiang Flashforge 3D Technology Co., Ltd., Zhejiang, China). The printing parameters established for the duration of the study were as follows: top and bottom layers set to 0, infill density at 30%, nozzle temperature maintained at 90 °C, and build plate temperature at 70 °C.

The main response evaluated was the percentage of drug release, using USP Apparatus II (paddle method) in phosphate buffer (pH 6.8) at 37 ± 0.5 °C. Statistical analysis utilized Design-Expert® software (version 8.0.6, Stat-Ease Inc., Minnesota,

USA). An analysis of variance was performed to evaluate the significance of main effects and interactions. Regression models were constructed to explain and predict the correlation between printing parameters and drug release behavior.

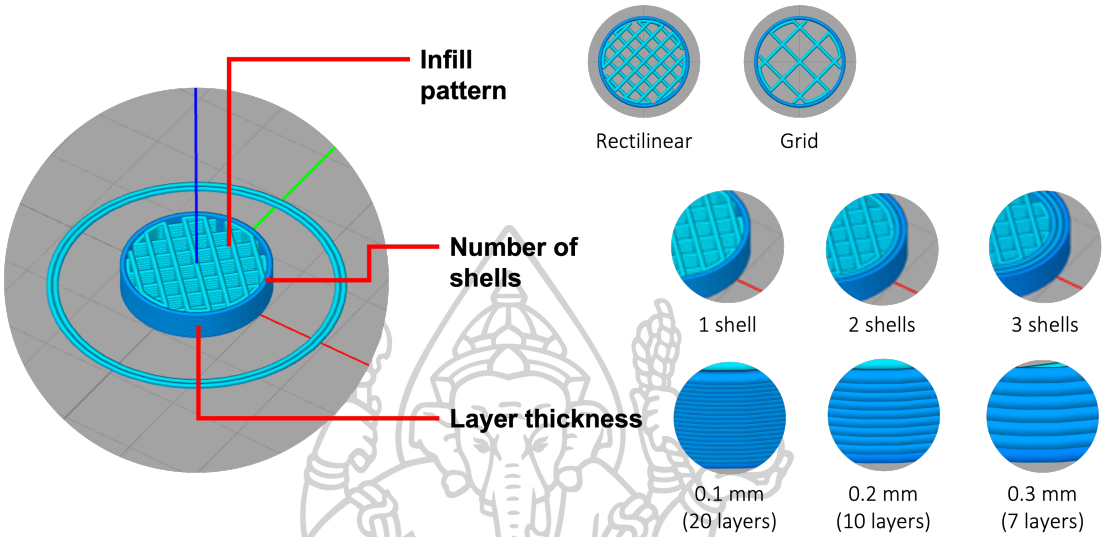

Figure 24. Schematic representation of 3D printing parameters investigated in GPZ-3D printed tablets using a mixed-level factorial design.

To scale up of GPZ 3D-printed tablets for dose adjustment, the tablet height was modified while keeping the tablet diameter constant at 10 mm. The tablet thickness required for a specified dose was determined using Equation (1):

$$Tablet\ thickness\ (h) = \frac{h_i D}{D_i} \quad (1)$$

Where h is tablet thickness (mm), h_i is initial tablet thickness (mm), D is target GPZ dose (mg), D_i is initial GPZ dose (mg).

The initial tablet thickness was 2 mm. The initial dose of GPZ was determined based on the drug content analysis

4.2.4. Characterization of GPZ-loaded filament and 3D-printed tablets

4.2.4.1. Morphological characteristics of filament and 3D-printed tablets

The morphology of the GPZ-loaded filament and 3D-printed tablets were analyzed using a SEM (Mira 3, Tescan, Brno, Czech Republic). Intact and cross-sectioned filament and tablet were dried, mounted on aluminum stubs, and

sputter-coated with a thin layer of gold to improve conductivity, following preparation with a precision cutter. SEM imaging was performed at an accelerating voltage of 5 kV and a working distance of approximately 30 mm. High-resolution images of the tablet surfaces and cross-sections were acquired for morphological evaluation.

4.2.4.2. Mechanical properties of filament

The GPZ-loaded filaments were evaluated for mechanical properties, including feedability and flexibility, before 3D printing. The feedability test evaluated the ability of the filament to be extruded through the 3D printer nozzle under standard printing conditions. The filament was put in into the Flashforge Creator Pro 3D printer at a nozzle temperature of 90 °C, and the duration to extrude 10 cm of filament was recorded (Figure 25A). The feeding speed derived from this test was utilized to establish the suitable test speed for the flexibility testing.

The flexibility test was conducted utilizing a Texture Analyzer (TA.XT Plus, Stable Micro Systems, UK) in compression mode. Filament samples were collected from six different parts of each batch, cut into 10 cm lengths, and evaluated for diameter uniformity. The samples were fixed to a custom-designed filament holder (Figure 25B-C), which was 3D printed and modified for stable attachment to the analyzer. The design was based on the Spaghetti Flexure Rig [103]. The test was conducted under the following parameters: a compression distance of 50 mm, a test speed of 3.0 mm/s, a trigger force of 0.05 N, and a load cell with a capacity of 5 kg. The flexibility of each filament was evaluated through the analysis of force-displacement profiles obtained during compression.

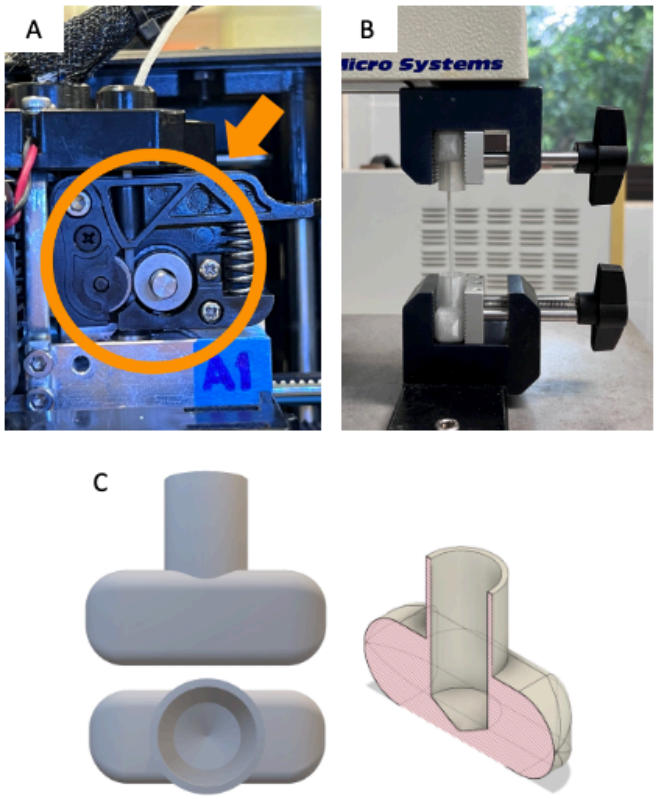

Figure 25. Mechanical evaluation setup for GPZ filament feedability and flexibility. (A) feedability test using the filament feeding mechanism of a 3D printer; (B) flexibility test setup using a texture analyzer; (C) custom-designed filament holder fabricated via 3D printing for mechanical testing.

4.2.4.3. Differential scanning calorimetry

The thermal properties of the individual materials—GPZ, KVA 64, and mannitol—along with their physical mixtures and GPZ-loaded filaments, were evaluated using a DSC (DSC 8000, PerkinElmer, Waltham, MA, USA). Each sample, weighing approximately 3–5 mg, was accurately assessed, placed in sealed aluminum pans, and subjected to a heating program from 20 °C to 250 °C at a constant rate of 10 °C/min. A nitrogen gas was sustained during the analysis at a flow rate of 20 mL/min. The thermograms obtained were processed and analyzed utilizing Pyris™ software.

4.2.4.4. Thermogravimetric analysis

TGA was performed to assess the thermal stability of the materials throughout the processes of filament extrusion and 3D printing. A simultaneous thermal analyzer (STA 6000, PerkinElmer, Waltham, MA, USA) was used for these measurements. Each sample, weighing approximately 3–5 mg, was accurately measured into open ceramic pans and tested by heating from 35 °C to 600 °C at a consistent rate of 10 °C/min. Nitrogen gas was continuously maintained at a flow rate of 20 mL/min during the analysis to ensure inert conditions.

4.2.4.5. Powder X-ray diffractometry

The solid-state characteristics of the materials (GPZ, KVA64, mannitol, physical mixture and GPZ-loaded filament), particularly their crystalline or amorphous nature, were investigated using a powder X-ray diffractometer (MiniFlex II, Rigaku, Tokyo, Japan). The measurements were conducted under the following parameters: an accelerating voltage of 30 kV, a current of 15 mA, and a scanning range of 5° to 45° (2θ). The scanning rate was kept constant at 4°/min, employing Cu-Kα radiation with a wavelength of 0.154 nm.

4.2.5. Drug content of GPZ-loaded filaments and 3D-printed tablets

The drug content in both GPZ-loaded filaments and 3D-printed GPZ tablets was measured using HPLC with an Agilent 1100 Series system (Agilent Technologies, CA, USA). Three different parts of filament were sampled for analysis to ensure uniformity along the filament. Each filament (weighing approximately 100 mg) and tablet sample was accurately measured and dissolved in 25 mL of phosphate buffer (pH 6.8) with 1% w/v polysorbate 80. The solutions were filtered using a 0.45 µm membrane filter before injection. Chromatographic separation was performed utilizing a Luna 5 µm C18 100Å column (250 × 4.6 mm; Phenomenex, Cheshire, UK). A mobile phase including acetonitrile, methanol, and phosphate buffer (pH 6.0) in a 20:10:70 (v/v/v) ratio was delivered at a flow rate of 1 mL/min. The column temperature was maintained at 40 °C, with the detection wavelength set at 276 nm. Measurements were performed in triplicate to guarantee precision and reproducibility.

4.2.6. *In vitro* drug release of 3D-printed tablets

The *in vitro* drug release profile of the GPZ 3D-printed tablets was analyzed using the United States Pharmacopeia (USP 43–NF 38) method for glipizide tablets with minor modifications. Dissolution testing was conducted utilizing a USP Apparatus II (paddle method) integrated with the AT Xtend™ system (Sotax, Westborough, MA, USA). Each tablet was soaked in 900 mL of phosphate buffer at pH 6.8, maintained at a temperature of 37 ± 0.5 °C. The paddle speed was maintained at 50 rpm for the duration of the experiment. The sample solution of 3 mL was collected at specified time intervals (5, 10, 15, 30, and 45 minutes) and was immediately replaced with a similar amount of fresh dissolution medium to maintain sink conditions. The samples that were withdrawn were analyzed for GPZ content utilizing HPLC, as outlined in Section 4.2.5.

4.3. Results and discussions

4.3.1. Filament formulation screening

The formulations for a GPZ filament were developed, containing 12% w/w GPZ as the API, KVA64 as the main water-soluble polymer, 10% w/w mannitol as a disintegrating agent, and TEC as a plasticizer. The ratios of KVA64 and TEC varied across various formulations, as shown in Table 10. All components were blended and extruded into a filament using an extruder at 60°C. Afterwards, the GPZ filament was selected based on an evaluation of three critical characteristics such as flexibility, feedability into a 3D printer, and hygroscopic time.

The results showed that the concentration of TEC was essential to the mechanical characteristics of filament. Formulation F1, which has the highest amount of TEC (15% w/w), showed high flexibility (6.98 ± 0.27 mm) and softness faster after the extrusion process, leading to its failure in the feedability test due to jamming in the gear of the 3D printer. F6, which lacked TEC, showed brittleness and fractured easily, causing it to be unfeedable. F2 to F5, produced by decreasing TEC concentrations, showed a reduction of flexibility (3.48 ± 0.53, 3.05 ± 0.25, 2.10 ± 0.42, and 2.04 ± 0.43 mm, respectively). Nonetheless, F2 and F3 demonstrated an appropriate property

suitable for printer feeding without fracture. Moreover, the amount of TEC influenced the hygroscopic time, defined as the duration before the filament absorbs moisture and becomes sticky and soft under the condition of 20°C with 50% relative humidity. The results showed that formulations with a higher amount of TEC displayed reduced hygroscopic times in comparison to those with lower TEC content. The reason for this behavior can be explained by the chemical structure of TEC, which has polar ester functional groups (-COO-) that can form hydrogen bonds with water molecules [104]. Increasing the concentration of TEC in the polymer matrix creates more polar sites that bind water molecules, which accelerates moisture absorption from the air. Considering all results, both F2 and F3 were successfully feedable; however, formulation F3 exhibited superior performance by showing the best moisture resistance, beginning hygroscopic only after 30 hours. Consequently, F3 was the best formulation for the subsequent 3D printing of GPZ tablets.

4.3.2. Morphological characteristics and drug content of GPZ-loaded filament.

The formulation screening identified filament F3 as the most suitable for 3D tablet printing. The filament produced was characterized by smooth, cylindrical rods, exhibiting a color range from white to off-white, with a diameter of 1.74 ± 0.11 mm, as showed in Figure 26A. The GPZ content measured in the filament was 10.94 ± 0.14%, slightly lower than the initial GPZ content added during mixing. This difference is probably because of minor material losses during the extrusion process.

The SEM analysis of the filament's cross-sectional morphology indicated a porous internal structure characterized by uniformly distributed voids within the matrix (Figure 26B1–B2). This porosity is commonly observed in hot-melt extrusion processes and may result from the air in the powder mixture before extrusion or from the evaporation of residual moisture in the raw materials during processing at 60°C, resulting in the production of small voids upon cooling [105-107].

In Figures 26B2-B3, which have higher magnification (800X and 5000X, respectively), small particles were observed dispersed throughout the polymer matrix within filament [108, 109]. These appear to be incompletely melted crystalline particles of either GPZ or mannitol. Because the extrusion temperature of 60°C is lower than the

melting points of GPZ (approximately 212°C) and mannitol (around 169°C), which limits their complete melting and dispersion during the extrusion process [110, 111].

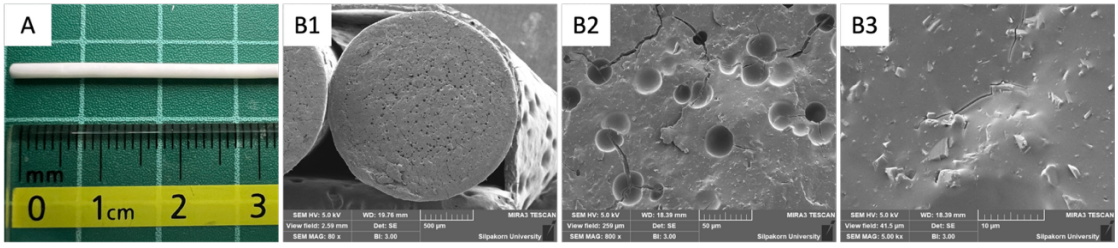

Figure 26. Photograph and surface morphology of GPZ-loaded filament. (A) Macroscopic image of the GPZ-loaded filament; (B1) SEM image of the cross-sectional surface of the filament at 80X magnification, (B2) SEM image at 800X magnification, and (B3) SEM image at 5,000X magnification.

4.3.3. Thermal properties, crystallinity properties and thermal stability of raw materials and GPZ-loaded filament.

The thermal properties of each component utilized in the preparation of the GPZ-loaded filament were analyzed using DSC, as illustrated in the thermograms (Figure 27A). Pure GPZ displayed a distinct endothermic peak at 212.47°C, indicating melting point of GPZ. The sharp melting peak indicates that GPZ is in a crystalline state under the initial conditions. KVA64 showed a slight baseline at approximately 58.52°C, characteristic of a Tg, confirming its amorphous nature as a polymer. Mannitol showed a sharp endothermic peak at 169.27 °C, thus confirming its crystalline structure similar to that of GPZ. When the three components and TEC were mixed in the same amounts as in formulation F3 (without heating), the resulting DSC thermogram of the mixture showed combined thermal behavior with some changes compared to the individual components. The GPZ melting peak at 204.50°C was still there but appeared shifted and less intense because the drug was diluted in the polymer matrix. Similarly, the mannitol melting peak reduced visibly around 135.76°C but appeared slightly broader. The KVA64 glass transition became partially obscured by overlapping thermal events from other components. The DSC thermogram of GPZ filament exhibited an endothermic peak at 155.98°C which is likely related to mannitol. The broader shape

and slight temperature decrease indicate that mannitol retains its crystalline structure, exhibiting minimal thermal modification, and did not completely melt or blend into the polymer matrix during extrusion at 60 °C. Whereas the characteristic melting peak of GPZ at approximately 200°C was absent in the DSC thermogram of the filament. The absence indicates that the low concentration of GPZ in the filament likely results from loss during the extrusion process. Therefore, the amount of GPZ in the filament might not have been enough to generate a detectable melting peak in the DSC analysis.

Figure 28 illustrated the crystallinity characteristics of the components of filament, physical mixture, and GPZ filament. GPZ displayed a distinct crystalline diffraction pattern, characterized by moderate to high intensity peaks at various 2θ angles, such as 7.24°, 9.78°, 10.78°, 15.55°, 17.84°, 18.38°, and 21.68° [112] which confirmed it has a crystalline structure. Conversely, the polymer KVA64 exhibited a broad halo, characteristic of an amorphous structure. Mannitol exhibited high-intensity peaks at 10.42°, 14.52°, 18.62°, 21.00°, and 23.30°, hence confirming its crystalline structure and especially indicating the β-polymorph form of mannitol [113]. The PXRD patterns of the physical mixture and the GPZ-loaded filament exhibited overlapping profiles characteristic of the individual components of GPZ and mannitol. Peaks related to both GPZ and mannitol remained observable, although with lowered intensity. These results correlate with the results of SEM imaging (Figure 26B3), which show crystalline particles dispersed within the filament matrix. Consequently, the crystalline structures were probably mannitol and GPZ that did not completely melt during the extrusion process, which is significantly temperature below the melting points of both compounds.

The thermal stability of the components was analyzed using TGA to evaluate the effects of processing temperatures during filament extrusion (60°C) and 3D printing (90°C). The findings demonstrated that all components displayed significant thermal stability (Figure 27B). GPZ started decomposition at approximately 250 °C, whereas mannitol and KVA64 exhibited the onset of thermal degradation at higher temperatures of around 300 °C and 350 °C, respectively. Additionally, the GPZ-loaded filament showed remaining thermal stability until 200°C, which was significantly higher than the actual processing temperatures. These results

confirmed that GPZ and its excipients are thermally stable for both the filament extrusion and 3D printing processes.

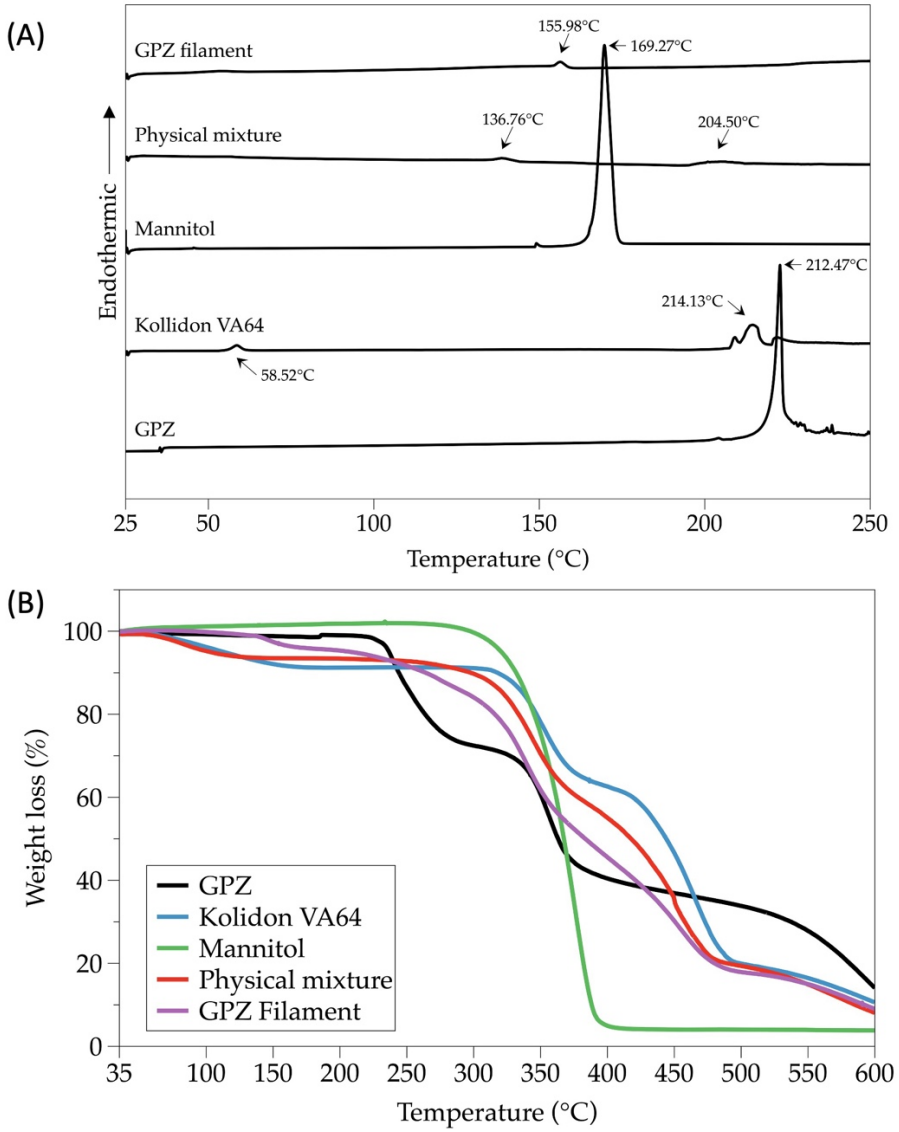

Figure 27. (A) DSC thermograms and (B) TGA thermograms of GPZ, Kollidon® VA64, mannitol, physical mixture, and GPZ filament.

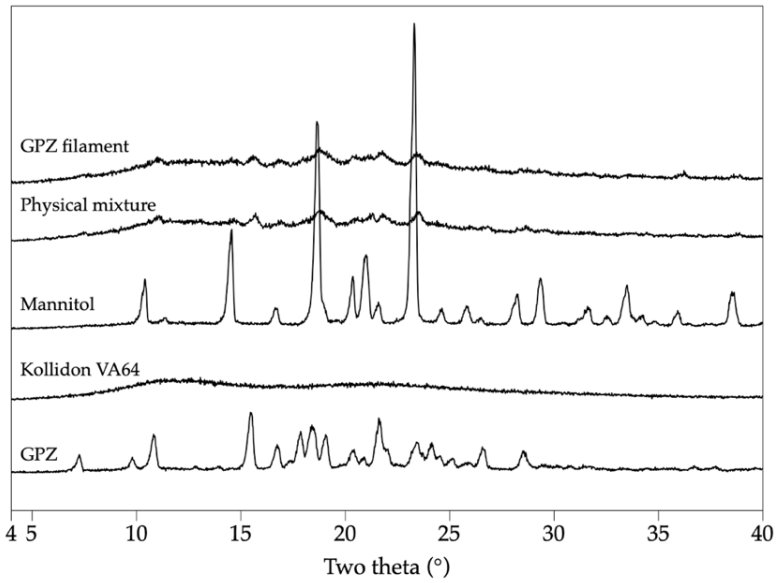

Figure 28. PXRD diffractograms of GPZ, Kollidon® VA64, mannitol, physical mixture, and GPZ filament.

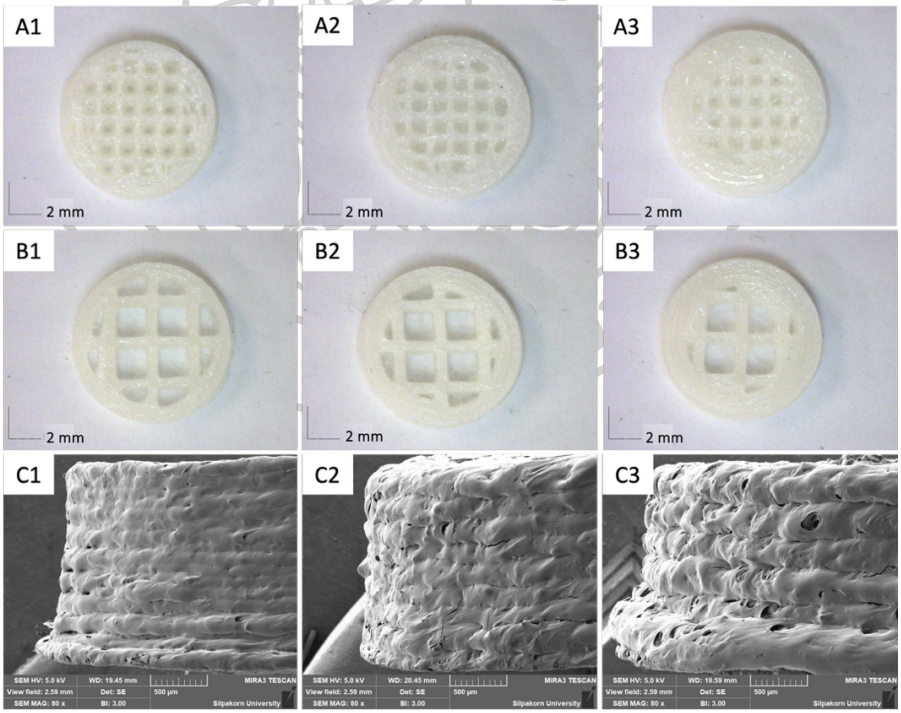

Figure 29. GPZ 3D-printed tablets with varying infill patterns, shell numbers, and layer thicknesses. (A1–A3) Rectilinear pattern with 1, 2, and 3 shells; (B1–B3) grid pattern with 1, 2, and 3 shells; and (C1–C3) SEM images showing layer thicknesses of 0.1 mm, 0.2 mm, and 0.3 mm, respectively.

4.3.4. Effect of 3D printing parameters on drug release of GPZ-3D printed tablet.

In this study, GPZ 3D-printed tablets were fabricated using pre-extruded drug-loaded filaments to evaluate the effect of printing parameters on the percent of drug release. A factorial design was utilized to create predictive models and evaluate the influence of three critical 3D printing parameters such as infill pattern, layer thickness, and shell number on the drug release. The 18 experiments showed a significantly statistical model (F-value = 36.84, $p < 0.0001$), indicating a strong relationship between the printing parameters and the percentage of drug release. The model demonstrated reliability, evidenced by high adjusted R^2 (0.9365) and predicted R^2 (0.8791) values, which indicate significant accuracy and predictive capability in identifying the factors affecting GPZ release.

Analysis of variance indicated that all three main printing parameters had a significant effect on the percentage of drug release from GPZ 3D-printed tablets. The infill pattern and shell number ($p < 0.0001$) significantly influenced the drug release. Tablets with a grid infill pattern exhibited higher drug release compared to those with a rectilinear pattern (Figure 30). The increase in drug release is due to the larger internal voids generated by the grid pattern (Figure 29B1- B3), allowing faster penetration of the dissolution medium into the tablet. In contrast, the rectilinear pattern (Figure 29A1-A3) created smaller voids, with one side of tablet lacking the channels compared to the grid pattern. During the initial printing layer, the nozzle was positioned slightly lower than in subsequent layers to ensure adhesion to the printing platform, causing the extruded polymer to spread and fuse without creating voids. This significantly decreased the contact area between the dissolution medium and the polymer matrix. Consequently, the dissolution of polymer with linear-designed tablet was reduced compared to that with grid-designed tablet at the same sampling time, thereby lowering percentage of GPZ release. Increasing the shell number from one to three layers (Figure 32) resulted in a significant decrease in drug release. Increasing the shell number led to a greater wall thickness of the tablets, which created a physical barrier that slowed medium penetration and subsequently decreased the drug release rate. Regarding layer thickness (0.1 to 0.3 mm), SEM images (Figures 29C1-C3) indicated that thinner layers resulted in fewer gaps between the printed layers when compared to thicker layers. Statistical analysis indicated that layer thickness had a significant impact on drug

release (*p = 0.0313*); however, the relationship exhibited notable complexity. As illustrated in Figure 31, the relationship between layer thickness and drug release was not linear and varied depending on other fixed parameters. For instance, under certain conditions, drug release decreased when layer thickness increased from 0.1 mm to 0.2 mm before rising again at 0.3 mm. This intricate behavior emphasizes the importance of the significant interaction effect between infill pattern and layer thickness (AB interaction, *p = 0.0016*). As clearly depicted in Figure 33, the influence of layer thickness on drug release strongly depended on the internal structure dictated by the infill pattern. From these findings, the optimal conditions to achieve rapid drug release from GPZ 3D-printed tablets were identified as follows: grid infill pattern, one shell, and a layer thickness of 0.3 mm.

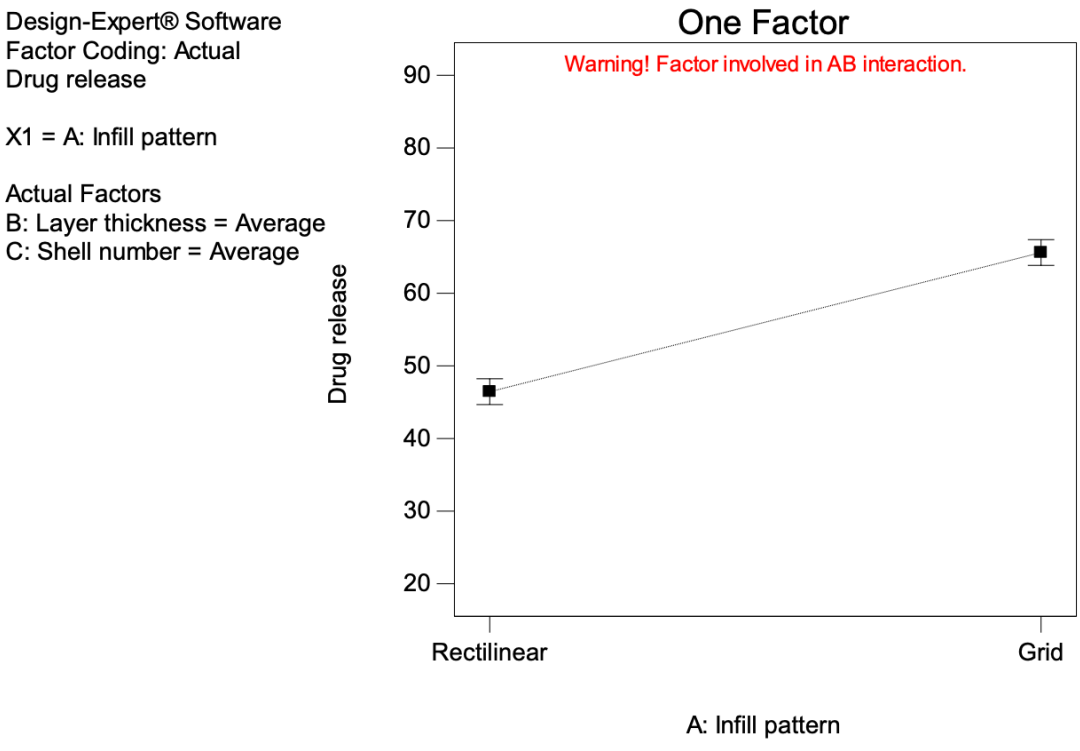

Figure 30. Main effect of infill pattern (rectilinear vs. grid) on GPZ drug release at varying layer thicknesses (0.1, 0.2, 0.3 mm) and shell numbers (1, 2, 3 shells).

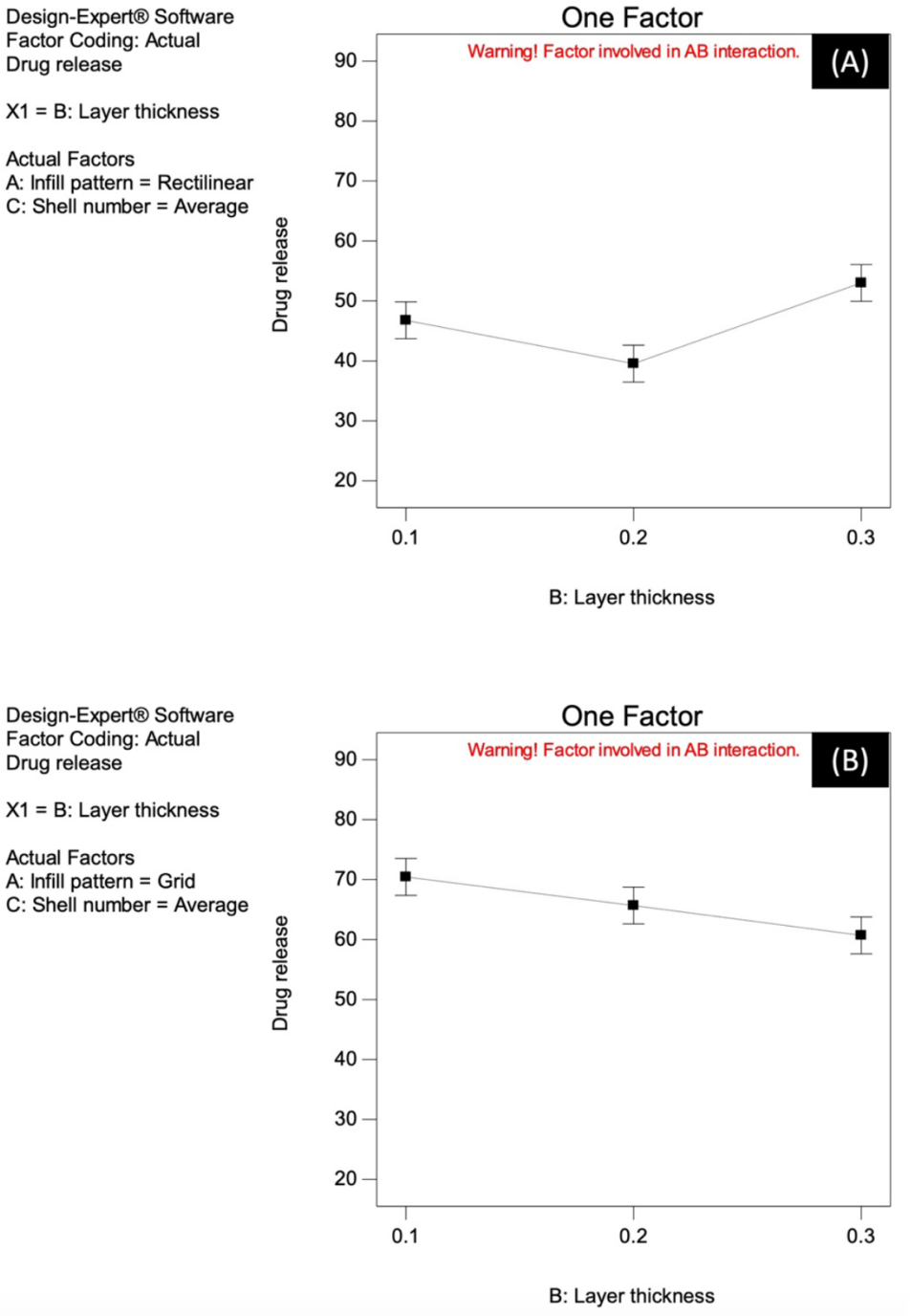

Figure 31. Main effect of layer thicknesses (0.1, 0.2, and 0.3 mm) on GPZ drug release at varying infill pattern ((A) rectilinear, (B) grid) and shell numbers (1, 2, 3 shells).

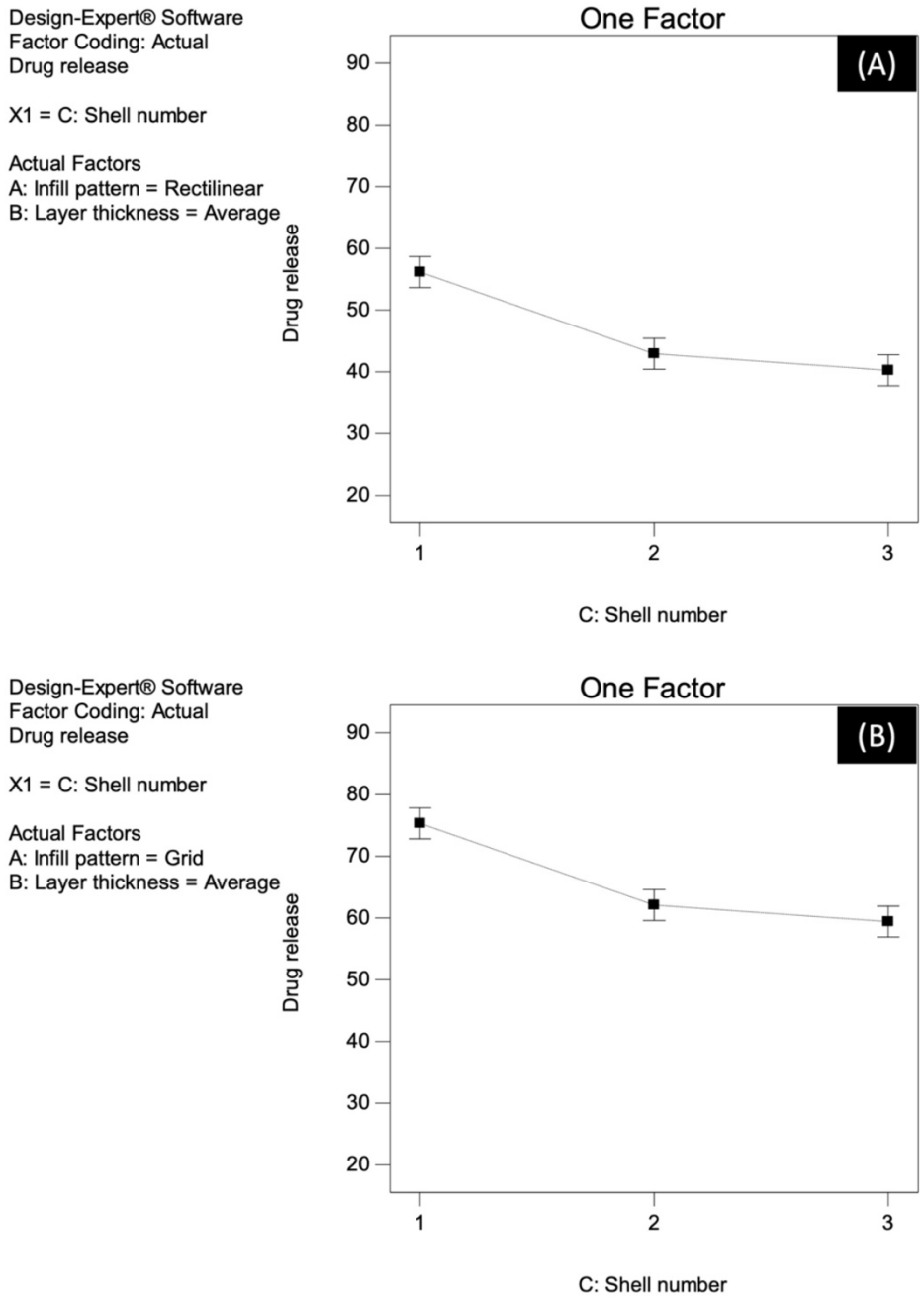

Figure 32. Main effect of shell numbers (1, 2, and 3 shells) on GPZ drug release at varying infill pattern ((A) rectilinear, (B) grid) and layer thicknesses (0.1, 0.2, and 0.3 mm).

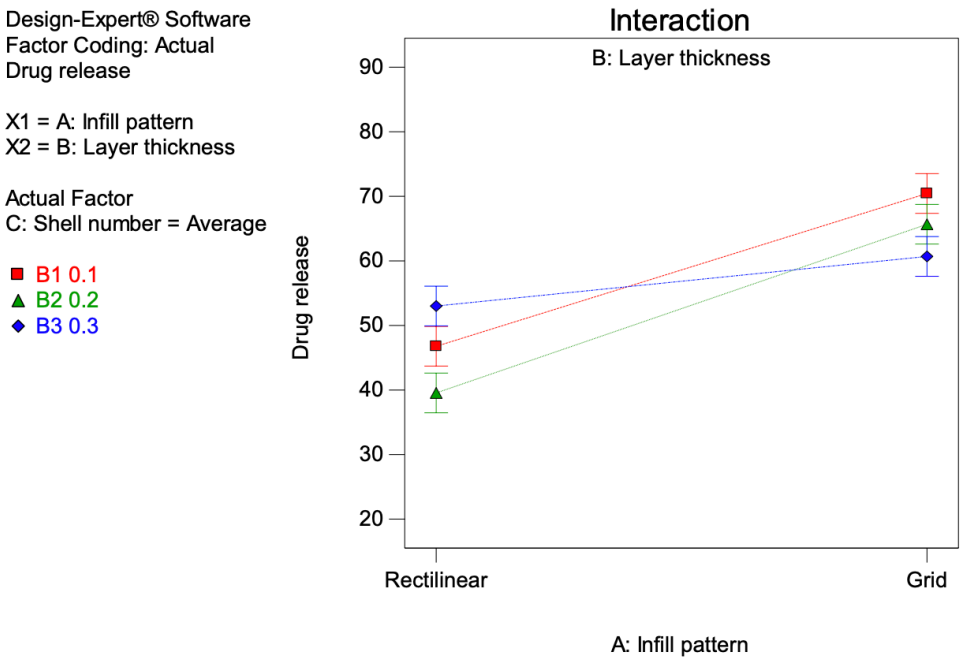

Figure 33. Interaction plots illustrating the effect of infill pattern and layer thicknesses on GPZ drug release at varying shell numbers (1, 2, 3 shells).

Table 12. Dimensional and drug content of GPZ 3D-printed tablets with varying dosages.

Dosage (mg)	Tablet thickness (mm)		3D-printed tablet diameter (mm)	Surface area; *SA* (mm^2)	Volume; *V* (mm^3)	*SA/V* ratio	Drug content (%)
	Calculated	Actual					
5	1.08	1.18 ± 0.07	9.95 ± 0.07	184.79	25.47	7.26	5.47 ± 0.20
7.5	1.62	1.67 ± 0.08	9.73 ± 0.06	265.92	38.21	6.96	7.71 ± 0.21
10	2.00	2.08 ± 0.16	9.72 ± 0.17	322.89	47.12	6.85	9.25 ± 0.21
15	3.24	3.18 ± 0.12	10.18 ± 0.36	508.82	76.41	6.66	14.49 ± 0.60

Note. Surface area (*SA*) and volume (*V*) were calculated using fusion 360 software. 3D printed tablet diameter was fixed at 10 mm for all formulations.

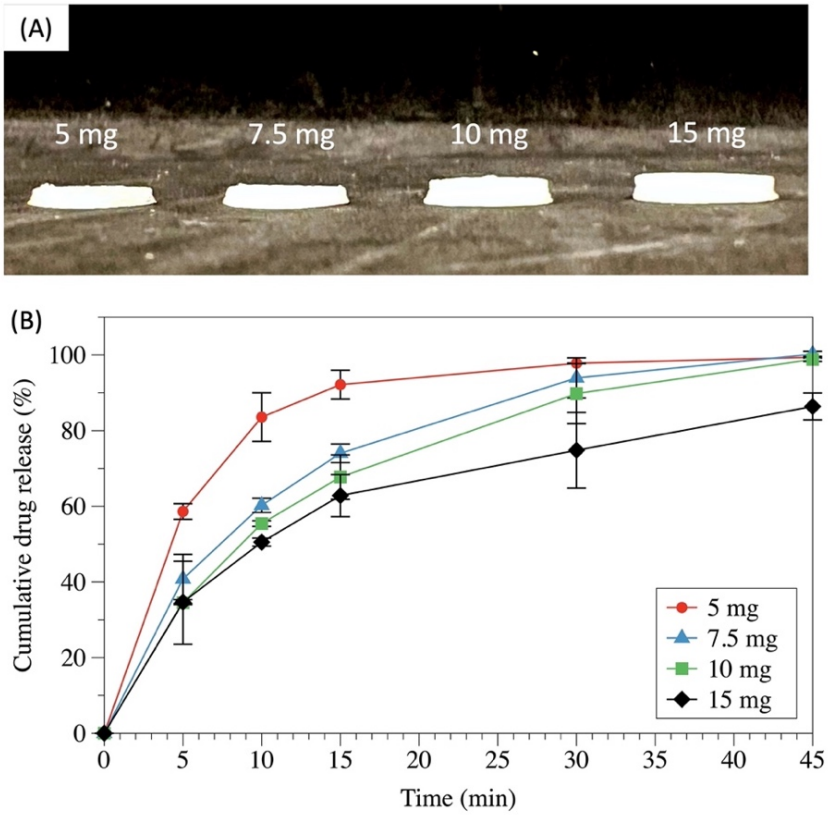

Figure 34. Appearance and drug release profiles of GPZ 3D-printed tablets with varying dosages. (A) Photographs of GPZ 3D-printed tablets prepared with adjusted GPZ dosages (5, 7.5, 10, and 15 mg). (B) In vitro dissolution profiles representing cumulative drug release (%) of the GPZ 3D-printed tablets over 45 min.

4.3.5. Dosage adjustment of GPZ 3D-printed tablets

The study of adjusting the dosage of GPZ 3D-printed tablets was conducted using a mathematical equation (Equation 1) to calculate tablet thickness required for GPZ dosages of 5, 7.5, 10, and 15 mg. The equation showed excellent predictive accuracy, with calculated thicknesses (1.08, 1.62, 2.00, and 3.24 mm) corresponding closely with the actual values (1.18 ± 0.07, 1.67 ± 0.08, 2.08 ± 0.16, and 3.18 ± 0.12 mm, respectively), as showed in Table 12 and Figure 34A. All tablets had consistent dimensions of approximately 10 mm (range: 9.7-10.2 mm). The drug content analysis exhibited GPZ contents of 5.47 ± 0.20%, 7.71 ± 0.21%, 9.25 ± 0.21%, and 14.49 ± 0.60% for tablets containing 5, 7.5, 10, and 15 mg GPZ, respectively, closely with the target dosages. Consequently, these results proved the mathematical equations efficacy in predicting both tablet thickness and drug loading.

The dissolution analysis of GPZ 3D-printed tablets with different dosages was showed in Figure 34B. Tablets with the lowest dosage (5 mg) and minimal thickness exhibited the fastest drug release, with nearly 100% of GPZ released within 30 minutes. Whereas, the 15 mg tablets, being the thickest, exhibited the slowest drug release profile, with around 85% of GPZ released after 45 minutes. These results can be explained through changes in the SA/V ratio. The 5 mg tablet exhibited the highest SA/V ratio of 7.26, resulting in a relatively larger surface area exposed to the dissolution medium, thereby enhancing drug release. The increase in tablet thickness with higher dosages corresponded to a decrease in the SA/V ratio, with the 15 mg tablet exhibiting the lowest SA/V ratio of 6.66, leading to slower dissolution rates.

4.4. Conclusion

This study successfully fabricated immediate-release GPZ tablets using a low-temperature FDM 3D printing technology, thereby fully accomplishing the primary research objective. A key development was the formulation of an optimal drug-loaded filament (Formulation F3) comprising GPZ, KVA64, mannitol, and TEC. This formulation exhibited appropriate mechanical properties (flexibility and feedability) for the printing process and proved the most moisture stable of all evaluated formulations at 20°C and 50% relative humidity. Subsequently, characterization through DSC and PXRD confirmed that the low-temperature (60°C) hot-melt extrusion process induced a partial amorphous transition in both GPZ and mannitol. These components were distributed as a solid within the polymer matrix, however some residual crystalline forms were still observable in SEM. Furthermore, TGA confirmed that all components were stable well above the temperatures used during filament extrusion process and printing process (90°C). Moreover, the investigation revealed a highly significant correlation between the 3D printing parameters—namely, the infill pattern, shell count, and layer thickness-and the resultant drug release rate. It was determined that a grid infill pattern, combined with a minimal shell count (one layer) and a layer thickness of 0.3 mm, constituted the optimal conditions for accelerating drug release. This result was attributable to the designing of a more porous interior tablet structure, which

increased the surface area accessible for contact with the dissolution medium. Furthermore, this study established the feasibility of a mathematical model for accurate dosage customization by adjusting tablet thickness. This allowed for the successful producing of 3D-printed tablets with various dosages (5, 7.5, 10, and 15 mg). Importantly, the drug release was shown to be directly proportional to the SA/V ratio of the tablets.

CHAPTER 5
DESIGN AND FABRICATION OF MULTI-RELEASE FIXED-DOSE COMBINATION TABLETS VIA 3D PRINTING: A FELODIPINE-GLIPIZIDE MODEL SYSTEM

5.1. Introduction

Chronic, non-communicable diseases (NCDs) like cardiovascular disorders and metabolic syndromes are one of the biggest challenges to modern healthcare systems. Hypertension and type 2 diabetes mellitus (T2DM) are common, often coexisting in the same patient population due to insulin resistance, inflammation, and endothelial dysfunction [114]. This comorbidity raises the risk of myocardial infarction, stroke, renal failure, and retinopathy, which required extensive and lifelong treatment. Patients with hypertension and type 2 diabetes are typically treated with multiple medications or polypharmacy. Complex dosage schedules that require patients to take multiple tablets throughout the day increase the problem of non-adherence. Poor patient compliance hinders chronic disease management, resulting in suboptimal clinical control, higher healthcare utilization, and higher medical costs [115]. The pharmaceutical industry has prioritized fixed-dose combination (FDC) products to combat polypharmacy. An FDC, also known as a polypill, is a single dosage form with more than one APIs. This approach has many advantages over administering individual medications. FDCs raise the treatment regimen by decreasing pill dosage and increasing patient acceptance. It has been shown to significantly improve adherence [116]. As a result, FDCs prevent patients from forgetting their medications by combining them into a single tablet.

The conventional pharmaceutical manufacturing technologies struggle to produce a single oral dosage form with both immediate and controlled release APIs. The multi-layer tableting or coated core-tablets, which is traditional methods, can achieve dual-release profiles but require complex, multi-step, and expensive manufacturing. Poor layer adhesion and inconsistent drug release limit the design flexibility, precision, and release kinetics of these methods [117, 118]. Additive manufacturing, or 3D printing, has revolutionized pharmaceutical sciences in recent years. This technology builds objects layer-by-layer from digital designs, giving unprecedented control over the product's internal and external architecture [119]. 3D printing in pharmaceutical enables personalized medicine, where dosage forms can be customized to a patient's needs, including doses, shapes for easier swallowing, and, most importantly, sophisticated drug release profiles [69]. FDM is popular for pharmaceutical

development due to its accessibility, cost-effectiveness, and solvent-free operation [120].

FDM printing builds an object layer-by-layer by extruding molten thermoplastic filament through a heated nozzle. Drug-loaded filaments produced by hot-melt extrusion are the printer's "ink" in pharmaceuticals. HME is a well-established industrial process that mixes an API with a thermoplastic polymer and other excipients to form a solid dispersion that is extruded into a precise-diameter filament [121]. The filament can be fed into an FDM printer. FDM technology excels at material spatial distribution control. A printer with multiple extruders can print discrete compartments in a tablet using filaments containing different drugs or polymers. This allows the creation of multi-drug tablets with complex internal geometries that achieve independent and highly specific release kinetics for each drug [34]. Geometric control unlocks complex, multi-modal release profiles that conventional manufacturing cannot achieve.

Accordingly, this study aimed to fabricate and characterize a dual-release fixed-dose combination tablet combining an immediate-release glipizide and a controlled-release felodipine by using FDM 3D printing technique. Three geometric designs were evaluated to determine their influence on the in vitro drug release kinetics of both active pharmaceutical ingredients within a single 3D-printed dosage form.

5.2. Materials and methods

5.2.1. Materials

FDP was obtained from Xilin Pharmaceutical Raw Material Co., Ltd. (Jiangsu, China), while GPZ was supplied by Siam Pharmaceutical Co., Ltd. (Bangkok, Thailand). Beside Plendil® 5 mg/tab (AstraZeneca, Cambridge, England) and Dipazide® 5 mg/tab (Siam Pharmaceutical Co., Ltd., Bangkok, Thailand), which are commercial reference tablets, were used for comparing dissolution profiles with 3D-printed tablets in this study. For filament preparation, the polymeric materials included PVA powder (Parteck® MXP) purchased from Merck (Darmstadt, Germany), PLA filament donated by IRPC Public Company Limited (Rayong, Thailand), and KVA 64, a vinylpyrrolidone-vinyl acetate copolymer supplied by BASF Pharma (Ludwigshafen,

Germany). The additional ingredients in the filament included erythrosine (FD&C Red No. 3, E127) purchased from Bangkok Chemical Co., Ltd. (Bangkok, Thailand), triethyl citrate (TEC) as a plasticizer from Sigma-Aldrich (MO, USA) and D-mannitol from Shandong Tianli Pharmaceutical Co., Ltd. (Shandong, Chaina). For chemical analysis, HPLC solvents consisting of acetonitrile and methanol were purchased from RCI Labscan (Bangkok, Thailand), while monobasic sodium phosphate, dibasic sodium phosphate, and sodium hydroxide (analytical grade) were purchased from Ajax Finechem (NSW, Australia). In addition, sodium lauryl sulfate (SLS) was purchased from Kemaus (NSW, Australia).

5.2.2. Preparation of FDP-loaded filament and GPZ-loaded filaments.

The preparation of drug-loaded filaments for this study followed methods from two previous studies, which were described in Chapters 3 and 4. The formulation for FDP-loaded filament was modified from Chapter 3 by using erythrosine as a coloring agent to visually differentiate the drug areas from the PLA filament during multi-material printing. The modified formulation contained 5% w/w FDP, 94% w/w PVA, and 1% w/w erythrosine. The extrusion processes were performed at 185°C with a screw speed of 12 rpm using single-screw extruder (Wellzoom™ C desktop extruder, Shenzhen Mistar Technology Co., Ltd., Shenzhen, China) with a nozzle diameter of 1.75 mm. For GPZ-loaded filament, follow the methods described in Chapter 4. The GPZ-loaded filament contained 12% w/w GPZ, 69% w/w KVA 64, 10% w/w mannitol, and 9% w/w TEC. The powder mixtures were thoroughly blended and extruded by a single-screw extruder at 60°C with a screw speed of 10 rpm. Before the printing process, both filaments were kept in desiccators at room temperature to protect them from moisture in the air.

5.2.3. Density of drug-loaded filaments measurement.

The density of the filament was evaluated using Gas pycnometer (Ultrapyc 5000, Anton Paar, Graz, Austria). The sample filaments were dried at 40°C for 24 hours to remove residual moisture before measurement. After the filament was cut into pieces of approximately 10 mm, and weighed to 10 ± 0.5 mg. Each sample was placed in a

small sample cell, which has a volume of 10 cm^3 (0.03% accuracy, 0.015% repeatability). The measurements were conducted at 25°C using nitrogen gas at a target pressure of 18 psi (1.24 bar) in monolith flow mode.

5.2.4. Design and fabrication of FDP-GPZ 3D-printed tablets

This study focused on the development of a fixed-dose combination tablet using 3D printing technology. Figure 35 demonstrated the design of three types of FDP-GPZ 3D-printed tablets using Shapr3D software (education license version, Siemens Parasolid®, Budapest, Hungary). The target dose of each drug layer was calculated from the thickness of the tablet layer. This calculation was based on the relationship between the density of drug-loaded filament, the specific geometry of the designed tablet, and the mass of the tablet.

The first tablet model (Figure 35A) features a stacked-layer structure. The FDP layer was cylindrical in shape and enclosed on its side and base by a PLA wall. The thickness of this layer (h_F) was calculated using Equation 1. Whereas the GPZ layer was placed above the FDP layer as a cylindrical structure with a grid pattern (30% infill density). Equation 2 determined the thickness of this layer (h_G).

$$Thickness\ of\ FPD\ layer\ (h_F) = \frac{m_F}{\rho_F \pi r_F^2} \quad (1)$$

Where h_F is thickness of the FDP layer (mm), m_F is target mass of FDP layer (mg), ρ_F is density of the FDP filament (mg/mm^3) and r_F is radius of the FDP layer (mm).

$$Thickness\ of\ GPZ\ layer\ (h_G) = \frac{m_G}{0.3 \cdot \rho_G \pi r_G^2} \quad (2)$$

Where h_G is thickness of the GPZ layer (mm), m_G is target mass of GPZ layer (mg), ρ_G is density of the GPZ filament (mg/mm^3), r_G is radius of the GPZ layer (mm) and 0.3 is the factor corresponding to the 30% infill density

The second table model (Figure 35B) features a core-shell design in which a cylindrical FDP core is surrounded by a GPZ shell. The FDP core was enclosed by a PLA wall and base and maintains the same thickness calculation as model 1 (Equation 1). The GPZ layer surrounding the FDP core was printed with a grid pattern at 30% infill density. Its thickness (h_G) is calculated using Equation 3.

$$\textit{Thickness of GPZ layer } (h_G) = \frac{m_G}{0.3 \cdot \rho_G \pi (R_G^2 - r_G^2)} \tag{3}$$

Where R_G is outer radius of the GPZ shell (mm), r_G is inner radius of the GPZ shell (mm), and other variables are as defined in Equation 2.

The third tablet model (Figure 35C) was designed on an inverted core-shell structure. The GPZ was a core layer that printed in a cylindrical structure with 30% grid infill density (grid pattern). The thickness (h_G) was calculated by Equation 2. Whereas the FDP shell was formed as a solid hollow cylinder surrounding the GPZ core, with thickness (h_F) determined by Equation 4.

$$\textit{Thickness of FDP layer } (h_F) = \frac{m_F}{\rho_F \pi (R_{FO}^2 - R_{FI}^2)} \tag{4}$$

Where R_{FO} is outer radius of the FDP shell (mm), R_{FI} is inner radius of the FDP shell (mm) and other variables are as defined in Equation 1.

In the printing process, the FDP-GPZ 3D-printed tablets were employed in a sequential printing approach using a 3D printer (Flashforge Creator Pro, Zhejiang Flashforge 3D Technology Co., Ltd., Zhejiang, China). The printing of the FDP layer followed the methodology from chapter 3, utilizing the left nozzle for FPD core printing at 195°C, with parameters set at 60°C bed temperature, 50 mm/s printing speed, 70 mm/s travel speed, 100% infill density with a rectilinear pattern, and 0.12 mm layer thickness, while the right nozzle was used for PLA shell printing at 200°C. The GPZ layer fabrication followed Chapter 4. The GPZ tablets were printed at 90°C with 30% infill density using a grid pattern, a single shell perimeter, and a 0.3 mm layer thickness.

After the individual FDP and GPZ layers were assembled into a single complete tablet using 20% w/w PVA solution as a binding agent. The FDP-GPZ 3D-printed tablets were stored in desiccators at room temperature before analytical testing.

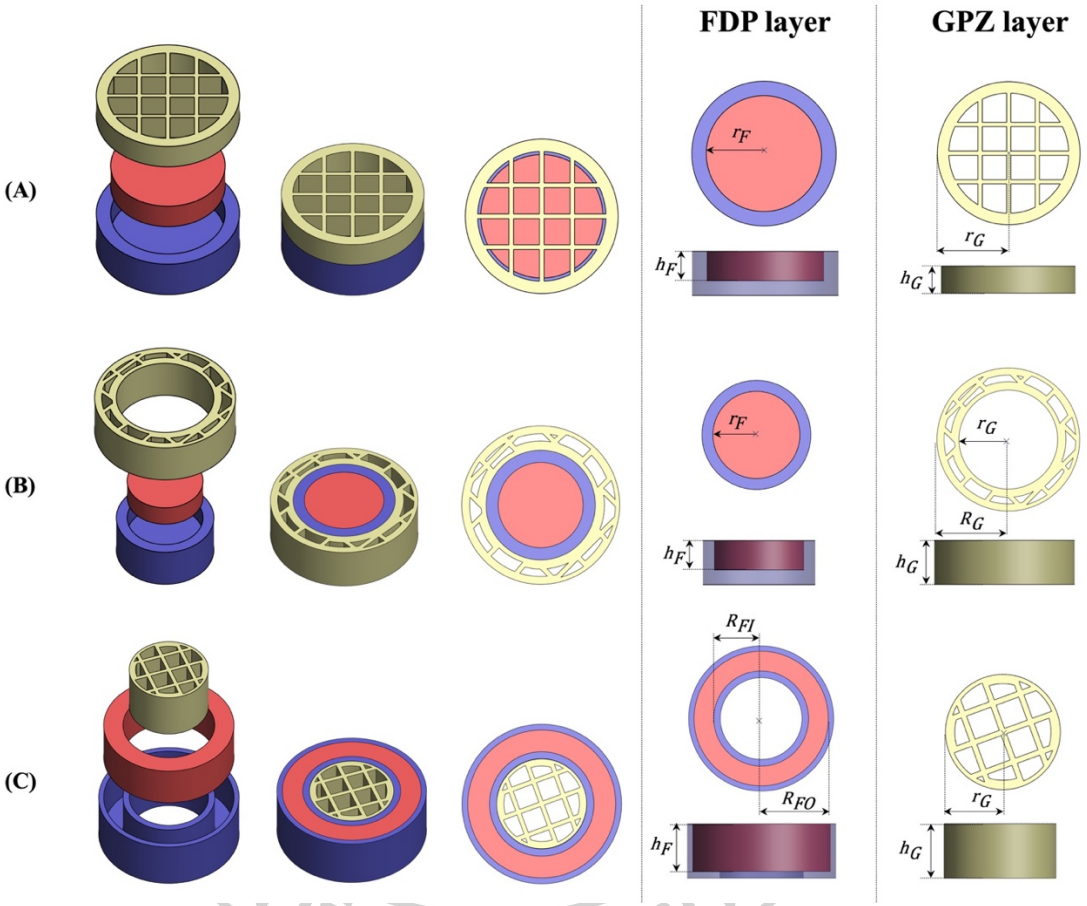

Figure 35. Three-dimensional architectural designs of FDP-GPZ 3D-printed tablets with 100% and 30% infill densities, respectively: (A) Stacked-layer structure with discrete horizontal drug layers; (B) Core-shell design with GPZ outer layer and FDP inner core; and (C) Inverted core-shell structure with FDP outer layer and GPZ inner core. (Red: FDP layer; Yellow: GPZ layer; Blue: PLA polymer matrix).

Table 13. Dimensional parameters and drug content analysis: calculated versus actual values for FDP-GPZ tablet designs.

Tablet models	Calculated parameters		Actual parameters		Drug content (%)	
	FDP layer	**GPZ layer**	**FDP layer**	**GPZ layer**	**FDP layer**	**GPZ layer**
Tablet A	m_F = 100 mg r_F = 3.5 mm h_F = 2.13 mm	m_G = 100 mg r_G = 6 mm h_G = 2.54 mm	m_F = 101.43 ± 1.85 mg r_F = 3.79 ± 0.20 mm	m_G = 98.03 ± 4.25 mg r_G = 6.01 ± 0.32 mm h_G = 2.44 ± 0.06 mm	5.22 ± 0.57	9.18 ± 0.19
Tablet B	m_F = 100 mg r_F = 3.5 mm h_F = 2.13 mm	m_G = 100 mg R_G = 6.5 mm r_G = 4.5 mm h_G = 4.16 mm	m_F = 103.73 ± 1.46 mg r_F = 3.67 ± 0.15 mm	m_G = 99.45 ± 1.78 mg R_G = 6.60 ± 0.06 mm r_G = 4.60 ± 0.10 mm h_G = 4.10 ± 0.10 mm	6.04 ± 0.52	9.41 ± 0.92
Tablet C	m_F = 100 mg R_{FO} = 7 mm R_{FI} = 6 mm h_F = 2.00 mm	m_G = 100 mg r_G = 5 mm h_G = 3.66 mm	m_F = 104.02 ± 1.68 mg R_{FO} = 7.03 ± 0.14 mm R_{FI} = 5.90 ± 0.04 mm	m_G = 97.87 ± 1.52 mg r_G = 4.88 ± 0.19 mm h_G = 3.63 ± 0.05 mm	6.52 ± 0.68	8.99 ± 0.30

Note. Details of all parameters are described in Section 5.2.4.

5.2.5. Drug content of drug-loaded filaments and FDP-GPZ 3D-printed tablets

The drug content of FDP and GPZ was followed, and some modifications were made to the drug content method in chapters 3 and 4 of the study. Drug filaments were selected from three sections during the extrusion process, with an approximate weight of 100 ± 0.5 mg. The FDP filament and tablet layer of each model were dissolved in 25 mL of 1% w/v polysorbate 80 for 3 hours. Similarly, the GPZ filament and tablet layer of each model were dissolved in 25 mL of phosphate buffer (pH 6.8) containing 1% w/v polysorbate 80 for the same duration. After that the drug-polymer solutions from filaments and tablets were filtered using a 0.45 μm membrane filter before injection.

HPLC analysis was conducted utilizing a Phenomenex Luna C18 100Å column (250 × 4.6 mm; Cheshire, UK), with the temperature maintained at 40°C. Each drug required specific analytical conditions. FDP quantification used a mobile phase consisting of acetonitrile, methanol, and phosphate buffer (pH 3.0) in a 45:25:30 (v/v/v) ratio, delivered at a flow rate of 1 mL/min with UV detection at 362 nm. In contrast, GPZ analysis utilized a binary mobile phase consisting of methanol and phosphate buffer at pH 6.0 in a 52:48 v/v ratio, with a flow rate of 1 mL/min and UV detection at 220 nm. Analytical precision and reproducibility were ensured through triplicate analysis of all samples.

5.2.6. *In vitro* drug release of FDP-GPZ 3D-printed tablets

Drug release studies were performed on three dial-drug 3D-printed tablets and reference commercial products (Plendil® 5 mg FDP tablets and Dipazide® 5 mg GPZ tablets). The dissolution testing employed an AT Xtend™ dissolution system (Sotax, Westborough, MA, USA) with USP dissolution apparatus II paddle configuration. These testing conditions consisted of 500 mL phosphate buffer (pH 6.5) added with 1% w/v SLS as the dissolution medium, 50 rpm paddle speed, and temperature at 37 ± 0.5°C. The specified sampling time occurred at 5, 10, 15, 30, 45, and 60 minutes, followed by 2, 3, 4, 6, 8, 10, 12, 14, 16, 18, and 24 hours. 3 mL of the sampling solutions were withdrawn and promptly replaced with equivalent volumes of

fresh medium to maintain sink conditions. The concentrations of FDP and GPZ in the samples were analyzed using HPLC, as explained in Section 5.2.5.

5.2.7. Mathematical modeling of drug release kinetics from 3D-printed tablets

The mechanism and kinetics of drug release from the 3D-printed tablets were analyzed by fitting the dissolution profiles of the controlled-release FDP layer and the immediate-release GPZ layer to six mathematical models using DDSolver in Microsoft Excel [76]. The six mathematical models included the zero-order model, first-order model, Higuchi model, Korsmeyer–Peppas model, Peppas–Sahlin model, and Hopfenberg model. The goodness of fit for each model was assessed using the highest R^2 value and the lowest AIC. Additionally, the f_2 value was calculated to compare the dissolution profiles of the 3D-printed tablets with commercial reference tablets. The f_2 value between 50 and 100 indicates that the two dissolution profiles were similar. The details of each mathematical model equation and similarity factor equation were described in chapter 3, section 3.2.7.

5.3. Results and discussion

5.3.1. Drug-loaded filament characterizations

The FDP and GPZ filaments were successfully prepared according to the filament extrusion methods described in chapters 3 and 4. Figure 36 exhibited great physical characteristics and mechanical properties in accordance with previous studies. The FDP filament presented smooth and red filament with an average diameter of 1.73 ± 0.01 mm. The mechanical properties were evaluated as excellent flexibility due to no fracture occurred during compression over 50 mm. Furthermore, this filament could be fed through 3D printer without bending or breaking. The drug content analysis performed at three different points of the filament during hot melt extrusion process—proximal, central, and distal—yielded an average FDP concentration of 4.92 ± 0.02% w/w. This result indicated a uniform drug distribution throughout the filament and was in close agreement with the theoretical drug loading (5% w/w of FDP).

The GPZ filaments exhibited a white or cream-colored appearance with a smooth surface and an average diameter of 1.77 ± 0.16 mm. The flexibility of GPZ filament was 3.13 ± 0.28 mm, and it also exhibited feedability during the 3D printing process. These mechanical properties were consistent with prior research findings. The average GPZ content was 11.75 ± 0.32% w/w (12% w/w of GPZ theoretical drug loading) , suggesting consistent drug incorporation with a uniform distribution similar to the FDP filament.

Moreover, the density of both filament types was analyzed using a gas pycnometer. The results showed that the densities of the FDP and GPZ filaments were 1.2219 mg/mm³ and 1.1586 mg/mm³, respectively. The slightly higher density of the FDP filament might be attributed to the higher density of PVA polymer (1.10-1.31 mg/mm^3) [73] compared to that of KVA 64 (1.2 mg/mm^3) [122], as well as the higher proportion of polymer incorporated in its formulation. Whereas GPZ filament formulations had higher drug loading and inclusion of additional excipients such as mannitol and TEC, exhibited a lower overall density. This reduction might be influenced by the presence of structural voids, as evidenced by the SEM results presented in Section 4.3.2 which revealed distributed porosity within the GPZ filament.

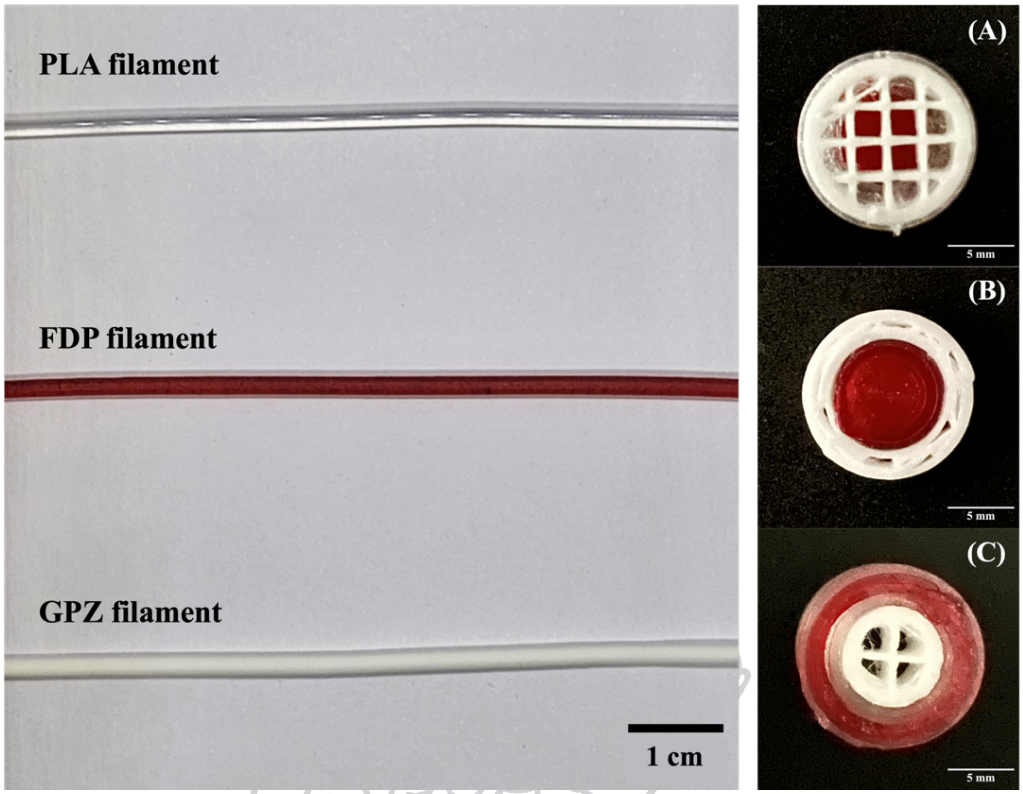

Figure 36. Drug-loaded filaments and resulting FDP-GPZ 3D-printed tablets. Left images: PLA filament, FDP filament, and GPZ filament. Right images: (A) stacked-layer, (B) core-shell (FDP core/GPZ shell), and (C) inverted core-shell (FDP shell/GPZ core) tablet designs.

5.3.2. Physical characterization and drug content analysis of FDP-GPZ 3D-printed tablet

The FDC tablets containing two different drugs, FDP and GPZ, were designed and fabricated using FDM 3D printing in this study. The three tablet structures were designed with different compositions of the FDP layer and GPZ layer, as illustrated in Figure 35. The resulting FDP-GPZ 3D-printed tablets exhibited physical characteristics consistent with their respective design models, as shown in Figures 36A-C. The dimensional analysis of tables was demonstrated a Table 13. The results showed that the actual weight of each drug layer was significantly close to the target value of 100 mg, ranging from 97.02 to 105.03 mg. In addition, the actual dimensions of the tablets were in good agreement with the calculated design values. However, the drug

content analysis revealed an interesting difference between the printed layers and the original filaments. For the FDP layers, the drug content in across three models (5.22 ± 0.57% in Model A, 6.04 ± 0.52% in Model B, and 6.52 ± 0.68% in Model C) was slightly higher the FDP content in the filament (4.92 ± 0.02%). Conversely, the GPZ layers exhibited lower drug content (9.18 ± 0.19% in Model A, 9.41 ± 0.92% in Model B, and 8.99 ± 0.30% in Model C) than that of its filament (11.75 ± 0.32%).

These variations in drug content between the 3D-printed tablets and the filaments can be observed by the slight deviations in mass and dimension of the tablets that occurred during the printing process. The causes of these phenomena might be the material behavior during the printing process. The FDP layers, which were slightly larger and heavier than their theoretical values, likely experienced die swell, also known as extrudate swell or Barus effect. Die swell is a phenomenon where elastic recovery of polymer melts that have been subjected to shear stress during flow through the nozzle, causing the extrudate to expand upon exit [123-125]. This results in a slightly thicker deposited line, leading to a higher overall volume and mass, and consequently, a higher measured drug content [126].

In contrast, the smaller diameter and lighter GPZ layers could be attributed to one or more factors. The first factor was post-extrusion shrinkage due to the GPZ filament's composition, which included KVA 64, TEC, and mannitol. Because TEC can increase polymer chain mobility, accelerating crystallization kinetics and densification during cooling. In addition, mannitol might act as a nucleating agent, promoting faster crystal formation and higher crystallinity, further increasing shrinkage Alternatively, the second factor was the under-extrusion mechanism, where the material flow is marginally less than intended. This mechanism might be caused by plasticizers reducing melt viscosity, but mannitol increases viscosity by disrupting polymer flow, potentially reducing volumetric output during the printing process.

5.3.3. *In vitro* drug release profiles of GPZ layers

The dissolution studies of the GPZ layers across all three tablet designs demonstrated immediate-release characteristics, achieving >80% drug release within 30 minutes and complete release (>95%) within 60 minutes (Figure 37B), satisfying

USP criteria for immediate-release formulations. The immediate drug release behavior of the GPZ layer can be attributed to the tablet's structural design and formulation. The combination of KVA64, a water-soluble polymer, and mannitol, a highly hydrophilic excipient that induced porosity during dissolution, caused the tablet disintegration. Furthermore, TEC enhanced the flexibility of the polymer matrix and also allowing water penetration, resulting in faster drug release [54, 127] .

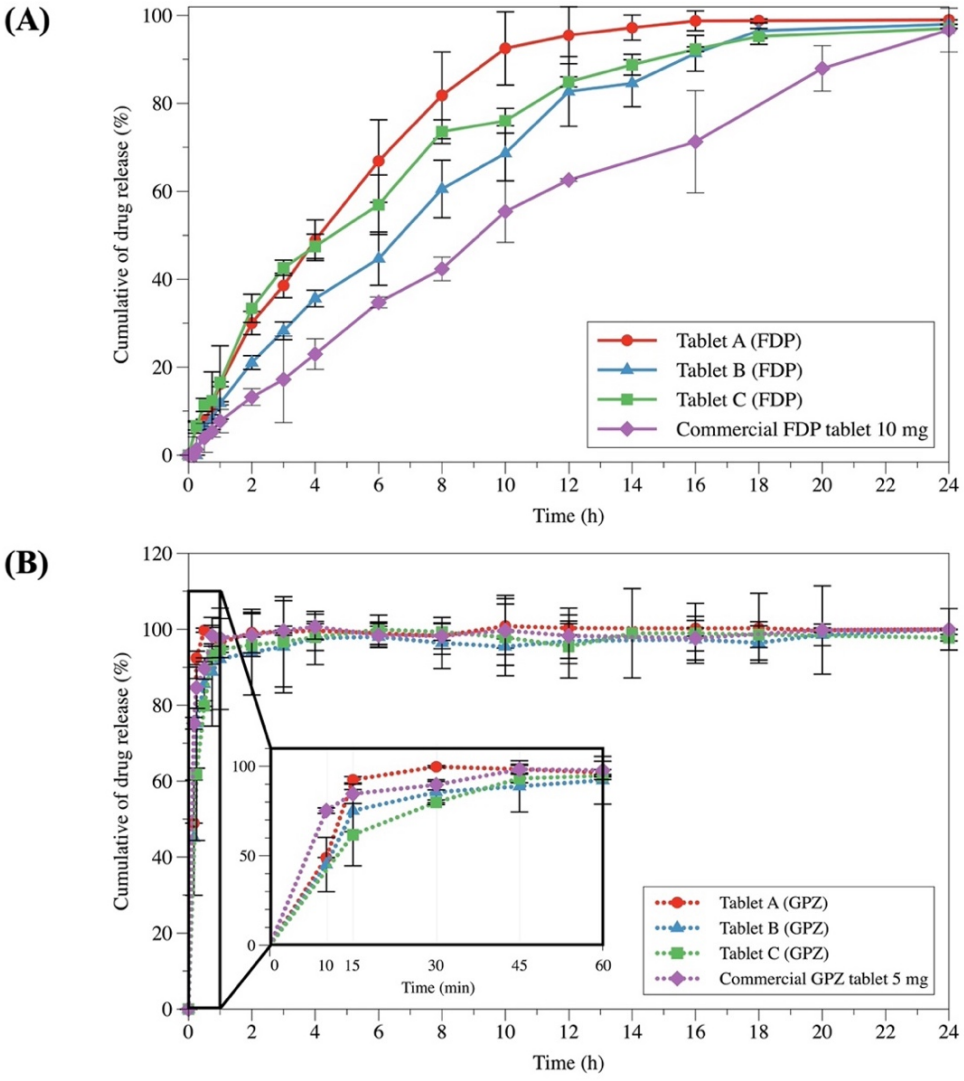

Figure 37. Comparative in vitro dissolution profiles showing cumulative drug release (%) versus time for FDP-GPZ 3D-printed tablets and commercial reference tablets. (A) FDP controlled-release layer; (B) GPZ immediate-release layer.

Table 14. Tablet contact area, tablet volume and surface area-to-volume ratios of FDP-GPZ 3D-printed tablet models calculated using Shapr3D software.

Tablet models	Contact area (mm^2)		Tablet volume (mm^3)		SA/V ratio	
	FDP layer	GPZ layer	FDP layer	GPZ layer	FDP layer	GPZ layer
Tablet A	38.4845	515.4467	81.972	115.7907	0.469	4.452
Tablet B	38.4845	650.6884	81.972	206.1285	0.469	3.157
Tablet C	40.8407	440.0565	81.6814	124.616	0.500	3.531

Structurally, the GPZ layer was designed with a 30% infill density grid pattern, forming an interconnected porous network throughout the tablet. The design of this structure is different from conventional solid tablets by providing 70% void space within the structure. Although the tablets contain only 30% solid material, their design improves the surface area exposed to the dissolution medium. The interconnected channels enable rapid medium penetration into the tablet core, as compared with conventional solid tablets, which dissolve only on the external surface [63, 128].

When the position and design of the GPZ layer in each model was evaluated, the dissolution profiles of all three tablet types showed similarly rapid release patterns. However, Model A showed the fastest initial release, followed by Model C and Model B. The result correlated with the theoretical SA/V ratios calculated using Shapr3D software, as summarized in Table 14: Model A (SA/V = 4.452), Model C (SA/V = 3.531), and Model B (SA/V = 3.157). A higher SA/V ratio implies greater surface exposure relative to volume, which facilitates faster dissolution, as described by the Noyes–Whitney equation [129].

Further investigation indicated that the position and internal porosity of the GPZ layer influenced its relationship with the dissolution medium. Model A, the medium was able to access the surface from all directions which featured a large internal pore structure and the GPZ layer positioned on top. Its rapid drug release was facilitated by the complete exposure of its 515.45 mm^2 surface area to the medium. In contrast, Model B had the largest total surface area (650.69 mm^2), but its GPZ layer encased the FDP core, preventing direct contact with the dissolution medium. The

dissolution efficiency was further diminished by the smaller internal pores in Model B (Figure 37B), which further restricted medium penetration.

Comparison of the drug release profiles of the 3D-printed tablets with a commercial GPZ tablet (Dipazide®) was showed in Table 16. The results revealed that Models A and B had f_2 values below 50, indicating a difference from the commercial profile. In contrast, Model C demonstrated a f_2 value of 60.06, which indicates that its release behavior was similar to that of the commercial product. This similarity might be attributed to the GPZ core structure in Model C, which more closely resembles the disintegration and drug release mechanism of the conventional tablet.

Table 15. Release kinetics of different FDP layer in 3D-printed tablets

Model	Type of Tablet	R^2	AIC	Parameters
Zero-order	Control	0.9980	23.4907	k_0 = 5.421
	Tablet A	0.9197	43.5339	k_0 = 10.296
	Tablet B	0.8951	59.1801	k_0 = 6.480
	Tablet C	0.9765	71.5108	k_0 = 7.046
First-order	Control	0.9793	28.6098	k_1 = 0.074
	Tablet A	0.9752	35.2898	k_1 = 0.188
	Tablet B	0.9736	46.7694	k_1 = 0.120
	Tablet C	0.9747	43.0075	k_1 = 0.160
Higuchi	Control	0.8315	43.2987	k_H = 15.361
	Tablet A	0.9339	43.1497	k_H = 26.790
	Tablet B	0.9269	55.9271	k_H = 21.546
	Tablet C	0.9854	38.0403	k_H = 23.991
Korsmeyer–Peppas	Control	0.9956	18.5764	k = 6.643, n = 0.907
	Tablet A	0.9968	21.7380	k = 17.852, n = 0.723
	Tablet B	0.9880	40.4961	k = 13.500, n = 0.702
	Tablet C	0.9863	39.4788	k = 24.919, n = 0.483
Peppas–Sahlin	Control	0.9944	20.5747	k_1 = 0.259, k_2 = 6.433, m = 0.456
	Tablet A	0.9979	19.2135	k_1 = −23.486, k_2 = 39.514, m = 0.271
	Tablet B	0.9884	40.7951	k_1 = −32.469, k_2 = 41.932, m = 0.237
	Tablet C	0.9880	37.6672	k_1 = 22.624, k_2 = -1.230, m = 0.658
Hopfenberg	Control	0.9953	18.9813	k_{HB} = 0.040
	Tablet A	0.9962	22.8691	k_{HB} = 0.067
	Tablet B	0.9907	38.2074	k_{HB} = 0.038
	Tablet C	0.9710	45.0171	k_{HB} = 0.00006

Note: R^2 = correlation coefficient values, AIC = Akaike information criterion, control tablet is Plendil® 5 mg/tab.

Table 16. Similarity factor (f_2) results for dissolution profile comparison of FDP-loaded 3D-printed tablets.

Comparison	FDP layer tablet		GPZ layer tablet	
	f_2 value	Interpretation	f_2 value	Interpretation
Control tablet vs. Tablet A	27.19	Not accept	46.07	Not accept
Control tablet vs. Tablet B	44.11	Not accept	42.85	Not accept
Control tablet vs. Tablet C	32.19	Not accept	60.06	Accept
Tablet A vs. Tablet B	39.68	Not accept	53.27	Accept
Tablet A vs. Tablet C	53.34	Accept	54.83	Accept
Tablet B vs. Tablet C	48.62	Not accept	55.51	Accept

Note. Control tablets are Plendil® 5 mg/tab and Dipazide® 5 mg/tab.

5.3.4. *In vitro* drug release and kinetic modeling of FDP layers

The *in vitro* dissolution profiles (Figure 37A) reveal that all 3D-printed FDP layers (Models A, B, and C) had a controlled-release pattern over 24 hours, but the rates and extents of release differed from the commercial Plendil® 5 mg tablet. Model A demonstrated the fastest FDP release among the 3D-printed models, achieving nearly complete drug release within 16 hours. Model C exhibited intermediate release. and Model B exhibited the slowest FDP release among the 3D-printed tablets. Although all tablet models were similar in design, with the FDP layer enclosed by a non-dissolving PLA wall and base that allowed drug release only from the top surface, their release behaviors differed significantly. Notably, despite Models A and B having a similar diameter, Model B released the drug at a slower rate than Model A. his result may be attributed to differences in the spatial arrangement and function of the GPZ layer in each model. In Model A, the GPZ layer was attached to the top of the FDP layer. This condition accelerated drug release by allowing the initial hydration of the PVA-based FDP layer [130-132]. Even though this configuration enabled the FDP surface to be exposed to the dissolution medium from the beginning, it lacked a rapidly dissolving overlayer to facilitate initial wetting. Thus, PVA polymer hydration and swelling were slower, which led to delaying FDP release. The FDP layer in Model C displayed a

slower dissolution rate than Model A, which can be attributed to the lower surface area exposed to the dissolution medium.

Table 15 shows an analysis of the mathematical modeling of the release kinetics for the FDP layers in the 3D-printed tablets compared to the commercial Plendil® 5 mg tablet. For the commercial Plendil® tablet, the release data for the control tablet best fit the Korsmeyer-Peppas model ($R^2 = 0.9956$, AIC = 18.5764) with a release exponent of n = 0.907, signifying Super Case-II transport where release is governed by polymer swelling and erosion. For Models A and C, the data for both models were best described by the Peppas-Sahlin model (Model A: $R^2 = 0.9979$, AIC = 19.2135; Model C: $R^2 = 0.9880$, AIC = 37.6672). This result indicated a significant contribution from both Fickian diffusion and Case II transport (polymer chain relaxation) polymer relaxation. This suggests a combined or coupled mechanism where drug release is driven not only by diffusion but also by the structural changes, such as swelling and relaxation, of the polymer matrix upon exposure to the fluid [133]. For Model B, the release profile demonstrated the best fit with the Hopfenberg model ($R^2 = 0.9907$, AIC = 38.2074) which describing drug release from systems undergoing surface erosion, where the rate of release is proportional to the surface area of the tablet. In addition, A crucial observation for Model B was that the R^2 and AIC values for the Korsmeyer-Peppas and Peppas-Sahlin models are also very high and closely ranked. This strongly suggests a complex, multi-factorial release mechanism rather than a single process. The Korsmeyer-Peppas model yields a release exponent of n = 0.702 for this model. For a cylindrical tablet, a value of n between 0.45 and 0.89 indicates Anomalous (non-Fickian) transport, which is defined as a combination of both diffusion and polymer swelling/relaxation mechanisms The best fit of the Peppas-Sahlin model (R^2=0.9884) further corroborates that a combination of diffusion and polymer relaxation was significant. Consequently, the release from FDP model B was best described as a complex process where surface erosion is the dominant rate-limiting step, but it occurs concurrently with, and is influenced by, polymer swelling and drug diffusion.

The analysis of the f_2 values in Table 16 showed that none of the three FDP layer 3D-printed tablets were similar to the dissolution profile of the commercial reference tablet. All f_2 values of FDP layers (Model A, B and C) were below the similarity threshold of 50 (27.19, 44.11, and 32.19, respectively), confirming a

significant dissimilarity. Because the release from the 3D-printed tablets was governed by their unique geometric configurations and surface area-to-volume ratios, a mechanism fundamentally different from the likely complicated matrix system used in the commercial product. Interestingly, the comparisons among the 3D-printed tablets themselves revealed more nuanced relationships. The comparison of Models A and B yielded a f_2 value of 39.68, confirming that their profiles were not similar. whereas Models A and C yielded a f_2 value of 53.34, indicating that their profiles are statistically similar. This suggests that, despite their different initial release patterns, the mathematical shape of their release curves over 24 hours is almost the same. Finally, the comparison of the two core-shell designs, Models B and C, yielded a f_2 value of 48.62, which was just short of similarity. This demonstrated that simply inverting the roles of the FDP and GPZ layers as core or shell is sufficient to generate a statistically distinct release profile.

5.4. Conclusion

This study successfully achieved its objective, demonstrating the proof-of-concept for using FDM 3D printing technology to prepare a fixed-dose combination tablet containing FDP and GPZ, two active pharmaceutical ingredients with distinctly different release profiles within a single dosage form. The process involved the successful and uniform production of FDP-loaded filaments for controlled release and GPZ-loaded filaments for immediate release. These were subsequently fabricated into three different architectural designs: a stacked-layer, a core-shell, and an inverted core-shell model, all of which exhibited high physical accuracy when compared to their digital counterparts. The results indicated that the structure of the tablet directly influences drug release kinetics. All GPZ layer models achieved immediate release, with the rate correlating to the SA/V ratio of each individual design. Furthermore, the FDP layer provided a sustained release over 24 hours, with mechanisms that were highly dependent on the tablet's architecture. Kinetic modeling revealed that FDP release from Models A and C was best described by the Peppas-Sahlin model, indicating a combined mechanism of Fickian diffusion and polymer relaxation. In contrast, Model B followed a more complex process best fitted to the Hopfenberg

model, suggesting that surface erosion was the dominant rate-limiting step, occurring concurrently with drug diffusion and polymer swelling. Notably, the Model C tablet (GPZ core/FDP shell) was the only design to exhibit a GPZ release profile similar to the commercial reference product (f_2=60.06), whereas the FDP release from all models differed significantly from its commercial reference.

CHAPTER 6
SUMMARY AND GENERAL CONCLUSION

This study successfully demonstrated the comprehensive development of 3D-printed pharmaceutical tablets using FDM technology for the treatment of chronic diseases. The research addressed a critical healthcare challenge—improving patient compliance in managing multiple chronic conditions such as hypertension and diabetes—by developing innovative drug delivery systems that combine personalized dosing capabilities with controlled release profiles.

The first study (Chapter 3) focused on development of a controlled-release 3D printing tablet for FDP which a poorly water-soluble antihypertensive agent. The objective of the study is to fabricate internal tablet geometry on drug release kinetics. A drug-loaded filament consisting of FDP and PVA, a water-soluble polymer, was prepared using HME. This filament was used to print the drug core, which was enclosed within a non-soluble PLA shell. The FDP 3D-printed tablets were fabricated with four different internal surface geometries (round, square, hexagonal, and triangular) with maintaining constant volume. The critical discovery was that drug release was not simply dependent on surface area but rather governed by the SA/V ratio. Tablets with round geometry exhibited the highest SA/V ratio (0.55) and fastest drug release. Whereas triangular designs showed the lowest SA/V ratio (0.41) and slowest drug release. Mathematical modeling of release kinetics found that all formulations followed the Peppas-Sahlin model, indicating a swelling-controlled mechanism where polymer relaxation dominate over Fickian diffusion ($k_2 > k_1$ in all cases). This finding was further validated by similarity factor analysis, where tablets with comparable SA/V ratios demonstrated statistically similar dissolution profiles ($f_2 > 50$), establishing a predictive relationship between inner surface geometry of tablet and drug release behavior. To demonstrate dose flexibility, triangular geometry tablets were selected for dosage adjustment studies. By doubling the inner compartment volume from 79.97 mm^3 (TX) to 159.94 mm^3 (T2X), the felodipine dose could be precisely increased from 5 mg to 10 mg while maintaining controlled release characteristics. The larger T2X tablets showed slightly extended-release profiles due to their lower SA/V ratio (0.26)

compared to TX tablets (0.41), confirming that both dose and release kinetics could be independently controlled through geometric design. Furthermore, long-term stability studies (12 months at 28°C/40% RH) confirmed that the 3D-printed tablets maintained their drug content without significant degradation.

The second study (Chapter 4) aimed to develop a GDZ immediate-release 3D-printed tablet using a low-temperature FDM process to ensure drug stability under processing at only 60°C for filament extrusion and 90°C for printing. Because the chemical structure of GPZ could be changed when exposed to high temperatures. The optimized filament comprised 12% GPZ, 69% KVA64, 10% mannitol, and 9% TEC, demonstrating excellent mechanical properties and printability. The investigation of a systematically factorial design evaluated the influence of critical 3D printing parameters, such as infill pattern, shell number, and layer thickness, on drug release. The optimal conditions for rapid release were identified as a grid infill pattern, a single shell, and the thickest layer height (0.3 mm), a combination that maximized internal porosity and the surface area available for contact with the dissolution medium. Furthermore, a mathematical model was successfully employed to accurately adjust tablet thickness to produce various dosage (5, 7.5, 10, and 15 mg). Interestingly, the dissolution revealed that increasing the dosage by increasing thickness led to a slower drug release rate. As a result, the SA/V ratio of the tablet affects the efficient contact with the dissolution media and the timing of drug release.

The final study (Chapter 5) involved developing fixed-dose combination tablets that integrated both controlled-release FDP 3D-printed tablets (Chapter 3) and immediate-release GPZ 3D-printed tablets within a single dosage form. Three distinct tablet designs were investigated including a stacked-layer model, (2) a core-shell model with an FDP core and a GPZ shell, and (3) an inverted core-shell model with a GPZ core and an FDP shell. Experimental results confirmed that all three different dual-drug release success models achieved their intended release patterns. All GPZ layer designs consistently exhibited immediate release (>80% within 30 minutes), with release rates collimating to SA/V ratios. In contrast, the FDP layer exhibited controlled release over 24 hours. However, the mechanisms involved are dependent on the design. The stacked-layer design (Model A) showed the fastest FDP release due to enhanced polymer hydration from the overlying GPZ layer. Whereas the core-shell design (Model

B) demonstrated the slowest release, described by the Hoffenberg model indicating surface erosion and the colocation with the Korsmeyer-Peppas and Peppas-Sahlin models. Therefore, the release from FDP model B was best described as a complex process where surface erosion is the dominant rate-limiting step, but it occurs concurrently with, and is influenced by, polymer swelling and drug diffusion. Notably, the inverted care-shell design (Model C) produced a GPZ release profile statistically similar to commercial tablets (f_2 = 60.06), suggesting it could be a comparable option for formulation. The GPZ layer consistently exhibited immediate release (>80% within 30 minutes) which is similar to commercial drug product.

In conclusion, this research successfully demonstrates the flexibility and profound potential of FDM 3D printing technology for developing complex pharmaceutical dosage forms. By processing from controlling release via surface geometry to achieving immediate release by tuning printing parameters and culminating in the facilitation of a sophisticated dual-release polypill, this work provides a significant proof of concept. The findings give rise to the development of personalized medicine tailored to individual patient needs, which could ultimately lead to improved patient compliance and therapeutic efficacy in long-term treatment.

Future direction of research

The successful establishment of FDM 3D printing principles for pharmaceutical tablets in this thesis opens multiple promising research avenues. Clinical translation remains the immediate priority, requiring bioequivalence studies, quality control protocol development, and regulatory guideline establishment for personalized medicines. Advanced material development should focus on creating pharmaceutical-grade filaments with enhanced capabilities including taste-masking, stimuli-responsive properties, and higher drug loading capacities. Building upon the fixed-dose combination concept, future investigations could explore multi-drug tablets containing three or more active ingredients with independent release profiles, including pulsatile and chronotherapeutic patterns for specific clinical needs. The integration of artificial intelligence and machine learning algorithms could revolutionize tablet design by predicting drug release profiles based on geometric and material parameters, enabling rapid personalization according to patient-specific pharmacokinetics. Point-of-care

manufacturing systems need development to bring this technology directly to pharmacies and hospitals, with automated systems capable of converting prescriptions into customized tablets. Special attention should be given to vulnerable populations through pediatric and geriatric formulations, including mini-tablets and orodispersible films to address swallowing difficulties. Finally, sustainability considerations through biodegradable polymers and recycling protocols will ensure environmental responsibility. As 3D printing technology converges with pharmaceutical sciences, the integration of these advanced approaches will fundamentally transform medicine manufacturing and delivery, ultimately enhancing therapeutic outcomes and quality of life for patients managing chronic diseases.

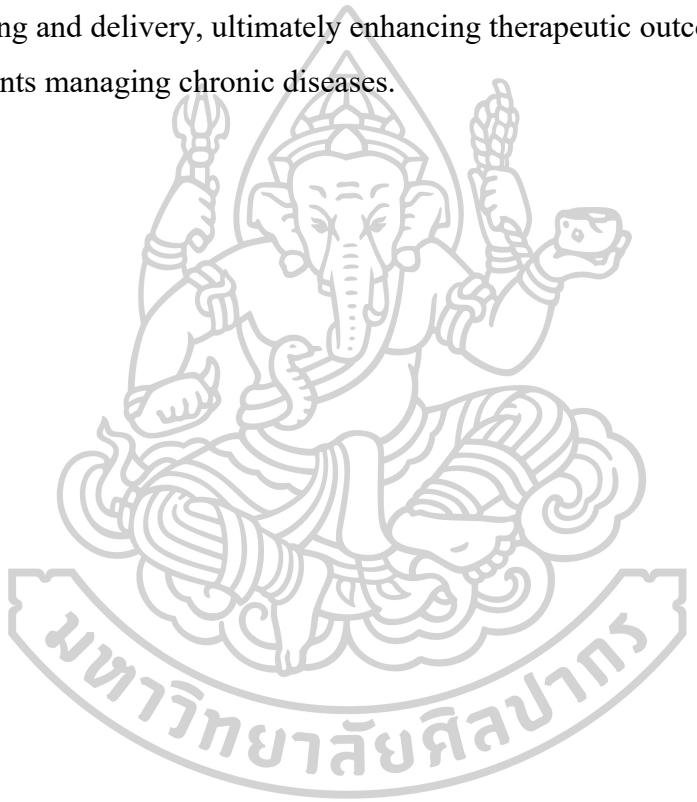

REFERENCES

1. Annaji M, Ramesh S, Poudel I, Govindarajulu M, Arnold RD, Dhanasekaran M, et al. Application of extrusion-based 3d printed dosage forms in the treatment of chronic diseases. J Pharm Sci 2020;109:3551-68.
2. Acosta-Vélez GF, Wu BM. 3D pharming: direct printing of personalized pharmaceutical tablets. Polym Sci 2016;2.
3. Alhnan MA, Okwuosa TC, Sadia M, Wan KW, Ahmed W, Arafat B. Emergence of 3D printed dosage forms: opportunities and challenges. Pharm Res 2016;33:1817-32.
4. Palo M, Holländer J, Suominen J, Yliruusi J, Sandler N. 3D printed drug delivery devices: perspectives and technical challenges. Expert Rev Med Devices 2017;14:685-96.
5. Awad A, Gaisford S, Basit AW. Fused deposition modelling: advances in engineering and medicine. In: Basit AW, Gaisford S, editors. 3D Printing of Pharmaceuticals. Cham: Springer International Publishing; 2018. p. 107-32.
6. Klein GT, Lu Y, Wang MY. 3D printing and neurosurgery--ready for prime time? World Neurosurg 2013;80:233-5.
7. Chia HN, Wu BM. Recent advances in 3D printing of biomaterials. J Biol Eng 2015;9:4.
8. Jakab K, Neagu A, Mironov V, Markwald RR, Forgacs G. Engineering biological structures of prescribed shape using self-assembling multicellular systems. Proc Natl Acad Sci USA 2004;101:2864-9.
9. Barron JA, Ringeisen BR, Kim H, Spargo BJ, Chrisey DB. Application of laser printing to mammalian cells. Thin Solid Films 2004;453-454:383-7.
10. Duan B, Hockaday LA, Kang KH, Butcher JT. 3D bioprinting of heterogeneous aortic valve conduits with alginate/gelatin hydrogels. J Biomed Mater Res A 2013;101:1255-64.
11. Goole J, Amighi K. 3D printing in pharmaceutics: A new tool for designing customized drug delivery systems. Int J Pharm 2016;499:376-94.
12. Roopavath U, Kalaskar D. Introduction to 3D printing in medicine. 2017. p. 1-10.
13. Xu X, Awad A, Robles-Martinez P, Gaisford S, Goyanes A, Basit AW. Vat photopolymerization 3D printing for advanced drug delivery and medical device applications. J Control Release 2021;329:743-57.

14. Pagac M, Hajnys J, Ma Q-P, Jancar L, Jansa J, Stefek P, et al. A Review of Vat Photopolymerization Technology: Materials, Applications, Challenges, and Future Trends of 3D Printing. Polymers 2021;13:598.

15. Murphy C, Lim K, Woodfield T. Next evolution in organ-scale biofabrication: bioresin design for rapid high-resolution vat polymerization. Adv Mater 2022;34.

16. Sing SL, An J, Yeong WY, Wiria FE. Laser and electron-beam powder-bed additive manufacturing of metallic implants: A review on processes, materials and designs. J Orthop Res 2016;34:369-85.

17. Fina F, Goyanes A, Madla CM, Awad A, Trenfield SJ, Kuek JM, et al. 3D printing of drug-loaded gyroid lattices using selective laser sintering. Int J Pharm 2018;547:44-52.

18. Gueche YA, Sanchez-Ballester NM, Cailleaux S, Bataille B, Soulairol I. Selective laser sintering (SLS), a new chapter in the production of solid oral forms (SOFs) by 3D printing. Pharmaceutics 2021;13:1212.

19. Mancilla-De-la-Cruz J, Rodriguez-Salvador M, An J, Chua CK. Three-dimensional printing technologies for drug delivery applications: processes, materials, and effects. Int J Bioprint 2022;8:622.

20. Wang Y, Müllertz A, Rantanen J. Additive manufacturing of solid products for oral drug delivery using binder jetting three-dimensional printing. AAPS PharmSciTech 2022;23:196.

21. Kozakiewicz-Latała M, Nartowski KP, Dominik A, Malec K, Gołkowska AM, Złocińska A, et al. Binder jetting 3D printing of challenging medicines: From low dose tablets to hydrophobic molecules. Eur J Pharm Biopharm 2022;170:144-59.

22. Acosta-Vélez GF, Linsley CS, Zhu TZ, Wu W, Wu BM. Photocurable bioinks for the 3D pharming of combination therapies. Polymers (Basel) 2018;10.

23. Trenfield SJ, Madla CM, Basit AW, Gaisford S. Binder jet printing in pharmaceutical manufacturing. In: Basit AW, Gaisford S, editors. 3D Printing of Pharmaceuticals. Cham: Springer International Publishing; 2018. p. 41-54.

24. Pervaiz S, Qureshi TA, Kashwani G, Kannan S. 3D printing of fiber-reinforced plastic composites using fused deposition modeling: a status review. Materials 2021;14:4520.

25. Majrashi MAA, Yahya EB, Mushtaq RY, H.P.S AK, Rizg WY, Alissa M, et al. Revolutionizing drug delivery: Exploring the impact of advanced 3D printing technologies on polymer-based systems. J Drug Deliv Sci Tech 2024;98:105839.

26. Zhang X, Xu Y, Li L, Yan B, Bao J, Zhang A. Acrylate-based photosensitive resin for stereolithographic three-dimensional printing. J Appl Polym Sci 2019;136:47487.

27. Han W, Kong L, Xu M. Advances in selective laser sintering of polymers. Int J Extrem Manuf 2022;4:042002.

28. Khaled SA, Burley JC, Alexander MR, Yang J, Roberts CJ. 3D printing of five-in-one dose combination polypill with defined immediate and sustained release profiles. J Contr Release 2015;217:308-14.

29. Sadia M, Isreb A, Abbadi I, Isreb M, Aziz D, Selo A, et al. From ‘fixed dose combinations’ to ‘a dynamic dose combiner’: 3D printed bi-layer antihypertensive tablets. Eur J Pharm Sci 2018;123:484-94.

30. Gioumouxouzis CI, Baklavaridis A, Katsamenis OL, Markopoulou CK, Bouropoulos N, Tzetzis D, et al. A 3D printed bilayer oral solid dosage form combining metformin for prolonged and glimepiride for immediate drug delivery. Eur J Pharm Sci 2018;120:40-52.

31. Pereira BC, Isreb A, Forbes RT, Dores F, Habashy R, Petit J-B, et al. ‘Temporary Plasticiser’: A novel solution to fabricate 3D printed patient-centred cardiovascular ‘Polypill’ architectures. Eur J Pharm Biopharm 2019;135:94-103.

32. Trenfield SJ, Tan HX, Goyanes A, Wilsdon D, Rowland M, Gaisford S, et al. Non-destructive dose verification of two drugs within 3D printed polyprintlets. Int J Pharm 2020;577:119066.

33. Xu X, Robles-Martinez P, Madla CM, Joubert F, Goyanes A, Basit AW, et al. Stereolithography (SLA) 3D printing of an antihypertensive polyprintlet: Case study of an unexpected photopolymer-drug reaction. Addit Manuf 2020;33:101071.

34. Khaled SA, Burley JC, Alexander MR, Yang J, Roberts CJ. 3D printing of tablets containing multiple drugs with defined release profiles. Int J Pharm 2015;494:643-50.

35. Zhu C, Tian Y, Zhang E, Gao X, Zhang H, Liu N, et al. Semisolid Extrusion 3D Printing of Propranolol Hydrochloride Gummy Chewable Tablets: an Innovative Approach to Prepare Personalized Medicine for Pediatrics. AAPS PharmSciTech 2022;23:166.

36. Goyanes A, Madla CM, Umerji A, Duran Piñeiro G, Giraldez Montero JM, Lamas Diaz MJ, et al. Automated therapy preparation of isoleucine formulations using 3D printing for the treatment of MSUD: First single-centre, prospective, crossover study in patients. Int J Pharm 2019;567:118497.

37. Goh O, Goh WJ, Lim SH, Hoo GS, Liew R, Ng TM. Preferences of healthcare professionals on 3d-printed tablets: a pilot study. Pharmaceutics 2022;14:1521.

38. Isreb A, Baj K, Wojsz M, Isreb M, Peak M, Alhnan MA. 3D printed oral theophylline doses with innovative 'radiator-like' design: Impact of polyethylene oxide (PEO) molecular weight. Int J Pharm 2019;564:98-105.

39. Jin Y-a, Li H, He Y, Fu J-z. Quantitative analysis of surface profile in fused deposition modelling. Addit Manuf 2015;8:142-8.

40. Long J, Gholizadeh H, Lu J, Bunt C, Seyfoddin A. Application of fused deposition modelling (FDM) method of 3D printing in drug delivery. Curr Pharm Des 2017;23:433-9.

41. Cunha-Filho M, Araújo MR, Gelfuso GM, Gratieri T. FDM 3D printing of modified drug-delivery systems using hot melt extrusion: a new approach for individualized therapy. Ther Deliv 2017;8:957-66.

42. Wei C, Solanki N, Vasoya J, Shah A, Serajuddin A. Development of 3D printed tablets by fused deposition modeling using polyvinyl alcohol as polymeric matrix for rapid drug release. J Pharm Sci 2020.

43. Kollamaram G, Croker DM, Walker GM, Goyanes A, Basit AW, Gaisford S. Low temperature fused deposition modeling (FDM) 3D printing of thermolabile drugs. Int J Pharm 2018;545:144-52.

44. Fanous M, Gold S, Hirsch S, Ogorka J, Imanidis G. Development of immediate release (IR) 3D-printed oral dosage forms with focus on industrial relevance. Eur J Pharm Sci 2020:105558.

45. Cuiffo M, Snyder J, Elliott A, Romero N, Kannan S, Halada G. Impact of the fused deposition (FDM) printing process on polylactic acid (PLA) chemistry and structure. Appl Sci 2017;7:579.

46. Da Silva Siqueira A, Braga NF, Muñoz PAR, De Freitas LF, Ferreira AH, Fechine G. Biodegradable scaffold: integration of polylactic acid, hydroxyapatite, and graphene oxide via FDM 3D printing. Express Polymer Letters 2024.

47. Pérez-Davila S, Garrido-Gulías N, González-Rodríguez L, López-Álvarez M, Serra J, López-Periago J, et al. Physicochemical properties of 3D-printed polylactic acid/hydroxyapatite scaffolds. Polymers 2023;15.

48. Korte C, Quodbach J. Formulation development and process analysis of drug-loaded filaments manufactured via hot-melt extrusion for 3D-printing of medicines. Pharm Dev Technol 2018;23:1117-27.

49. Tran N-H, Nguyen V-N, Ngo A-V, Nguyen C. Study on the effect of fused deposition modeling (FDM) process parameters on the printed part quality. Int J Eng Res Appl 2017:71-7.

50. Patil H, Tiwari RV, Repka MA. Hot-melt extrusion: from theory to application in pharmaceutical formulation. AAPS PharmSciTech 2016;17:20-42.

51. Fuenmayor E, Forde M, Healy AV, Devine DM, Lyons JG, McConville C, et al. Material considerations for fused-filament fabrication of solid dosage forms. Pharmaceutics 2018; 10(2).

52. Omnexus. Elongation at Yield 2025 [cited 2025 6 July 2025]. Available from: https://omnexus.specialchem.com/polymer-property/elongation-at-yield.

53. Bandari S, Nyavanandi D, Dumpa N, Repka MA. Coupling hot melt extrusion and fused deposition modeling: Critical properties for successful performance. Adv Drug Deliv Rev 2021;172:52-63.

54. Zhang J, Feng X, Patil H, Tiwari RV, Repka MA. Coupling 3D printing with hot-melt extrusion to produce controlled-release tablets. Int J Pharm 2017;519:186-97.

55. Zhang J, Xu P, Vo AQ, Bandari S, Yang F, Durig T, et al. Development and evaluation of pharmaceutical 3D printability for hot melt extruded cellulose-based filaments. J Drug Deliv Sci Tech 2019;52:292-302.

56. Xu P, Li J, Meda A, Osei-Yeboah F, Peterson ML, Repka M, et al. Development of a quantitative method to evaluate the printability of filaments for fused deposition modeling 3D printing. Int J Pharm 2020;588:119760.

57. Wang H, Dumpa N, Bandari S, Durig T, Repka MA. Fabrication of taste-masked donut-shaped tablets via fused filament fabrication 3D printing paired with hot-melt extrusion techniques. AAPS PharmSciTech 2020;21:243.

58. Nasereddin JM, Wellner N, Alhijjaj M, Belton P, Qi S. Development of a simple mechanical screening method for predicting the feedability of a pharmaceutical FDM 3D printing filament. Pharm Res 2018;35:151.

59. Wang T-M, Xi J-T, Jin Y. A model research for prototype warp deformation in the FDM process. Int J Adv Manuf Tech 2007;33:1087-96.

60. Roberson DA. Comparison of extruder systems for 3D printer filament fabrication: University of Texas at El Paso; 2017.

61. Christiyan KGJ, Chandrasekhar U, Venkateswarlu K. A study on the influence of process parameters on the mechanical properties of 3D printed ABS composite. IOP Conference Series: Materials Science and Engineering 2016;114:012109.

62. Comotti C, Regazzoni D, Rizzi C, Vitali A. Additive manufacturing to advance functional design: an application in the medical field. J Comput Inf Sci Eng 2017;17.

63. Goyanes A, Buanz ABM, Basit AW, Gaisford S. Fused-filament 3D printing (3DP) for fabrication of tablets. Int J Pharm 2014;476:88-92.

64. APhA APA. Drug Information Handbook with International Trade Names Index. 23, editor. Hudson, Ohio: Lexi-Comp Inc; 2014. 2663 p.

65. Bethesda. PubChem Compound Summary for CID 3333, Felodipine.: National Library of Medicine (US), National Center for Biotechnology Information; 2025 [cited 2025 6 July]. Available from: https://pubchem.ncbi.nlm.nih.gov/compound/Felodipine.

66. Bethesda. PubChem Compound Summary for CID 3478, Glipizide: National Library of Medicine (US), National Center for Biotechnology Information; 2025 [cited 2025 5 July]. Available from: https://pubchem.ncbi.nlm.nih.gov/compound/3478.

67. Durga Prasad Reddy R, Sharma V. Additive manufacturing in drug delivery applications: A review. Int J Pharm 2020;589:119820.

68. Shahrubudin N, Lee TC, Ramlan R. An Overview on 3D printing technology: technological, materials, and applications. Procedia Manuf 2019;35:1286-96.

69. Norman J, Madurawe RD, Moore CM, Khan MA, Khairuzzaman A. A new chapter in pharmaceutical manufacturing: 3D-printed drug products. Adv Drug Deliv Rev 2017;108:39-50.

70. Pereira GG, Figueiredo S, Fernandes AI, Pinto JF. Polymer selection for hot-melt extrusion coupled to fused deposition modelling in pharmaceutics. Pharmaceutics 2020;12.

71. Patel SK, Khoder M, Peak M, Alhnan MA. Controlling drug release with additive manufacturing-based solutions. Adv Drug Deliv Rev 2021;174:369-86.

72. Shadambikar G, Kipping T, Di-Gallo N, Elia AG, Knüttel AN, Treffer D, et al. Vacuum compression molding as a screening tool to investigate carrier suitability for hot-melt extrusion formulations. Pharmaceutics 2020;12.

73. Merck. Parteck® MXP two polymers, unparalleled value. 2022 [cited 2025 6 July]. Available from: https://www.sigmaaldrich.com/deepweb/assets/sigmaaldrich/product/documents/943/464/parteck-mxp-br9695en-mk.pdf.

74. Paarakh MP, Jose PA, Setty C, Peterchristoper G. Release kinetics–concepts and applications. Int J Pharm Res Technol 2018;8:12-20.

75. Bruschi ML. Mathematical models of drug release. Woodhead Publishing Cambridge, UK; 2015. p. 63-86.

76. Zhang Y, Huo M, Zhou J, Zou A, Li W, Yao C, et al. DDSolver: an add-in program for modeling and comparison of drug dissolution profiles. AAPS J 2010;12:263-71.

77. Crișan AG, Porfire A, Ambrus R, Katona G, Rus LM, Porav AS, et al. Polyvinyl alcohol-based 3D printed tablets: novel insight into the influence of polymer particle size on filament preparation and drug release performance. Pharmaceuticals 2021;14:418.

78. Li R, Pan Y, Chen D, Xu X, Yan G, Fan T. Design, preparation and in vitro evaluation of core–shell fused deposition modelling 3D-printed verapamil hydrochloride pulsatile tablets. Pharmaceutics 2022;14:437.

79. Goyanes A, Buanz AB, Hatton GB, Gaisford S, Basit AW. 3D printing of modified-release aminosalicylate (4-ASA and 5-ASA) tablets. Eur J Pharm Biopharm 2015;89:157-62.

80. Li Q, Wen H, Jia D, Guan X, Pan H, Yang Y, et al. Preparation and investigation of controlled-release glipizide novel oral device with three-dimensional printing. Int J Pharm 2017;525:5-11.

81. He Y, Zhan C, Pi C, Zuo Y, Yang S, Hu M, et al. Enhanced oral bioavailability of felodipine from solid lipid nanoparticles prepared through effervescent dispersion technique. AAPS PharmSciTech 2020;21:1-10.

82. Tapas A, Kawtikwar P, Sakarkar D. Enhanced dissolution rate of felodipine using spherical agglomeration with Inutec SP1 by quasi emulsion solvent diffusion method. Res Pharm Sci 2009;4:77.

83. Du Plessis A, Yadroitsev I, Yadroitsava I, Le Roux SG. X-ray microcomputed tomography in additive manufacturing: a review of the current technology and applications. 3D Print Addit Manuf 2018;5:227-47.

84. Cano S, Lube T, Huber P, Gallego A, Naranjo JA, Berges C, et al. Influence of the infill orientation on the properties of zirconia parts produced by fused filament fabrication. Materials 2020;13:3158.

85. Utz J, Zubizarreta J, Geis N, Immonen K, Kangas H, Ruckdäschel H. 3D printed cellulose-based filaments—processing and mechanical properties. Materials 2022, 15, 6582.

86. Quodbach J, Bogdahn M, Breitkreutz J, Chamberlain R, Eggenreich K, Elia AG, et al. Quality of FDM 3D printed medicines for pediatrics: considerations for formulation development, filament extrusion, printing process and printer design. Ther Innov Regul Sci 2021:1-19.

87. Goyanes A, Kobayashi M, Martínez-Pacheco R, Gaisford S, Basit AW. Fused-filament 3D printing of drug products: microstructure analysis and drug release characteristics of PVA-based caplets. Int J Pharm 2016;514:290-5.

88. Kadry H, Al-Hilal TA, Keshavarz A, Alam F, Xu C, Joy A, et al. Multi-purposable filaments of HPMC for 3D printing of medications with tailored drug release and timed-absorption. Int J Pharm 2018;544:285-96.

89. Sriamornsak P, Nunthanid J, Cheewatanakornkool K, Manchun S. Effect of drug loading method on drug content and drug release from calcium pectinate gel beads. AAPS PharmSciTech 2010;11:1315-9.

90. Windolf H, Chamberlain R, Quodbach J. Predicting drug release from 3D printed oral medicines based on the surface area to volume ratio of tablet geometry. Pharmaceutics 2021;13:1453.

91. Bacaita E, Ciobanu B, Popa M, Agop M, Desbrieres J. Phases in the temporal multiscale evolution of the drug release mechanism in IPN-type chitosan based hydrogels. Phys Chem Chem Phys 2014;16:25896-905.

92. Baggi RB, Kilaru NB. Calculation of predominant drug release mechanism using Peppas-Sahlin model, Part-I (substitution method): A linear regression approach. Asian J Pharm Sci 2016;6:223-30.

93. Thanawuth K, Sutthapitaksakul L, Konthong S, Suttiruengwong S, Huanbutta K, Dass CR, et al. Impact of drug loading method on drug release from 3D-printed tablets made from filaments fabricated by hot-melt extrusion and impregnation processes. Pharmaceutics 2021;13:1607.

94. Colombo P, Bettini R, Santi P, De Ascentiis A, Peppas N. Analysis of the swelling and release mechanisms from drug delivery systems with emphasis on drug solubility and water transport. J Control Release 1996;39:231-7.

95. Gorkem Buyukgoz G, Soffer D, Defendre J, Pizzano GM, Davé RN. Exploring tablet design options for tailoring drug release and dose via fused deposition modeling (FDM) 3D printing. Int J Pharm 2020;591:119987.

96. Alzahrani A, Narala S, Adel Ali Youssef A, Nyavanandi D, Bandari S, Mandati P, et al. Fabrication of a shell-core fixed-dose combination tablet using fused deposition modeling 3D printing. Eur J Pharm Biopharm 2022;177:211-23.

97. Fanous M, Bitar M, Gold S, Sobczuk A, Hirsch S, Ogorka J, et al. Development of immediate release 3D-printed dosage forms for a poorly water-soluble drug by fused deposition modeling: Study of morphology, solid state and dissolution. Int J Pharm 2021;599:120417.

98. Melocchi A, Parietti F, Loreti G, Maroni A, Gazzaniga A, Zema L. 3D printing by fused deposition modeling (FDM) of a swellable/erodible capsular device for oral pulsatile release of drugs. J Drug Deliv Sci Technol 2015;30:360-7.

99. Afkhami S, Abdi M, Baserinia R. Effect of geometry on the dissolution behaviour of complex additively manufactured tablets. J Manuf Mater Process 2025;9:11.

100. McDonagh T, Belton P, Qi S. An investigation into the effects of geometric scaling and pore structure on drug dose and release of 3D printed solid dosage forms. Eur J Pharm Biopharm 2022;177:113-25.

101. Pflieger T, Venkatesh R, Dachtler M, Cooke K, Laufer S, Lunter D. Influence of design parameters on sustained drug release properties of 3D-printed theophylline tablets. Int J Pharm 2024;658:124207.

102. Bruni G, Ghione I, Berbenni V, Cardini A, Capsoni D, Girella A, et al. The physico-chemical properties of glipizide: new findings. Molecules 2021;26:3142.

103. Systems SM. Spaghetti Flexure Rig 2025 [Available from: https://www.stablemicrosystems.com/texture-analysis/attachments/spaghetti-flexure-rig/#imageGallery.

104. Ikeda Y, Wada Y, Matoba Y, Murakami S, Kohjiya S. Characterization of comb-shaped high molecular weight poly(oxyethylene) with tri(oxyethylene) side chains for a polymer solid electrolyte. Electrochim Acta 2000;45:1167-74.

105. Costello MA, Liu J, Wang Y, Qin B, Xu X, Li Q, et al. Manufacturing dexamethasone intravitreal implants: Process control and critical quality attributes. Int J Pharm 2023;647:123515.

106. Ghalanbor Z, Körber M, Bodmeier R. Protein release from poly(lactide-co-glycolide) implants prepared by hot-melt extrusion: Thioester formation as a reason for incomplete release. Int J Pharm 2012;438:302-6.

107. Meißner P, Watschke H, Winter J, Vietor T. Artificial neural networks-based material parameter identification for numerical simulations of additively manufactured parts by material extrusion. Polymers 2020;12:2949.

108. Scott CE, Macosko CW. Morphology development during the initial stages of polymer-polymer blending. Polymer 1995;36:461-70.

109. Tidau M, Finke JH. Dispersion state analysis in hot melt extruded, highly drug-loaded 3D printing filaments applying Raman microscopy. RPS Pharm Pharmacol Rep 2024;3.

110. Kaialy W, Ticehurst M, Nokhodchi A. Dry powder inhalers aerosolisation performance enhancement by carrier mannitol recrystallisation 2010.

111. Zhao C, Jin C, Gao H, Wang L, Liu H, He Z. Effect of raw material variability of glipizide on the in vitro dissolution rate and in vivo bioavailability performance: The importance of particle size. Asian J Pharm Sci 2018;14.

112. Prakash O, Krishan B, G. J. Synthesis, spectral characterization and X-ray diffraction studies of cerium complex of glipizide, an oral antidiabetic drug. Orient J Chem 2013;29.

113. Nunes C, Suryanarayanan R, Botez CE, Stephens PW. Characterization and crystal structure of d-mannitol hemihydrate. J Pharm Sci 2004;93:2800-9.

114. Cheung BM, Li C. Diabetes and hypertension: is there a common metabolic pathway? Curr Atheroscler Rep 2012;14:160-6.

115. Cutler RL, Fernandez-Llimos F, Frommer M, Benrimoj C, Garcia-Cardenas V. Economic impact of medication non-adherence by disease groups: a systematic review. BMJ Open 2018;8:e016982.

116. Gupta AK, Arshad S, Poulter NR. Compliance, safety, and effectiveness of fixed-dose combinations of antihypertensive agents: a meta-analysis. Hypertension 2010;55:399-407.

117. Muhamad H, Bashir AB, Charlton-Harrison J, Abdulhussain R, Mawla N, Patel K, et al. Hot-melt extruded-FDM 3D-printed polyethylene oxide tablets: Dissolution imaging analysis of swelling and drug release. Eur J Pharm Biopharm 2025;208:114636.

118. Raje V, Palekar S, Banella S, Patel K. Tunable drug release from fused deposition modelling (FDM) 3D-printed tablets fabricated using a novel extrudable polymer. Pharmaceutics 2022;14:2192.

119. Sadia M, Sośnicka A, Arafat B, Isreb A, Ahmed W, Kelarakis A, et al. Adaptation of pharmaceutical excipients to FDM 3D printing for the fabrication of patient-tailored immediate release tablets. Int J Pharm 2016;513:659-68.

120. Jamróz W, Szafraniec-Szczęsny J, Kurek M, Jachowicz R. 3D printing in pharmaceutical and medical applications – recent achievements and challenges. Pharm Res 2018;35.

121. Maniruzzaman M, Boateng JS, Snowden MJ, Douroumis D. A review of hot-melt extrusion: process technology to pharmaceutical products. ISRN Pharm 2012;2012:436763.

122. BASF. Safety data sheet Kollidon® VA 64 Fine: BASF Corporation or BASF AG; 2004 [cited 2025 6 July]. Available from: https://www.stobec.com/DATA/PRODUIT/1844~v~msds_8326.pdf.

123. Colon AR, Kazmer DO, Peterson AM, Seppala JE. Characterization of die-swell in thermoplastic material extrusion. Addit Manuf 2023;73:103700.

124. Spanjaards MMA, Hulsen MA, Anderson PD. Die shape optimization for extrudate swell using feedback control. J Nonnewton Fluid Mech 2021;293:104552.

125. Tranová T, Pyteraf J, Kurek M, Jamróz W, Brniak W, Spálovská D, et al. Fused deposition modeling as a possible approach for the preparation of orodispersible tablets. Pharmaceuticals (Basel) 2022;15.

126. Khan S, Ranjha NM. Effect of degree of cross-linking on swelling and on drug release of low viscous chitosan/poly(vinyl alcohol) hydrogels. Polym Bull 2014;71:2133-58.

127. Kempin W, Domsta V, Brecht I, Semmling B, Tillmann S, Weitschies W, et al. Development of a dual extrusion printing technique for an acid- and thermo-labile drug. Eur J Pharm Sci 2018;123:191-8.

128. Pietrzak K, Isreb A, Alhnan MA. A flexible-dose dispenser for immediate and extended release 3D printed tablets. Eur J Pharm Biopharm 2015;96:380-7.

129. Nokhodchi A, Raja S, Patel P, Asare-Addo K. The role of oral controlled release matrix tablets in drug delivery systems. Bioimpacts 2012;2:175-87.

130. Doty AC, Weinstein DG, Hirota K, Olsen KF, Ackermann R, Wang Y, et al. Mechanisms of in vivo release of triamcinolone acetonide from PLGA microspheres. J Contril Release 2017;256:19-25.

131. Sinha Roy D, Rohera BD. Comparative evaluation of rate of hydration and matrix erosion of HEC and HPC and study of drug release from their matrices. Eur J Pharm Sci 2002;16:193-9.

132. Sun X-T, Guo R, Wang D-N, Wei Y-Y, Yang C-G, Xu Z-R. Microfluidic preparation of polymer-lipid Janus microparticles with staged drug release property. J Colloid Interface Sci 2019;553:631-8.

133. Thanawuth K, Limmatvapirat S, Rojviriya C, Sriamornsak P. Controlled release of felodipine from 3D-printed tablets with constant surface area: influence of surface geometry. Pharmaceutics 2023;15:467.

APPENDIX

Standard curve of FDP in 1% w/v polysorbate 80 for chapter 3

Mehtod :	HPLC analysis
HPLC column :	Phenomenex Luna C18 column, 5 μm, 150 × 4.6 mm
Mobile phase :	acetonitrile, methanol, and phosphate buffer (40:20:40)
Flow rate :	1 mL/min at a controlled temperature of 35°C
UV detector :	wavelength 254 nm

Table A1. The concentration of FDP in 1% w/v polysorbate 80 for chapter 3.

Concentration (μg/mL)	Area under the curve
10	1.15×10^6
20	2.37×10^6
40	4.70×10^6
60	7.26×10^6
80	9.31×10^6
100	1.19×10^7

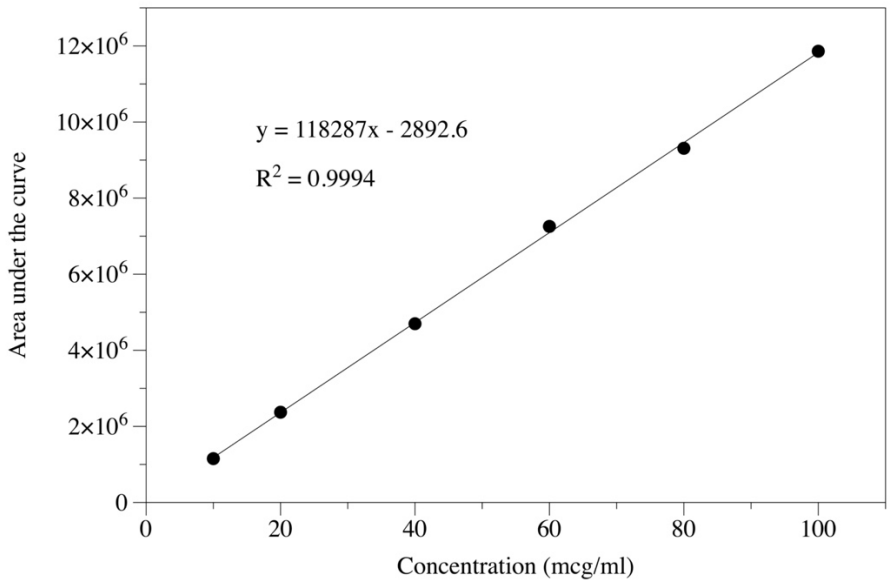

Figure A1. Standard curve of FDP in 1% w/v polysorbate 80 for chapter 3.

Standard curve of GPZ in phosphate buffer (pH 6.8) with 1% w/v polysorbate 80 for chapter 4

Mehtod :	HPLC analysis
HPLC column :	Phenomenex Luna C18 column, 5 μm, 150 × 4.6 mm
Mobile phase :	acetonitrile, methanol, and phosphate buffer pH 6.0 (20:10:70)
Flow rate :	1 mL/min at a controlled temperature of 40°C
UV detector :	wavelength 276 nm

Table A2. The concentration of GPZ in phosphate buffer (pH 6.8) with 1% w/v polysorbate 80 for chapter 4

Concentration (μg/mL)	Area under the curve
5	4.59×10^5
10	9.49×10^5
20	1.85×10^6
40	3.93×10^6
60	5.78×10^6
80	7.79×10^6
100	9.98×10^6

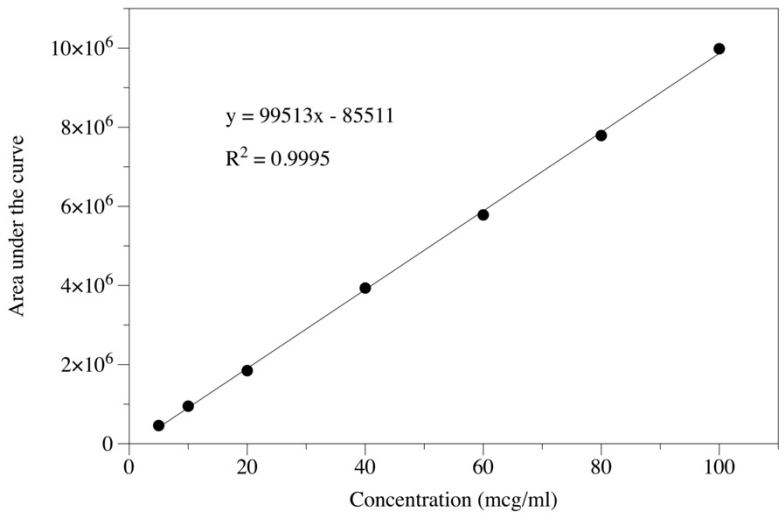

Figure A2. Standard curve of GPZ in phosphate buffer (pH 6.8) with 1% w/v polysorbate 80 for chapter 4

Standard curve of FDP in 1% w/v polysorbate 80 for chapter 5

Mehtod :	HPLC analysis
HPLC column :	Phenomenex Luna C18 column, 5 μm, 150 × 4.6 mm
Mobile phase :	acetonitrile, methanol, and phosphate buffer pH 3.0 (45:25:30)
Flow rate :	1 mL/min
UV detector :	wavelength 362 nm

Table A3. The concentration of FDP in 1% w/v polysorbate 80 for chapter 5

Concentration (μg/mL)	Area under the curve
10.44	3.69×10^5
20.88	7.78×10^5
41.76	1.62×10^6
62.64	2.50×10^6
83.52	3.34×10^6
104.4	4.12×10^6

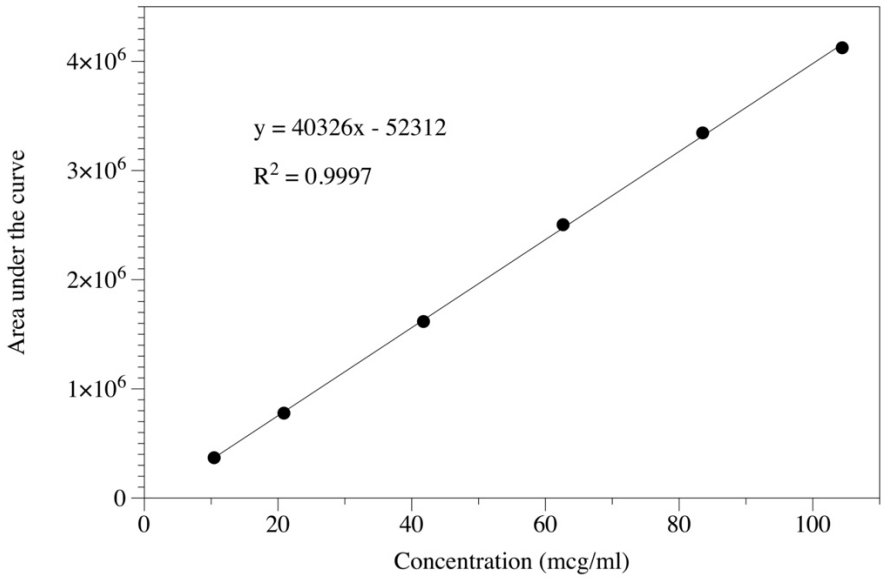

Figure A3. Standard curve of FDP in 1% w/v polysorbate 80 for chapter 5.

Standard curve of GPZ in phosphate buffer (pH 6.8) with 1% w/v polysorbate 80 for chapter 5

Mehtod :	HPLC analysis
HPLC column :	Phenomenex Luna C18 column, 5 μm, 150 × 4.6 mm
Mobile phase :	methanol and phosphate buffer pH 6.0 (52:48)
Flow rate :	1 mL/min
UV detector :	wavelength 220 nm

Table A4. The concentration of GPZ in phosphate buffer (pH 6.8) with 1% w/v polysorbate 80 for chapter 5

Concentration (μg/mL)	Area under the curve
10.02	1.65×10^6
40.08	5.30×10^6
60.12	7.76×10^6
80.16	1.04×10^7
100.2	1.27×10^7

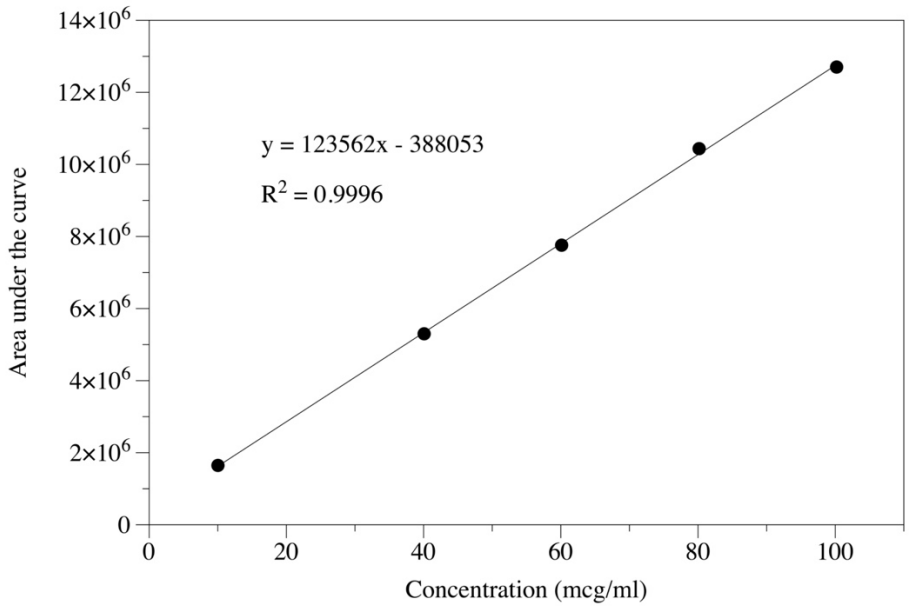

Figure A4. Standard curve of GPZ in phosphate buffer (pH 6.8) with 1% w/v polysorbate 80 for chapter 5

VITA

NAME	**KASITPONG THANAWUTH**
INSTITUTIONS ATTENDED	Bachelor Degree: College of Pharmacy, Rangsit University, Thailand
PUBLICATION	1.Thanawuth K, Limmatvapirat S, Rojviriya C, Sriam ornsak P. Controlled release of felodipine from 3D-printed tablets with constant surface area: influence of surface geometry. Pharmaceutics. 2023;15(2):467. 2. Thanawuth K, Sutthapitaksakul L, Konthong S, Suttiruengwong S, Huanbutta K, Dass CR, et al. Impact of drug loading method on drug release from 3D-printed tablets made from filaments fabricated by hot-melt extrusion and impregnation processes. Pharmaceutics. 2021;13(10):1607. 3. Thanawuth K, Sriamornsak P. Fabrication of indomethacin-loaded polyvinyl alcohol filaments through hot-melt extrusion. Key Eng Mater. 2020;859:247-251.
AWARD RECEIVED	-